SOLUBILITY OF HYDROGEN IN METALS AND ITS EFFECT ON POREFORMATION AND EMBRITTLEMENT

By

Hamid R. Shahani

STOCKHOLM
1984

Department of Casting of Metals
The Royal Institute of Technology

SOLUBILITY OF HYDROGEN IN METALS AND ITS EFFECT ON POREFORMATION AND EMBRITTLEMENT

Hamid R Shahani

Dept. of Casting of Metals

The Royal Institute of Technology

Stockholm, Sweden

April 1984

Avhandling

Som med tillstånd av Kungl. Tekniska Högskolan framläggs till offentlig granskning för avläggande av teknisk doktorsexamen fredag den 18 maj 1984, kl 10.15 i sal B1 Brinellvägen 23, Stockholm

Institutionen för Metallernas Gjutning, Stockholm 1984

ERRATA:

	written:	should be:
Introduction, Page 5, lines 6-8	The partial molar volume of hydrogen in the melt, $\bar{V}_H$, is not determined. Due to very low solubility of hydrogen in the melt, $\bar{V}_H$ can be substituted by the...	No Data of the partial molar volume of hydrogen in the melt has been found in the literature. Just as an example $\bar{V}_H$ has been substituted by the ...
Introduction, Page 5, lines 22-24	a-Silicon and iron decrease the solubility of hydrogen in aluminium, whereas with iron at higher temperature, and titanium it increases.	a-Silicon and iron decrease the solubility of hydrogen in aluminium and titanium increases it.
Introduction, Page 8, line 14	... using Fick' s first law:	... using Fick' s first law combined with common gas law:
Introduction, Page 9, line 15	... 20-40 seconder ...	... 20-40 seconds...
Introduction, Page 9, line 21	Pores size and number were...	The size and number of pores were...
Introduction, Page 9, line 28	... by collosion as...	... by collision as...
Introduction, Page 10, line 20	Het rogeneous...	heterogeneous...
Paper I, Page 1, line 14	Silicon and iron decrease the solubility of hydrogen while titanium increases it. At high temperature, iron also increases the hydrogen solubility.	Silicon and iron decrease the solubility of hydrogen while titanium increases it. (Last sentence should be omitted.)
Paper I, Page 8		Lines 11 to 23 should be omitted
Paper V, Page 5, line 10	Equation 5, reflects the solubility of hydrogen in the melt as a function of pressure and temperature, The partial molar volume of hydrogen in aluminium, $\bar{V}_H$, is not determined. In the present analysis, it is assumed that $\bar{V}_H$ and its variation with the temperature is the same as the molar volume of aluminium, V_m^{Al}. This is because the solubility of hydrogen in the aluminium melt, max 2×10^{-4} mole fraction is very small. Equation 5 then becomes;	... and temperature. No value on the partial molar volume of hydrogen in the melt has been found in the literature. For the calculations this value is not critical for the moderate pressures. In the present analysis. Just as an example it is assumed that $\bar{V}_H$ and its variation with the temperature is the same as the molar volume of aluminium V_m^{Al}. Equation 5 then becomes:
Paper I, Page 13, Table 3		Calculations for Ti and Fe are not valid.

This thesis comprises the following papers:

I. Solubility of dry hydrogen in liquid aluminum, Al-4%Ti, Al-7%Si and Al-10%Fe at one atmosphere
H. Shahani

II. Solubility of dry hydrogen in liquid gold, gold-copper and gold-palladium alloys at one atmosphere
H. Shahani, L. Wictorin

III. On the design of rapid heating and high pressure casting furnaces used in metal foam experiments
H. Shahani, R. Jönsson, S. Wallin

IV. On the mechanism of precipitation of pores in melts
H. Shahani, H. Fredriksson

V. Precipitation of gas pores in metallic melts during cooling under microgravity
H. Shahani, H. Fredriksson

VI. Effect of hydrogen on the shrinkage porosity of aluminum copper and aluminium silicon alloys
H. Shahani

VII. Hydrogen embrittlment in iron base alloys
H. Shahani, H. Söderhjelm, M. Nygren

ABSTRACT
========

Solubility of hydrogen in Al, Al-4%Ti, Al-7%Si, Al-10%Fe and also in Au-Cu, Au-Pd alloys is investigated. Effect of alloying elements on the hydrogen solubility are determined by evaluating solubility equations and interaction coefficients.

Formation of rounded pores in hydrogen supersaturated Al, Al- 4%Ti, and Al-10%Fe alloys is investigated. A model for nucleation and growth of rounded pores in the melt is presented, and is applied for pure aluminium. These samples were remelted in reduced gravity and reduced ambient pressure. The resulting materials consisted of numerous expanded pores, dispersed in the metallic matrix. Al-4%Ti samples, saturated at 0.5 and 1 atm hydrogen and remelted at 0.1 atm ambient pressure, achieved 50% relative reduction in density with a uniform pore distribution.

The effect of hydrogen, alloying elements, modifiers and pressure drop, caused by solidification on the shrinkage porosity in aluminium silicon and aluminium copper alloys are studied. A model for formation of shrinkage pores, regarding these parameters is also presented.

Effect of hydrogen on the transition from ductile to brittle in iron base amorphous ribbon is studied. The presented results indicate that small amount of hydrogen in the melt prior to rapid quenching can cause embrittlement in the amorphous ribbons.

Key words:

Hydrogen, aluminium, gold, palladium, poreformation, nucleation, growth, shrinkage, metallic foam, microgravity, amorphous, embrittlement.

INTRODUCTION

Pores in most cases are formed in metals during casting and solidification and may reduce the desired properties. However, pores can be useful in some special applications i.e. producing very light materials or materials with a high damping capacity. In these cases, a large number of pores should be evenly distributed in the metallic matrix and the material is known as metallic foam.

Whether the problem is to eliminate or to enhance the formation of pores, a basic understanding of the mechanisms involved in the poreformation is necessary. In this respect, a fundamental knowledge of gas solubility in the melt, induced pressure by the dissolved gas, nucleation and growth of the pores, and solidification mechanism are all essential. Finally, from these informations, the production of metallic foam can be considered. All these mechanisms have been investigated in this thesis, and the results thus obtained were used in investigation of poreformation in aluminium alloys.

1. GAS SOLUBILITY

Hydrogen is one of the most common gases dissolving in metals. It is, for instance, the only gas which dissolves in aluminium. Diatomic gases, such as hydrogen, dissolve in the melts as atom by gradual steps (1). The total reaction for hydrogen dissolution can be written as:

$$H_2(g) \rightleftharpoons 2\underline{H} \qquad (1)$$

At equilibrium, the chemical potential of hydrogen in the gas phase and in the melt, should be equal. Considering the effect of external pressure (2) on the above reaction

gives:

$$2(\mu_H^o + RT \ln X_H - \bar{V}_H(P_t - P_o)) = \mu_{H_2}^o + RT \ln(P_{H_2}/P_o) \quad (2)$$

$$X_H = (P_{H_2}/P_o)^{\frac{1}{2}} \exp((\mu_{H_2}^o - 2\mu_H^o)/2RT) \exp(\bar{V}_H(P_t - P_o)/RT) \quad (3)$$

which normally is expressed by:

$$X_H = (P_{H_2}/P_o)^{\frac{1}{2}} A \exp(-B/T) \exp(\bar{V}_H(P_t - P_o)/RT) \quad (4)$$

The partial molar volume of hydrogen in the melt, $\bar{V}_H$, is not determined. Due to very low solubility of hydrogen in the melt, $\bar{V}_H$ can be substituted by the molar volume of melt V_m^ℓ. The amount of dissolved gas can thus be calculated from equation 5.

$$X_H = (P_{H_2}/P_o)^{\frac{1}{2}} A \exp(-B/T) \exp(V_m^\ell(P_t - P_o)/RT) \quad (5)$$

In the absence of external pressure and with moderate pressures of hydrogen, equation 5 reduces to:

$$X_H = (P_{H_2}/P_o)^{\frac{1}{2}} A \exp(-B/T) \quad (6)$$

This equation is known as Sieverts law (3). The values of constants A and B, for aluminium and gold alloys are determined experimentally at $P_{H_2} = P_o$. The Sieverts apparatus was employed for the measurements, and the results are presented in the papers I and II. Effect of alloying elements on the gas solubility are determined by calculating interaction coefficients (4). The results indicate that:

a-Silicon and iron decrease the solubility of hydrogen in aluminium, whereas with iron at higher temperature, and titanium it increases.

b-For gold alloyed with copper or palladium, hydrogen solubility increases with alloying content.

2. NUCLEATION

Nucleation of pores is normally treated by the method derived by Gibbs (5) more than 100 years ago. The pressure caused by the dissolved gas in the melt, P'_{H_2}, is the driving force for poreformation in castings. During cooling, the gas solubility in the melt decreases, see equation 5. Assuming that the gas content in the melt remains constant, P'_{H_2} increases, and can be evaluated as a function of initial gas content, applied ambient pressure and temperature from equation 5:

$$P'_{H_2} = \frac{P_G X_H^2 \exp(\frac{2B}{T})}{A^2 \exp(\frac{2V_m^2 (p_t - p_o)}{RT})} \qquad (7)$$

At mechanical equilibrium, the gas pressure in a bubble, P_b is related to the ambient pressure Pa, and surface tension Y

$$P_b = P_a + 2Y/r \qquad (8)$$

Gas pressure required for nucleating a bubble can be calculated by equating $P_b = P'_{H_2}$, and considering the activation energy for nucleation (6):

$$W^* = 60kT = 16\pi Y^3/(P'_{H_2} - P_a)^2 \qquad (9)$$

This indicates that P'_{H_2} of about 40000 atm, is required to form a bubble homogeneously. This pressure is too high to be achieved in even highly supersaturated melts computed by equation 7. It is thus, concluded that the pores, observed in the samples, must have formed hetrogeneously. The usual method to treat the hetrogeneous nucleation is to look at a gap, formed on a flat substrate. In paper IV, a model for hetrogeneous nucleation is presented. In a melt, there usually are particles which can cause hetrogeneous nucleation. In a spherical substrate, the size of the particles, as well as, the difference in surface tensions influence the nucleation. Assuming:

$$n = \frac{\gamma^{\ell/p}}{\gamma^{\ell/g}} > 1 \qquad (10)$$

the required work for nucleation can be calculated as a function of particle size.

$$W^* = 60kT = 16\pi\gamma^{3}_{\ell/g}/(P'_{H_2}-P_a)^2 - 4\pi r_p^2 n\gamma^{\ell/g} + 4\pi r_p^3(P_{H_2}-P_a)/3 \qquad (11)$$

P'_{H_2} obtained from equation 11, reduces from 40000 atm to low pressures of 10-20 atm with particles larger than 2 um, and it reduces further with larger particles. Aluminium oxide fulfills the condition set by expression 10, ref(7), and it is easily formed during melting and casting according to the following reaction:

$$2Al + 3H_2O \text{ ========== } Al_2O_3 + 6\underline{H} \qquad (12)$$

The sources of water in the above reaction, are due to moisture in the air, combustion products and etc. The resulting atomic hydrogen dissolves rapidly in the melt and precipitates as pore during solidification.

3. GROWTH PROCESS

In order to study the nucleation and growth of the pores and also the production of metallic foam, aluminium, Al-10%Fe and Al-4%Ti were saturated with hydrogen at 1000 C. Electromagnetic levitation technic was employed. The degree of saturation was controlled by varying the pressure of hydrogen during gas treatment. The equipment is described in the paper III. After equilibrium, they were quenched in a watercooled copper mould, at ambient pressure of 6 atm. This treatment enhances formation of finner pores (8-11), which were intended for producing metallic foam. The size of the pores in the samples increased with the hydrogen content between 50-200 μm. In the case of pure aluminium they were mostly spherical while in Al-4%Ti and Al-10%Fe they were irregular and influenced in shape by primary Ti(ρ) and Fe(θ). The growth mechanism for pores in aluminium samples has been treated by the

following model:

During quenching, P'_{H_2} increases. A sufficient pressure is achieved at a critical temperature with the presence of particles, which pores can nucleate. As the cooling continious, the degree of supersaturation increases. Hydrogen atoms with higher potential in the surrounding, diffuse into the bubble, and it expands. With the increase of radius, the pressure inside the bubble diminishes and causes a higher driving force for diffusion;

$$r>r^* \Longrightarrow P_b=P_a+2\gamma/r < P'_{H_2} \tag{13}$$

At the same time due to depletion , diffusion distance for hydrogen atoms increases and it reduces the rate of gas transport to the bubble. The rate of transport of hydrogen can be calculated using Fick's first law:

$$n_{H_2} = \frac{P_b V_b}{RT} \tag{14}$$

$$dn_H = 2n_{H_2} = \frac{2}{RT}\,(P_b dV_b + V_b dP_b) \tag{15}$$

$$dn_H = \frac{2}{RT}\left(\left(P_a + \frac{2\gamma}{r}\right) 4\pi r^2 + \frac{4}{3} r^3 \pi\left(\frac{-2\gamma}{r^2}\right)\right)dr \tag{16}$$

$$\frac{dn_H}{dt} = \frac{8\pi}{3RT}(3P_a r^2 + 4\gamma r)\,\frac{dr}{dt} \tag{17}$$

$$\frac{dn_H}{dt} = \frac{D_H 4\pi r^2}{V_m^{\ell}} \cdot \frac{dx_H}{dr} \simeq \frac{D_H 4\pi r^2}{V_m^{\ell}} \cdot \frac{X_H^o - X_H^P}{r} \tag{18}$$

The concentration of hydrogen in bulk melt X_H^o is obtained from the gas analyses. Hydrogen concentration in the melt at the gas bubble interface, X_H^P is given by equations 5 and 8 as:

$$X_H^P = A \exp\left(\frac{-B}{T}\right) \cdot (P_b/P_o)^{\frac{1}{2}} \exp\left(\frac{V_m^{\ell}(P_t - P_o)}{RT}\right) \tag{19}$$

Combining eqations 17-19 results:

$$\frac{3RTD_H(X_H^o - X_H^P)}{2V_m^{\ell}} = (3P_a r + 4\gamma)\,\frac{dr}{dt} \tag{20}$$

Inserting dr/dt=dT/dt.dr/dT and integration gives the final pore size.

$$\int_{r^*}^{r_f} \frac{2\left(\frac{dT}{dt}\right)(3P_a+4Y)}{3R}\,dr = \int_{T^*}^{T_m} \frac{D_H(X_H^o - X_H^P)}{V_m^\ell}\,TdT \qquad (21)$$

This model indicates that the final size of the pores increases with the hydrogen content, and decreases with higher ambient pressure and higher cooling rates. The results based on the presented model were in a good agreement with the measured values presented in the paper IV.

4.METALLIC FOAM

The above mentioned samples were remelted at reduced gravity and reduced ambient pressure. Reduced gravity was achieved either using a sounding rocket or an airplane flying a parabolic trajectory. The devices for remelting the samples are described in the paper III. A filament extracted from a halogen projector lamp was used as the heating element. It was inserted in a cavity in the sample. Sample was remelted in about 15 seconds and solidfy in about 20-40 seconde depending on the gas (He or Ar) and ambient pressure. During remelting, pores expanded and they remained whithin the samples during solidification. Thus, pieces of metallic foams, about 2-3 grams were made. Density of the samples before and after remelting were measured. Relative reduction of density was calculated for the samples. Pores size and number were measured. The results are presented in paper V .

Samples of Al-4%Ti treated at 0.5-1 atm hydrogen and remelted at 0.1 atm achieved 50% reduction in density with a uniform distribution of pores. In aluminium cases, relative reduction of density did not exceed more than 5%. Pore were irregular and relatively large. The shape of pores in these cases was influenced by collosion as well as expansion. Al, Al-10%Fe, and Al-4%Ti have solidification range of 0, 200, 390 C, respectively. Hydrogen solubilities as measured in previous work increases for the alloys in the same order. The results indicate that increasing solidification range and gas solubility are effective parameters in producing metallic foam. Expanded pores, are more effectively trapped in the

mushy zone, by primary Ti and Fe and collosion was reduced.

5. EFFECT OF SHRINKAGE

Formation of shrinkage pores in aluminium, aluminium copper and aluminium silicon alloys are studied and the results are presented in paper VI. The effect of hydrogen content, mode of solidification, impurities i.e aluminium oxide, and modifiers on the porosity are investigated. The hydrogen content of the alloys prior to casting was varied, with water saturated argon injected into the melt for different periods. They were subsequently cast in a rectangular cast iron mould. The hydrogen content, area fraction of porosity and size of the pores was then measured. The effect of modifiers was studied by adding 100 ppm Na or 250 ppm Sr after gas treatment. The results indicated that the porosity in the samples increases with duration of gas treatment more than the hydrogen content. With longer period of gas treatment, the amount of aluminium oxide in the melt increases which subsequently forms more nucleation sites for pores. This conclusion is in accordance with the model for hetrogeneous nucleation presented above. Porosity also increased with the silicon content and addition of modifiers. Silicon reduces reduce the surface tension (12), which facilitates the pore nucleation.

A model for formation of shrinkage pores in long solidification range alloys is also presented. The enrichment of hydrogen and the pressure drop in the melt caused by shrinkage are accounted for in this model. During solidification, melt in the interdendritic area is enriched with hydrogen and the pressure of hydrogen in the melt thus increases, and can be calculated through equation 7. It is becuase the hydrogen solubility in the solid is much less than in the liquid. Due to high diffusivity of hydrogen and also short distance for diffusion, 100um dendrite arm spacing, the lever rule can be applied. The pressure drop caused by shrinkage is calculated with a model presented by Piwonka (13). Assuming that pore nucleation is hetrogeneous and that the size of the pores are

less than the remaining liquid between the dendrite arms, maximum pore size can be calculated as function of hydrogen content, dendrite arm spacing, and distance from the raiser by equation:

$$\left(\frac{X^{o}_{H\lambda}}{2rK}\right)^2 + \frac{32\mu\beta'\theta^2 L^2 t^2 \lambda^2}{r^4 \pi h^2} - P_a = \frac{2\gamma}{r} \qquad (22)$$

That size of the shrinkage pores varies between 10-50 um close to the raiser and 40-60um close to the chill depending on the hydrogen content. These results are in a good agreement with the measured size of the shrikage pores presented in paper VI.

6. Hydrogen Embrittlement

The hydrogen embrittlement is a well known phenomena in metals and specially in steel. The mechanisms are different for various metals. In steels, an accepted mechanism appears to be associated with the migration of hydrogen atoms to lattice imperfections or strain fields associated with the imperfections. During the last stage of the pore growth, the pressure increases and causes the diffusion of hydrogen to the structure, which can lead to hydrogen embrittlement. This process can also occure in amorphous metals provided that they contain hydrogen before production. This matter has been studied in the paper VII.

Experiments were performed by injecting hydrogen gas to Fe(SiBC) alloy, before rapid quenching by chill block melt spinning method. Cooling rate and hydrogen content were varied. The X-ray measurements and bending test indicated amorphous structure but brittle. The effect of hydrogen on the amorphous transition was negligible. Embrittlement caused by hydrogen in these samples, has the same mechanism, although due to rapid quenching pores did not form and hydrogen is directly trapped in the structure.

CONCLUDING REMARKS

The papers presented in this thesis show that:

I) Pores nucleate heterogenously. Reducing hydrogen and foreign particles in the melt would reduce the porosity.

II) The possibility of producing metallic foam in reduced gravity is proved. Alloys with long solidification range and moderate hydrogen content and low remelting pressure inhance the process.

III) Existence of hydrogen in iron base amorphous ribbon, cause transition from ductile to brittle behaviour.

ACKNOWLEDGEMENT

I would like to express my gratitude to my supervisor Professor Hasse Fredriksson for his encouraging support throughout the work and for many stimulating discussions.I would like to thank the members of the department of casting of metals for their assistance during the experimental work. Many thanks also to Rolf Jönsson and Sven Wallin at the Swedish Space corporation for good cooperation throughout the work with the space experiments

The main part of this work was sponsored by the Swedish Board for Space Activities.Minor financial support recieved from Ardal og Sunndal Verk a.s., Norway. This support is greatfully acknowledged.

REFERENCES

==========

1. R. D. Pehlke Trans. of the Metal. Soc. of AIME vol 227, p. 844, Aug. 1963
2. R. A. Swalin, Thermodynamics of solids, John Wiley & sons New York, 1962, p. 143-169
3. A. Sieverts, Zeitschrift fur metallkunde 21, p. 16, 1910
4. J. Chipman, J. of the Iron and Steel Inst, p. 97, 1955
5. J. W. Gibbs, Trans. Conn. Acad. 3, 343 (1878)
6. J. C. Brice: The Growth of Crystals from Liquids, North-Holland Publ. Co., Amsterdam, 1973.
7. J. A. Campion, Journal of Material Science 4 (1969) 39-49
8. S. Z. Uram, et.al. Trans. AFS, vol. 66, 1958, p.129-134
9. D. Hanson, J. of Metals, 1935, p. 103-123
10. D. R. Kononow, Iron & Steel, Oct.1957, p.489-491
11. W. P. Desnizky, ibid, Feb. 1958, p. 51-52
12. A. M. Korol'kov, "Casting Properties of Metals and Alloys" Consultants Bureau, New York, 1960, p.37
13. T. S. Piwonka, M. C. Flemings, Trans. of the Metall. Soc. of AIME, vol. 236, Aug. 1966, p. 1157

LIST OF SYMBOLES		used in equation
$\mu^{o}_{H_2}$	standard chemical potential of hydrogen in the gas phase	3
μ^{o}_{H}	standard chemical potential of hydrogen in the melt	3
R	gas constant	3
T	temperature	3
X_H	mole fraction of hydrogen in melt	3
$\bar{V}_H$	partial molar volume of hydrogen	3
P_t	total pressure in the gas phase	3
P_o	standars pressure of hydrogen	
P_{H_2}	pressure of hydrogen	
A, B	constant	4
V^{ℓ}_m	molar volum of melt	5
P'_{H_2}	pressure of hydrogen in the melt	7
P_b	Pressure in the bubble	8
r	radius of the bubble	8
$\gamma^{\ell/g}$	surface tension between melt and gas	8
P_a	ambient pressure	8
W*	activation energy for nucleation	9
k	Boltzman constant	9
$\gamma^{\ell/p}$	surface tension between particle and melt	
n	$\gamma^{\ell/p}$/ $\gamma^{\ell/g}$	10,11
r_p	radius of the particle	11
n_{H_2}	number of moles of gas in the bubble	14
V_b	volume of the bubble	14
D_H	hydrogen diffusivity	19
dT/dt	cooling rate	20
X^{o}_H	initial hydrogen content	22
λ	dendrite arm spacing	22
K	Sieverts constant	22
r	radius of shrinkage pore	22
μ	viscosity	22
β'	corrected shrinkage coefficient	22
θ	solidification rate	22
L	length of the casting	22
t	trotosity factor	22
h	half of the mould height	22

PAPER I

H. SHAHANI

SOLUBILITY OF DRY HYDROGEN IN LIQUID ALUMINIUM, AL-4%TI, AL-7%SI, AND AL-10%FE AT ONE ATMOSPHERE

DECEMBER 1983

SOLUBILITY OF DRY HYDROGEN IN LIQUID ALUMINIUM, AL-4%TI, AL-7%SI AND Al-10%Fe AT ONE ATMOSPHERE PRESSURE

Hamid Shahani

Dept. of Casting of Metals
The koyal Institute of Technology
S-10044
Stockholm, Sweden
December 1983

1. ABSTRACT

Solubility of hydrogen in liquid aluminium and Al-Ti, Al-Si, and Al- Fe has been studied. The solubility equations, the standard heat of solution and the dependency of interaction parameters on temperature have been determined. Silicon and iron decrease the solubility of hydrogen while titanium increases it. At high temperature, iron also increases the hydrogen solubility.

2. INTRODUCTION

Different forms of porosity, like pinholes, blow-holes, inter-dendritical porosity, gas bubbles, etc. are directly related to the gas content of a melt prior to casting.

In aluminium alloys, hydrogen is the only gas which dissolves in a measureable amount. It is the main cause for pore formation in these alloys. Measuring the gas solubility in the melt provides basic information to understand and explain the mechanism of pore formation.

There are two main methods for measuring gas solubility in metals:

i) Sampling Method
ii) Hot Volume Method

The "Sampling Method" is based on first equilibrating the samples at the desired temperature and atmosphere, followed by a rapid quench. The gas content of the quenched samples is then measured by "Extraction method" or "Vacuum melting". The loss of gas from the samples during quenching and handling and also during gas determination causes inaccuracy with this method. However, this method has been widely used (1-14).

The "Hot Volume Method", originally developed by Siverts in 1910 (15-16), is based on the difference of volumes of an inert and a soluble gas which are required to fill the reaction chamber at constant temperature. The difference in volumes is the solubility of the reactive gas at that temperature. This method has also been widely used (17-25).

Some disadvantages with the "Hot Volume Method" are absorption and reaction of reactive gas with the crucible, the reaction chamber and oxides on the sample. The difference

in the heat conductivities of the gases also entails varying thermal gradients which further increases measurement errors. For example hydrogen has a thermal conductivity equal to 4.7×10^{-4} (cal/cm/sec/K) at $50^{o}C$ (26). It is 1.2 and 10 times larger than helium and argon respectively at the same temperature.

Ransley (27,28,5), Gpie(29) and Simensen (30) have measured the solubility of hydrogen in Al-Cu, Al-Si, Al-Mg alloys using both the above mentioned methods.

In the present investigation solubility of hydrogen in pure aluminium and under the alloying influence of titanium, silicon and iron have been determined using the "Hot Volume Method".

3. APPARATUS AND EXPERIMENTAL PROCEDURE

3.1 APPARATUS

The apparatus is shown in figure 1. It consists mainly of a 50 mm inner diameter (i.d) quartz reaction chamber and a mercury burette. The crucible, located in the reaction chamber, is of aluminium oxide. The dead volume of the reaction chamber was reduced by inserting two half-spheres of quartz at the top and bottom of the crucible. The temperature was measured with a chromel-alumel thermocouple protected by an aluminium oxide tube. A low frequency induction furnace was used as the heat source.

Reaction chamber was sealed by silicon greased glass joint which was cooled by a water-jacket system. Ambient pressure and temperature were registered within an accuracy of ± 0.25 mm Hg and $\pm 0.25^{o}C$ respectively. Melt temperature was controlled within $\pm 2^{o}C$. The main burette was also used as an internal manometer.

The burette was made of a 20 mm i.d. tube having a

height of 800 mm. The volume of the burette was larger than that of the reaction chamber. This reduced the errors that could have been caused by refilling.

The volume and pressure in the burette were controlled by varying the level of a mercury reservoir. This was activated by a modified screw system driven by an electric motor. The hot volume was measured with helium.It has the thermal properties close to hydrogen. Instead of constructing a purification train, gases of high purity were used. Both gases were supplied by AGA Stockholm. The impurity content of both gases were:

O_2 < 10 ppm
H_2O < 10 ppm
total purity > 99.995%

3.2 PREPARATION OF THE SAMPLES

Pure aluminium (99.98%) and ingots of Al-7% Si were supplied by A.S.V (Ardal og Sunndalsora Verk, Norway). Alloys of 4%Ti and 10%Fe were made as follows:

Pure aluminium was melted in a "Super Kanthal" furnace in a graphite crucible. The desired amount of alloying element was wrapped in an aluminium foil and added under protective argon atmosphere. Samples were then cast into a graphite mould with a diameter of 33 mm and cut to a height of 50 mm.A hole for placing the thermocouple was drilled in the center of each sample. The samples were then washed with aceton. The mass of the samples were measured. Samples were normally in the range of 110- 120 grams.

3.3 PROCEDURE OF THE EXPERIMENTS

Samples were inserted into the reaction chamber and degassed for half an hour at about 750 ^{o}C. The burette was filled with helium and then connected to the reaction chamber. Pressure in the burette was balanced with the

ambient pressure by varying the level of the reservoir. The volume of helium in the burette prior and after connection to the reaction chamber at a given melt temperature was adjusted to S.T.P. conditions. The hot volume for helium can thus be depicted by :

$$ {}^{o}V^{T}_{He} = \frac{(h_1 - h_2)\pi D^2 P_1 T_o}{4 P_o T_1} \qquad (1) $$

${}^{o}V^{T}_{He}$, is the volume which contains an equivalent amount of gas at $0^{o}C$ as the actual volume does at the investigated temperature and pressure. Hot volumes of helium were measured at different temperatures in the range of 665-920 ^{o}C . The same procedure was repeated with hydrogen.It took about 10-15 minutes to reach equilibrium.The difference in the hot volume for hydrogen and helium gave the amount of hydrogen dissolved in the melt at the temperature of interest and can be determined by equation (2):

$$ S^{T}_{H_2} = \frac{({}^{o}V^{T}_{H_2} - {}^{o}V^{T}_{H_e})100}{m} \sqrt{\frac{76}{P_1}} \qquad (2) $$

where:

m = mass of the sample (grams)
P_1= ambient pressure (cm Hg)
P_o= standard pressure (76 cm Hg)
T_1= room temperature (^{o}K)
T_o= standard temperature ($273^{o}K$)
D = diameter of the burette (2 cm)
h_1= height of the mercury in the burette before connection to the reactiom chamber (cm)
h_2= height of the mercury in the burette after connection to the reaction chamber (cm)
S = solubility of hydrogen (cc H_2/100 gr)

4. RESULTS

The results are presented in table 1. The volumetric solubility of hydrogen (cc H_2/100 grams) as a function of temperature for aluminium and Al- alloys are shown in figures 2-5. Figures 2-5 show that the solubility of hydrogen increases with increasing temperature. Titanium has a strong effect on the solubility with increasing temperature, figure 3. Silicon and iron both decrease the solubility, figures 4-5 .

5. THEORY

5.1 PURE ALUMINIUM

Dry hydrogen dissolves in liquid aluminium alloy by three gradual steps (31):

a: Dissociation of molecular hydrogen into atomic form in the boundary layer:

$$1/2\ H_2(g) \rightleftharpoons H\ (g)$$

b: Dissolving of atomic hydrogen in the boundary layer of the melt:

$$H\ (g) \rightleftharpoons H^*$$

c: Transport of hydrogen to the bulk of the melt by diffusion:

$$H^* \rightleftharpoons \underline{H}$$

Total reaction can be written as:

$$1/2\ H_2(g) \rightleftharpoons \underline{H} \qquad (3)$$

In pure aluminium we have :

$$\Delta G^{o} = -R.T.\ln(a_H / (P_{H_2})^{1/2}) \qquad (4)$$

In this treatment wt.pct of hydrogen is used as the standard state. It is further assumed that activity of hydrogen, f_H, goes to unity when the concentration of hydrogen goes to zero and P_{H_2} is equal to 1 atm. Thus:

$$\Delta G^{o} = -R.T.\ln(\%H \text{ pure}) \qquad (5)$$

$$\log(\%H \text{ pure}) = 0.434(-\Delta H^{o}/T + \Delta S^{o})/R \qquad (6)$$

In figure 6, log(%H) is plotted as a function of (1/T) for pure aluminium. A straight line is fitted to the points by the least square method. Assuming that ΔH^{o} and ΔS^{o} varies slightly at the investigated temperature range, their values may be calculated from the slope and intercept respectively. The solubility equation and value of ΔH^{o} are given in table 2. The respective volumetric function (cc H_2 /100 grams) as a function of temperature is presented in figure 2.

5.2 THE EFFECT OF ALLOYING ELEMENTS ON THE SOLUBILITY

Although, reaction (3) is valid for the solubility of hydrogen in aluminium alloys, however due to the interaction of the alloying elements, the value of f_H is not unity . The solubility data presented in figures 2-5 show a strong influence from the alloying elements. Therefore equation 4 should be treated as follows:

$$\Delta G^{o} = -R.T.\ln(f_H.\%H \text{ alloy}) = -R.T.\ln(f_H) - R.T.\ln(\%H \text{ alloy}) \qquad (7)$$

By defining ΔG_E as the excess free energy (31):

$$\Delta G_E = -R.T.\ln(f_H) \qquad (8)$$

$$\Delta G_1^{o} = \Delta G^{o} - \Delta G_E = -R.T.\ln(\%H \text{ alloy}) \qquad (9)$$

and rewritting equation (9) results in :

$$\log(\%H \text{ alloy}) = 0.434(-\Delta H_1^0/T + \Delta S_1^0)/R \qquad (10)$$

Figures 7-9 depict plots of log(%H alloy) as a function of (1/T) for the three investigated alloys. The values of ΔH_1^0 and ΔS_1^0 are evaluated in the same way as for pure aluminium. Solubility is calculated, converted to (cc H_2 /100gr) and plotted in figures 3- 5. The solubility equations and ΔH_1^0 are also given in table 2. Equation 8 may be rewritten to give:

$$f_H = \exp(-\Delta G_E/R.T) = (\%H \text{ pure})/(\%H \text{ alloy}) \qquad (11)$$

ΔG_E can be calculated as:

$$\Delta G_E = \Delta G^0 - \Delta G_1^0 = (\Delta H^0 - \Delta H_1^0) - T(\Delta S^0 - \Delta S_1^0) \qquad (12)$$

Wagner(33) and Chipman(34) have defined "interaction parameter" as the coefficients in the Taylor expansion of the logarithm of the activity coefficient:

$$\log(f_H) = \log(f_H) + \%H\left(\frac{\partial \log f_H}{\partial \%H}\right) + \%i\left(\frac{\partial \log f_H}{\partial \%i}\right) + \ldots \qquad (13)$$

The first and second terms in the right hand side of equation (13) are assumed to be zero and the third term ,"interaction parameter" may expressed in (wt.pct) as :

$$e_H^i = \left(\frac{\partial \log f_H}{\partial \%i}\right)_{P,T} \qquad (14)$$

- where the derivative is taken for the limiting case of zero concentration of the solute (35-37). Values of ΔG_E , are calculated from table 2 . Values of $\log(f_H)$ at 700-800-900 ^oC and the interaction coefficient, e_H^i , at these temperatures are calculated and presented in table 3.

6. CONCLUSION

Comparision of the present data on the solubility of hydrogen in pure aluminium with those reported by Opie (29) and Ransley (27) shows present values to be about 8% higher, compared to those reported by Ransley and about the same as Opie's results. For Al-7%Si the results are about 10% higher than that reported by Opie. No data was found on the solubility of hydrogen in Al-4%Ti and Al-10%Fe. Table 3 shows the effect of alloying elements and temperature dependency, and it can be concluded that:

1. Silicon decreases the solubility of hydrogen in aluminium at all of the investigated temperature of interests.
2. Iron decreases the solubility but this effect becomes less at increasing temperatures.
3. Titanium increases the solubility and the effect becomes larger at increasing temperatures.

The solubility of hydrogen in the solid state is always much lower than that in the liquid. It thus may be expected that there is a small effect from the alloying elements on the solubility in the solid state. It means that the risk for poreformation will increase in alloys containing titanium, but will decrease for silicon and at low temperatures also for iron.

7. ACKNOWLEDGEMENT

I wish to thank Professor H.Fredriksson for many helpful and stimulating discussions. This work was sponsored by the Årdal og Sunndal Verk a.s.,Norway

8. REFERENCES

1 -H.A.Slooman J.of the Inst.of Metals,71,p71,1945

2 -H.A.Slooman ibid,71,p612,1945

3 -N.A.Gokcen Trans.of the Metal.Soc.of AIME p93 Feb 1958

4 -T.J.Bosworth ibid,p489 Aug 1958

5 -C.E.Ransley J.of the Inst.of Metals,86,p212.1957-1958

6 -W.Fountain Trans.of the Metal.Soc.of AIME vol 212 p737,Dec 1958

7 -J.F.Martin ibid,p514 Aug 1958

8 -K.J.Brondyke ibid,p1542 Dec 1964

9 -J.S.Blakemore ibid,vol 242 p332 Feb1968

10-M.Uda AFS Transactions.(71-82) p577 1971

11-M.Uda ibid,(71-83) p584 1971

12-W.A.Oates Scripta Metalurgica vol 6 p349 1972

13-C.E.Ransley Z.Metalkunde,1955,46,328

14-L.A.Greenberg Ironmaking and Steelmaking vol 9 No.2 p58, 1982

15-A.Sieverts Zeitschrift fur metallkunde 21,p 16,1910

16-A.Sieverts ibid,21,p 37,1926

17-V.C.Kashyap Tran.of the Metal.Soc.of AIME p86 Feb 1958

18-N.M.Tayeb ibid,vol 227,p929 Aug 1963

19-M.Weinstein ibid,vol 227,p382 Apr 1963

20-N.A.Parlee ibid,vol 233,p1918 Oct 1965

21-F.E.Wooly ibid,vol 233,p1454 Aug 1965

22-C.E.Lundin ibid,vol 236,p978 Jul 1966

23-F.De Kazinczy,Jernkontorets Annaler 144,1960:4,p288

24-P.H.Turnock Trans.of the Metal.Soc.of AIME vol 236,p1540 Nov 1966

25-A.Jostsons ibid,vol 239,p1318 Sep 1967

26-Handbook of chemistry and physics,56th edition,1975-76, p.E-2 CRC

27-C.E.Ransley J.of the Inst. of Metals,74,p 599 1948

28-C.E.Ransley ibid,84,p455 1955-56

29-W.R.Opie Transactions AIME vol 188 p1237 J.of Metals 1950

30-C.J.Simensen ALUMINIUM 56,1980 part 2 p156

31-R.D.Pehlke Trans.of the Metal.Soc. of AIME vol 227 p844 Aug. 1963

32-P.T.Gallagher ibid,vol 245 p179 Jan 1969
33-C.Wagner"Thermodynamics of alloys"p51,1952,Cambridge,Mass.
Addisson-Wesley Press,Inc.
34-J.Chipman J.of the Iron and Steel Inst. p97 1955
35-R.D.Pehlke Trans.of the Metal.Soc.of AIME vol 218 p1088
Dec.1960
36-J.M.Dealy ibid,vol 227 p88 Feb1963
37-C.H.P.Lupis ibid,vol 233 p257 Jan1965

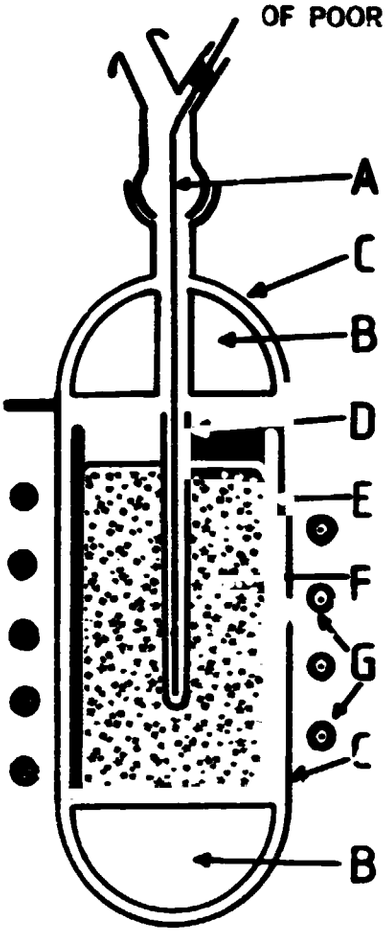

A -thermocouple
B -half spheres quartz bulbe
C -quartz reaction chamber
D -Al_2O_3 tube
E -Al_2O_3 crucible
F -melt
G -induction coil
H -water jacket
I -main burette
J -differential manometer
K -reservoir
V1-3 valve

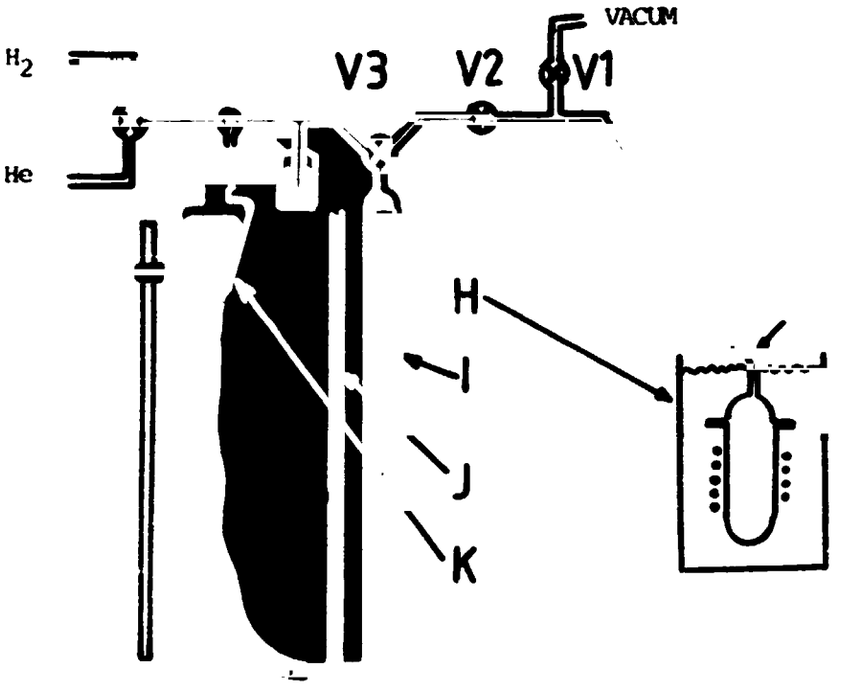

FIG.1 SCHEMATIC DRAWING OF THE REACTION CHAMBER AND APPARATUS.

TABLE 1: HYDROGEN SOLUBILITY MEASUREMENTS ($cc H_2$/100GRAMS)

TEMP(^oC)	660	675	700	750	775	780	800	815	825	840	850	860	920
Al	---	0.80	1.05	1.30	---	---	1.70	---	---	---	---	---	---
	---	0.9	1.1	1.46	---	---	1.88	---	---	---	---	---	---
	---	---	---	1.50	---	---	2.00	---	---	---	---	---	---
Al-4%Ti	---	---	1.00	1.78	---	1.58	3.04	---	---	---	2.30	---	---
	---	---	1.12	1.50	---	2.10	2.83	---	---	---	3.40	---	---
	---	---	---	---	---	---	---	---	---	---	3.63	---	---
Al-7%Si	0.60	---	0.68	0.90	---	---	1.00	---	---	1.35	---	---	---
	0.55	---	0.88	0.96	---	---	1.18	---	---	1.90	---	---	---
	---	---	---	---	---	---	---	---	---	2.05	---	---	---
Al-10%Fe	---	---	0.10	---	0.75	---	0.94	1.25	1.08	---	---	1.40	1.63
	---	---	0.20	---	0.45	---	---	---	---	---	---	1.50	1.85
	---	---	0.20	---	0.55	---	---	---	---	---	---	---	2.40
	---	---	0.25	---	---	---	---	---	---	---	---	---	---

TABLE 2: HYDROGEN SOLUBILITY EQUATIONS AND STANDARD HEAT OF SOLUTION

ALLOY	SOLUBILITY($cm^3 H_2$/100 grams)	SOLUBILITY(wt.pct)	ΔH (Kcal/mole)
Al	$\text{Log } S = (2.77 \pm 0.01) - (2683 \pm 11.7)/T$	$\text{Log}(\%H) = (-1.28 \pm 0.01) - (2683 \pm 11.7)/T$	12.28 ± 0.05
Al-4%Ti	$\text{Log } S = (3.61 \pm 0.03) - (3483 \pm 118)/T$	$\text{Log}(\%H) = (-0.44 \pm 0.03) - (3483 \pm 118)/T$	15.95 ± 0.05
Al-7%Si	$\text{Log } S = (2.50 \pm 0.18) - (2561 \pm 38)/T$	$\text{Log}(\%H) = (-1.55 \pm 0.18) - (2561 \pm 38)/T$	11.73 ± 0.17
Al-10%Fe	$\text{Log } S = (5.13 \pm 0.16) - (5664 \pm 168)/T$	$\text{Log}(\%H) = (1.08 \pm 0.16) - (5664 \pm 168)/T$	25.93 ± 0.77

TABLE 3: VARIATION OF ACTIVITY COEFFICIENT AND INTERACTION PARAMETER WITH TEMPERATURE(^oK)

		e_H^i for Al-alloys		
		700	800	900 (^oC)
$\text{Log } f_H^{Ti} = (800 \pm 106)/T - (0.84 \pm 0.02)$	at 4%Ti	-0.004	-0.024	-0.04
$\text{Log } f_H^{Si} = (-122 \pm 26)/T + (0.27 \pm 0.17)$	at 7 Si	+0.021	+0.022	+0.024
$\text{Log } f_H^{Fe} = (2981 \pm 156)/T - (2.36 \pm 0.15)$	at 10%Fe	+.070	+0.042	+0.018

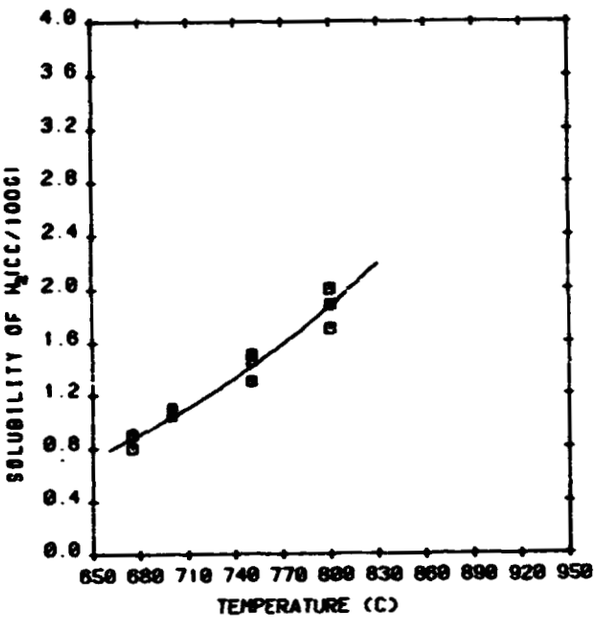

FIG 2:SOLUBILITY OF HYDROGEN IN PURE ALUMINIUM

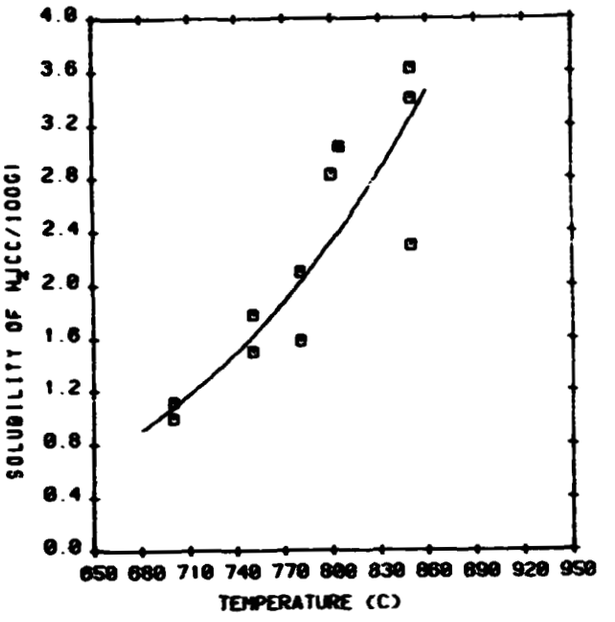

FIG 3:SOLUBILITY OF HYDROGEN IN AL-4%TI

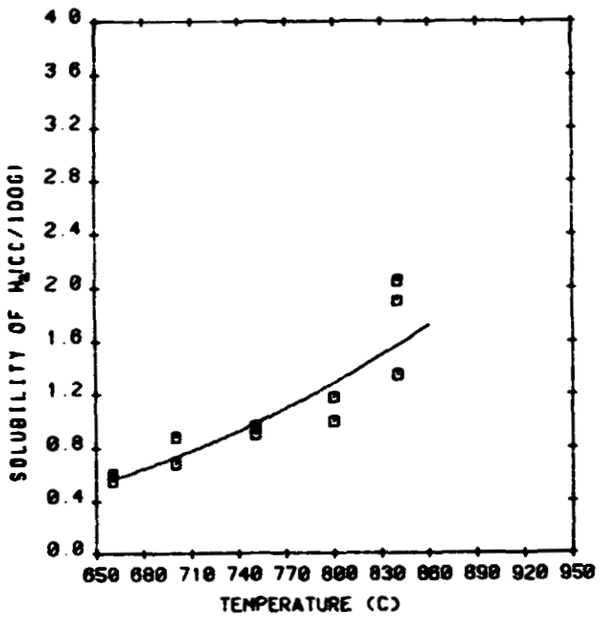

FIG 4:SOLUBILITY OF HYDROGEN IN AL-7%SI

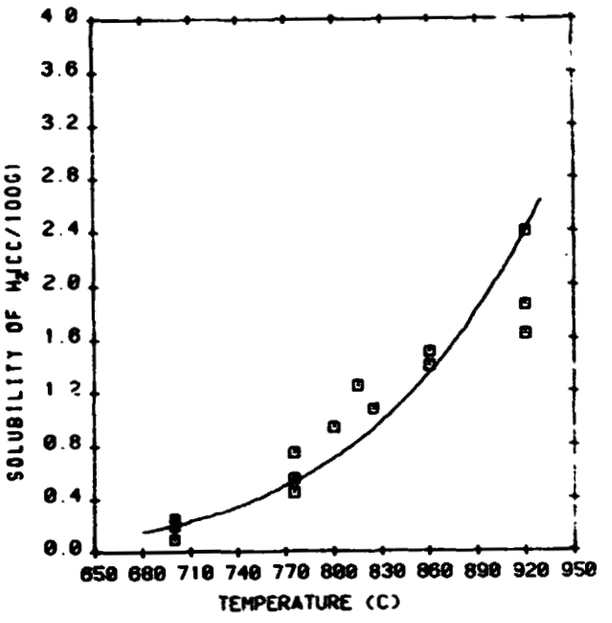

FIG 5:SOLUBILITY OF HYDROGEN IN AL-10%FE

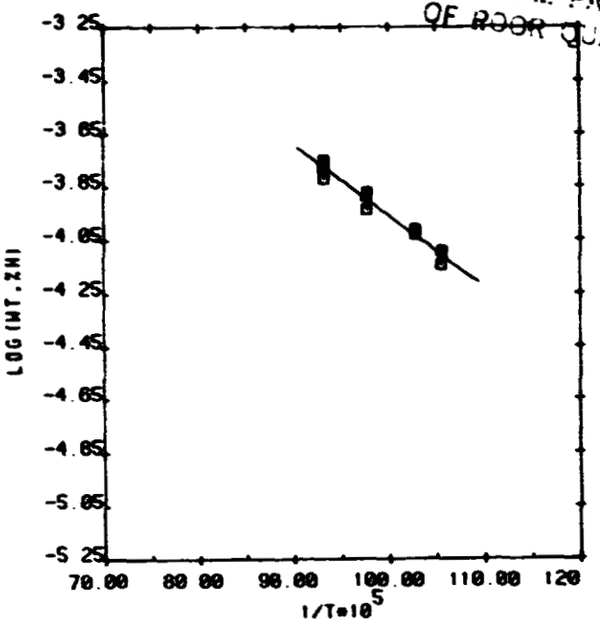

FIG.6: HYDROGEN SOLUBILITY FOR PURE AL WITH INVERSE OF TEMPERATURE(^{0}K).

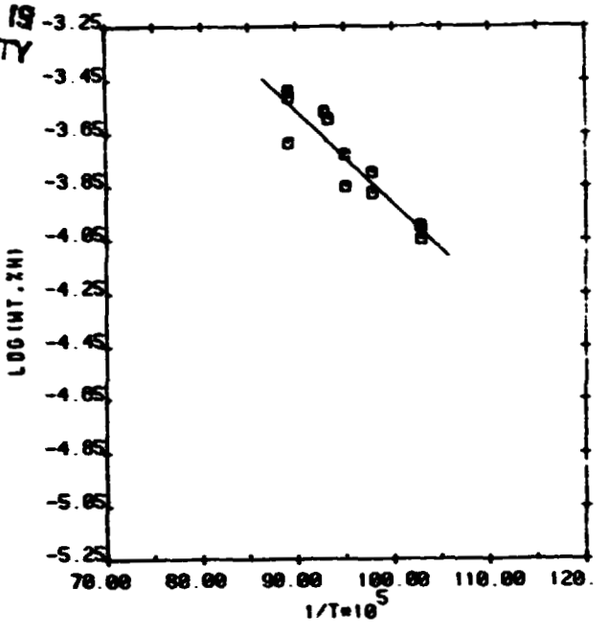

FIG.7: HYDROGEN SOLUBILITY FOR AL-4%TI WITH INVERSE OF TEMPERATURE(^{0}K)

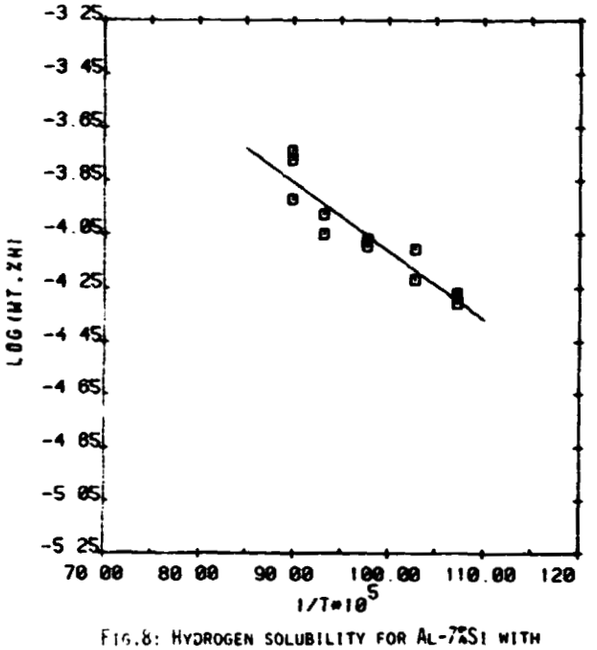

FIG.8: HYDROGEN SOLUBILITY FOR AL-7%SI WITH INVERSE OF TEMPERATURE(^{0}K)

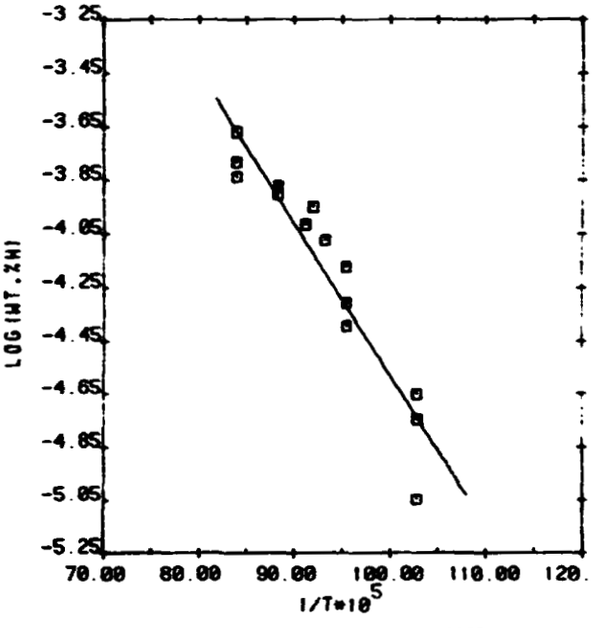

FIG.9: HYDROGEN SOLUBILITY FOR AL-10%FE WITH INVERSE OF TEMPERATURE(^{0}K)

PAPER II

H. SHAHANI, L. WICTORIN

SOLUBILITY OF DRY HYDROGEN IN LIQUID GOLD, GOLD-COPPER AND GOLD-PALLADIUM ALLOYS AT ON ATMOSPHERE PRESSURE

DECEMBER 1983

SOLUBILITY OF DRY HYDROGEN IN LIQUID GOLD, GOLD-COPPER AND GOLD-PALLADIUM ALLOYS AT ONE ATMOSPHERE PRESSURE

Hamid Shahani

Dept. of Casting of Metals
The Royal Institute of Technology

Lennart Wictorin

Div.of Oral Prosthetics
Eastman Institute

Stockholm, Sweden
December 1983

1. ABSTRACT

Hydrogen solubility in gold, gold-copper and gold-palladium alloys has been studied. Solubility equations, standard heat of solution and temperature dependency of the interaction parameter have been determined. Both copper and palladium increase the solubility. With increasing temperature, palladium has higher effect on the solubility of hydrogen than copper.

2. INTRODUCTION

The relationship between the gas content of the melt and defects due to porosity in the casting has been an interesting subject for years. In short, melts have gas solubilities about 5-10 times greater than in the solid state at the melting point. This solubility increases with increasing temperature. During casting, gas solubility decreases with diminishing melt temperatures. A sharp decrease of the solubility at the melting point also cause a concentration pile-up of the gas at the solidification front.

With the presence of proper nucleants in the liqiud, the pores will form and grow. Alloying elements influence the gas solubility of the melt which in turn affects the pore formation mechanism. Hydrogen is the only gas which dissolves in gold in small quantities (1-2). Adding alloying elements such as copper or palladium to pure gold in dental alloys is common. The practice, not only reduces costs but also enhances mechanical properties of the alloys. However, some draw backs are that they increase the hydrogen solubility in the liquid state. This increase in the solubility, in turn increases the tendency for poreformation in the casting.

Gas solubility measurements are performed by two main methods, namely "Sampling Method" (3-16) and "Hot Volume Method" (17-27). Solubility of hydrogen in pure gold in solid and liquid state has been studied earlier (1-2) using both methods. The aim of the present work is to study the effect of temperature and alloying elements, copper and palladium, on the hydrogen solubility using the "Hot Volume Method". This method was originally developed by Sieverts (17-18) and has been used in an earlier work by one of the authors (35). The method is based on the difference of volumes of an inert and a reactive gas which are required to fill the reaction chamber at constant temperature. The observed difference in volumes corresponds to the solubility of the reactive gas at the investigated temperature.

3. APPARATUS AND EXPERIMENTAL PROCEEDURE

3.1 APPARATUS

The Sieverts apparatus was used in this work. Figure 1 shows the schematic drawing of the apparatus.It was mainly composed of a quartz reaction chamber and a mercury burette. The crucible was also made of quartz. The reaction chamber and crucible had inner diameters of 15 and 6 mm respectively. Thermocouples of Pt,Pt-10%Rh and Pt-6%Rh,Pt-30%Rh were used for Au-Cu and Au-Pd alloys. They were protected by an aluminium oxide shield. Melt temperature was controlled within ± 2 ^{o}C. The mercury burette was made of a 6 mm i.d. tube with height of 850 mm. The height of mercury in the burette could be measured within ± 0.25mm. Helium was used as the insoluble gas to detect the hot volume. High purity helium and hydrogen were used. The impurities content are given below:

$O_2 < 10$ ppm
$H_2O < 10$ ppm
Total purity > 99.995%

A low frequency induction furnace was used for melting. The furnace enabled good stirring and fast response while adjusting temperatures. Silicon grease was used in the glass points. To cool the quartz joint, water jacket was utilized.

3.2 PREPARATION OF THE SAMPLES

Alloys were made of pure gold (24K), high purity copper and palladium. Experiments were initially performed with pure gold and subsequently by adding copper, to make alloys containing 4, 8, 10, 12, 13, 15, 20, 40% Cu. The same proceedure was repeated for palladium to make alloys of 2, 4, 6, 8, 10% Pd. The initial mass of pure gold was about 30 grams.

3.3 PROCEDURE OF THE EXPERIMENTS

Each experiment was initiated by evacuation of the apparatus for about 30 minuts at 1100^{o}C. Ambient pressure and temperature were recorded using a mercury thermometer (accuracy $\pm$0.25 C) and a mercury barometer (accuracy $\pm$0.25 mm Hg). The burette was first filled with helium and then connected to the reaction chamber. The hot volume of the system at S.T.P. and given melt temperature "T" could be calculated by:

$$ {}^{o}V^{T}_{He} = \frac{(h_1-h_2)D^2\pi P_1 T_o}{4P_o T_1} $$

-where:

P_1= ambient pressure (cm Hg)

P_o= standard pressure (76 cm Hg)

T_1= room temperature (^{o}K)

T_o= standard temperature (273^{o}K)

h_1, h_2= height of mercury in the burette before and after conection to the reaction chamber (cm)

D = diameter of the burette (0.6 cm)

The hot volume of the system was measured at different temperatures.The same procedure was applied with hydrogen in the same range of temperatures.It took about 20 minutes to reach equilibrium for each temperature.The amount of hydrogen dissolved in the melt could be calculated as:

$$ S^{T}_{H_2} = \frac{({}^{o}V^{T}_{H_2} - {}^{o}V^{T}_{He})100}{m} \sqrt{\frac{76}{P_1}} $$

where m is the mass of the sample in grams, and S is the solubility in (cc H_2/ 100 grams).

4. RESULTS

The results of the measurements are given in tables 1 and 2 for Au-Cu and Au-Pd alloys respectivly. The solubility measurements in (cc H_2/100 grams) as a function of temperature, ^{o}C, are also given in figures (2-16). All results indicate that the solubility increases with temperature and alloying element. They also show that Pd increases the solubility of hydrogen more than copper.This will be discussed later.

5. THEORY

5.1 PURE GOLD

Hydrogen dissolves in the melt by three gradual steps (28):

a: Dissociation of molecular hydrogen into atomic form at the boundary layer of the melt:

$$1/2\ H\ (g) \rightleftharpoons H(g)$$

b: Dissolving of atomic hydrogen in the boundary layer of the melt:

$$H(g) \rightleftharpoons H^*$$

c: Transport of hydrogen into the bulk of the melt by diffusion:

$$H^* \rightleftharpoons \underline{H}$$

The total reaction can be written as:

$$1/2\ H\ (g) \rightleftharpoons \underline{H} \qquad (1)$$

The standard free energy changes for this reaction is:

$$\Delta G^{o}=-R.T.\ln(a_H /(P_{H_2})^{1/2}) \qquad (2)$$

Concentration in weight percent and hydrogen pressure of one atmosphere are selected as the standard state. As the concentration goes to zero, activity coefficient of hydrogen, f_H, goes to unity, and;

$$\Delta G^{o}=-R.T.\ln(\%H \text{ pure}) \qquad (3)$$

and:

$$\log(\%H \text{ pure})=0.434(-\Delta H^{o}/T+\Delta S^{o})/R \qquad (4)$$

Neglecting small variation of ΔH^{o} and ΔS^{o} with temperature, the general form of the solubility can be depicted as a straight line in log(%H pure) as a function of (1/T). The best straight line was fitted to the points for the pure gold by the least square method. The value of ΔH^{o} and the corrected form of solubility with standard deviation are given in table 3.

5.2 THE EFFECT OF ALLOYING ELEMENTS ON THE SOLUBILITY

Although reaction (1) is still valid, but due to the interaction of alloying elements, the value of f_H is not oqual to unity anymore. The solubility data presented in figures (2-16) show a strong influence from the alloying elements. Equation 2 can thus be rewritten as:

$$\Delta G^{o}=-R.T.\ln(f .\%H \text{ alloy}) \qquad (5)$$

$$\Delta G^{o}=-R.T.\ln f_H-R.T.\ln(\%H \text{ alloy}) \qquad (6)$$

$$\Delta G^{o}=\Delta G_E+ \Delta G_1^{o} \qquad (7)$$

$$\Delta G_1^{o} =\Delta G^{o}- \Delta G_E=-R.T.\ln(\%H \text{ alloy}) \qquad (8)$$

$$\log(\%H \text{ alloy}) = 0.434(-\Delta H_1^0 /T+\Delta S_1^0)/R \qquad (9)$$

Again by neglecting the variation of ΔH_1^0 and ΔS_1^0 with temperature, a straight line should pass through these points in log(%H) and (1/T). The best straight line was passed by the least square method and values of ΔH_1^0 and ΔS_1^0 were calculated. They were transfered to the proper unit and plotted with solid line in relevant solubility diagrams. Equations 6 and 7 give the relation between excess free energy and activity coeficient:

$$f_H=\exp(-\Delta G_E/RT)=(\%H \text{ pure})/(\%H \text{ alloy}) \qquad (10)$$

$$\log f_H = \log f_H^0+\%H\left(\frac{\partial \log f_H}{\partial \%H}\right)+\%i\left(\frac{\partial \log f_H}{\partial \%i}\right) \qquad (11)$$

The first and second terms on the right hand side of the equation are assumed to be zero. Wagner (30) named the third term as interaction coefficient. It was modified slightly by Chipman(31) and is expressed in (wt.pct) as:

$$e_H^i = \left(\frac{\partial \log f_H}{\partial \%i}\right)_{P,T} \qquad (12)$$
$$\%i \to 0$$

In equation 12, the derivative is taken as the limiting case of zero concentration of the solute (29,32-34). To calculate the values of "f_H" at temperatures between 1100-1300, with interval of 100°C, the corrected form of solubility, as given in table (3) is used.

Values of interaction coefficient, e_H^i ,were calculated at mentioned temperatures and are presented in Table (4). The temperature dependency of the interaction coefficient is also given in the same table. Total heat of solution as a function of the alloying content for Au-Cu and Au-Pd are plotted in figure 17.

6. CONCLUSION

Hydrogen solubility in gold, gold-copper and gold-palladium alloys is related to the alloying content. Figures 2-16 show the increasing solubility with increasing alloying content. Palladium increases the solubility more than copper. It can also be realized by comparing the interaction coefficient values; e_H^{Pd} 3-4 times more than e_H^{Cu} was calculated when very small amount of alloy was added to pure gold. Comparison of the figures 2-10 for Au-Cu, also shows slightly lowered gas solubility for alloys of 10-12%Cu. Variation of the heat of solution indicates a minimum for Au-Pd at about 6%Pd. For Au-Cu alloys, the heat of solution decreases gradually with increasing copper content.

7. ACKNOWLEDGMENT

We wish to thank Professor Hasse Fredriksson for many helpful discussions. This project was sponsored by the Swedish Board for Technical Development, STU. Gold ,copper and palladium were kindly supplied by AB John Sjöding of Stockholm.

8. REFERENCES

1 -C.L.Thomas Transactions of the Metallurgical Soc. of AIME Vol.239 Apr.1967 p 485-490
2 -R.B.McLellan J.Phys.Chem.Solids,Vol.34 1973 p 1137-1141
3 -H.A.Slooman J.of the Inst.of Metals,71,p71,1945
4 -H.A.Slooman ibid,71,p612,1945
5 -N.A.Gokcen Trans.of the Metal.Soc.of AIME p93 Feb 1958
6 -T.J.Bosworth ibid,p489 Aug 1958
7 -C.E.Ransley J.of the Inst.of Metals,86,p212,1957-1958

8 -W.Fountain Trans.of the Metal.Soc.of AIME vol 212 p737, Dec.1958
9 -J.F.Martin ibid,p514 Aug 1958
10-K.J.Brondyke ibid,p1542 Dec 1964
11-J.S.Blakemore ibid,vol 242 p332 Feb1968
12-M.Uda AFS Transactions.(71-82) p577 1971
13-M.Uda ibid,(71-83) p584 1971
14-W.A.Oates Scripta Metallurgica vol 6 p349 1972
15-C.E.Ransley Z.Metalkunde,1955,46,328
16-L.A.Greenberg Ironmaking and Steelmaking vol 9 No.2 p58 1982
17-A.Sieverts Zeitschrift fur metallkunde 21,p 16,1910
18-A.Sieverts ibid,21,p 37,1926
19-V.C.Kashyap Tran.of the Metal.Soc.of AIME p86 Feb 1958
20-N.M.Tayeb ibid,vol 227,p929 Aug 1963
21-M.Weinstein ibid,vol 227,p382 Apr 1963
22-N.A.Parlee ibid,vol 233,p1918 Oct 1965
23-F.E.Wooly ibid,vol 233,p1454 Aug 1965.
24-C.E.Lundin ibid,vol 236,p978 Jul 1966
25-F.De Kazinczy,Jernkontorets Annaler 144,1960:4,p288
26-P.H.Turnock Trans.of the Metal.Soc.of AIME vol 236,p1540 Nov. 1966
27-A.Jostsons ibid,vol 239,p1318 Sep 1967
28-R.D.Pehlke Trans.of the Metal.Soc. of AIME vol 227 p844 Aug.1963
29-P.T.Gallagher ibid,vol 245 p179 Jan 1969
30-C.Wagner"Thermodynamics of alloys"p51,1952,Cambridge, Mass.Addisson-Wesley Press,Inc.
31-J.Chipman J.of the Iron and Steel Inst. p97 1955
32-R.D.Pehlke Trans.of the Metal.Soc.of AIME vol 218 p1088 Dec. 1960
33-J.M.Dealy ibid,vol 227 p88 Feb1963
34-C.H.P.Lupis ibid,vol 233 p257 Jan1965
35-H.Shahani Solubility of hydrogen in liquid aluminium alloys,this thesis

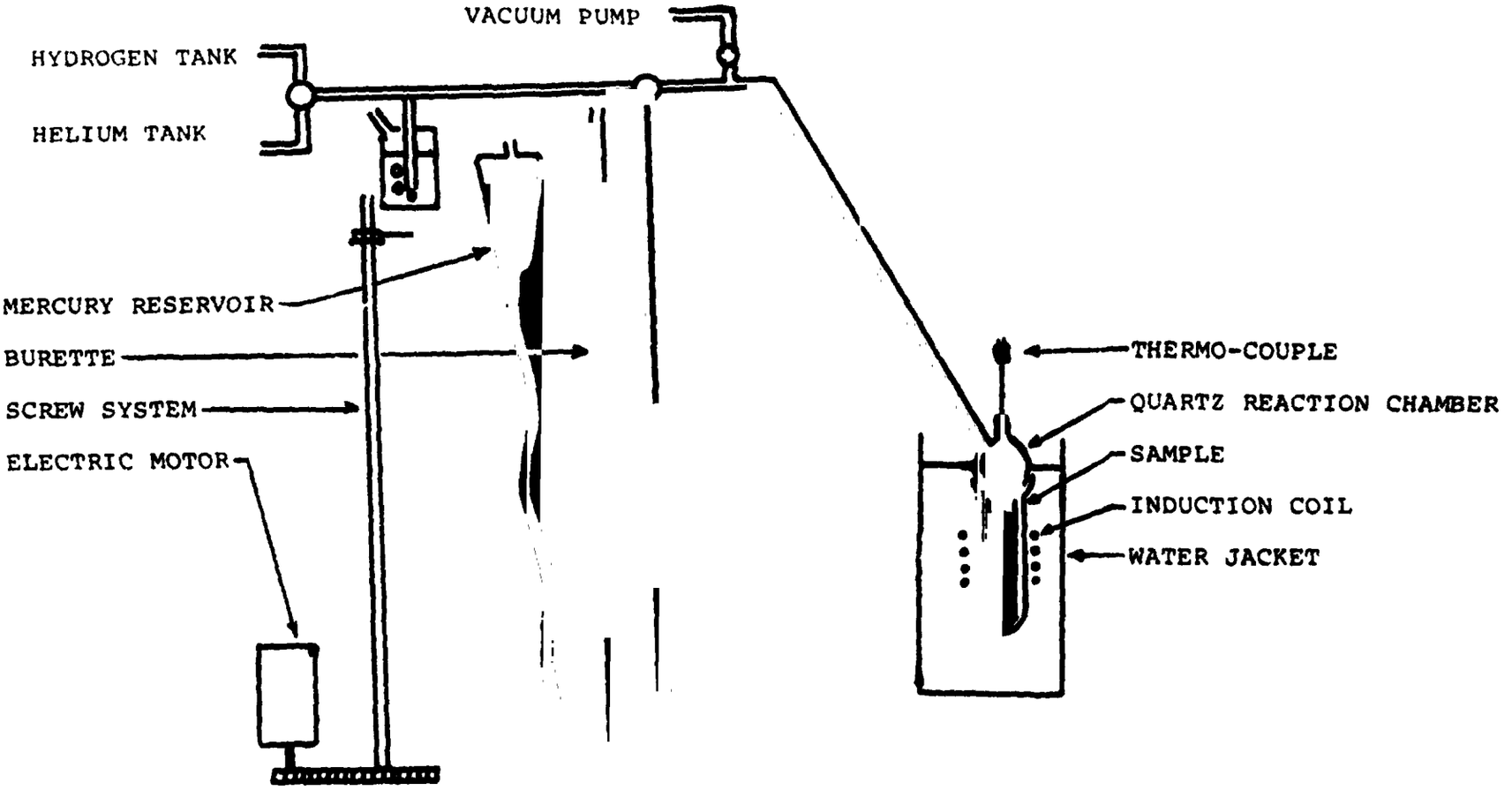

FIG.1:SCHEMATIC DRAWING OF THE APPARATUS.

TEMP(°C)	1010	1020	1045	1065	1090	1100	1112	1124	1130	1165	1173	1216	1233	1250	1267
0%CU	---	---	---	.06	---	.12	.17	---	---	.26	.32	.3	.55	---	.5
	---	---	---	---	---	.08	.19	---	---	---	---	.48	---	---	.75
	---	---	---	---	---	---	---	---	---	---	---	.36	---	---	---
4%CU	---	.18	---	---	---	---	---	---	.37	---	---	---	.54	---	---
	---	.24	---	---	---	---	---	---	.47	---	---	---	.78	---	---
8%CU	.38	---	---	---	.46	---	---	---	---	---	---	---	.78	---	---
10%CU	.14	---	---	---	---	---	---	---	---	---	.23	---	---	---	.2
	.25	---	---	---	---	---	---	---	---	---	.28	---	---	---	.26
	---	---	---	---	---	---	---	---	---	---	.39	---	---	---	.49
12%CU	.11	---	---	---	---	---	---	.14	---	.14	---	---	---	.22	.32
	.14	---	---	---	---	---	---	.25	---	---	---	---	---	.40	.34
	.17	---	---	---	---	---	---	.32	---	---	---	---	---	---	.58
13%CU	.46	---	---	---	---	---	---	---	.55	---	---	---	---	---	.57
	.58	---	---	---	---	---	---	---	.60	---	---	---	---	---	.68
	.61	---	---	---	---	---	---	---	.89	---	---	---	---	---	1.16
	.80	---	---	---	---	---	---	---	1.08	---	---	---	---	---	1.25
	---	---	---	---	---	---	---	---	---	---	---	---	---	---	.93
15%CU	.65	---	---	---	---	---	---	---	.96	---	---	---	---	---	1.13
	.85	---	---	---	---	---	---	---	1.48	---	---	---	---	---	1.59
	---	---	---	---	---	---	---	---	---	---	---	---	---	---	1.75
20%CU	---	---	1.43	---	---	---	---	---	---	1.35	---	---	---	---	2.05
	---	---	1.64	---	---	---	---	---	---	1.86	---	---	---	---	2.12
40%CU	1.74	---	---	---	---	---	---	---	---	1.85	---	---	---	---	2.06
	1.85	---	---	---	---	---	---	---	---	1.95	---	---	---	---	2.18
	1.88	---	---	---	---	---	---	---	---	2.06	---	---	---	---	2.39

TABLE 1: SOLUBILITY OF HYDROGEN ($cc H_2$/100GRAMS) FOR Au-Cu ALLOYS(°C)

TEMP	1100	1150	1200	1250	1300	1350
0%PD	0.09	---	0.42	---	0.97	---
	0.11	---	0.37	---	1.07	---
2%PD	---	0.65	1.05	1.40	1.58	---
	---	0.78	1.10	1.40	1.72	---
4%PD	0.70	---	1.35	---	2.00	---
	0.78	---	1.42	---	2.10	---
6%PD	---	0.72	---	2.70	---	3.22
	---	0.82	---	2.85	---	3.42
8%PD	---	1.82	---	3.82	---	6.8
	---	---	---	3.88	---	7.13
10%PD	---	1.88	---	---	5.88	8.81
	---	1.95	---	---	6.05	10.12

TABLE 2: SOLUBILITY OF HYDROGEN ($cc H_2$/100GRAMS) FOR Au-Pd ALLOYS(°C)

ALLOY	SOLUBILITY ($cm^3 H_2$/100 grams)	SOLUBILITY (wt.pct)	ΔH° (Kcal/mole)
Au-0 %Cu	Log S=(5.38±0.95)-(8592±453)/T	Log(%H)=(1.33±0.95)-(8592±453)/T	39.3±6.6
Au-4 %Cu	Log S=(2.84±0.04)-(4540±50)/T	Log(%H)=(-1.21±0.04)-(4540±50)/T	20.79±0.23
Au-8 %Cu	Log S=(1.7±0.01)-(2774±3)/T	Log(%H=(-2.35±0.01)-(2774±3)/T	12.70±0.01
Au-10%Cu	Log S=(0.4±0.18)-(1420±80)/T	Log(%H)=(-3.65±0.18)-(1420±80)/T	6.50±0.37
Au-12%Cu	Log S=(1.62±0.19)-(3200±270)/T	Log(%H)=(-2.43±0.19)-(3200±270)/T	14.65±1.24
Au-13%Cu	Log S=(0.78±0.15)-(1270±200)/T	Log(%H)=(-3.27±0.15)-(1270±200)/T	5.81±0.91
Au-15%Cu	Log S=(1.65±0.06)-(2246±81)/T	Log(%H)=(-2.40±0.06)-(2246±81)/T	10.28±0.37
Au-20%Cu	Log S=(1.06±0.04)-(1170±15)/T	Log(%H)=(-2.99±0.04)-(1170±15)/T	5.36±0.07
Au-40%Cu	Log S=(0.73±0.01)-(610±8)/T	Log(%H)=(-3.32±0.01)-(610±8)/T	2.79±0.04
Au-0 %Pd	Log S=(6.98±0.01)-(10940±23)/T	Log(%H)=(2.93±0.01)-(10940±23)/T	50.1±0.1
Au-2 %Pd	Log S=(3.71±0.02)-(5439±27)/T	Log(%H)=(-0.35±0.02)-(5439±27)/T	24.9±0.1
Au-4 %Pd	Log S=(2.82±0.01)-(3946±2.7)/T	Log(%H)=(-1.23±0.01)-(3946±2.7)/T	18.1±0.1
Au-6 %Pd	Log S=(1.71±0.01)-(1924±4.2)/T	Log(%H)=(-2.34±0.01)-(1924±4.2)/T	8.8±0.02
Au-8 %Pd	Log S=(4.78±0.01)-(6389±1.8)/T	Log(%H)=(0.73±0.01)-(6389±1.8)/T	29.25±0.01
Au-10%Pd	Log S=(7.25±0.02)-(10187±29)/T	Log(%H)=(3.2±0.02)-(10187±29)/T	46.6±0.1

TABLE 3: HYDROGEN SOLUBILITY EQUATION AND STANDARD HEAT OF SOLUTION FOR AU-CU AND AU-PD ALLOYS.

TEMP(°C)	1100	1200	1300	
Au-Cu	-0.14	-0.07	-0.02	$e_H^{Cu} = -0,96+5,9.10^{-4}.T$
Au-Pd	-0.34	-0.21	-0.09	$e_H^{Pd} = -2,05+1,25.10^{-3}.T$

TABLE 4: INTERACTION PARAMETER AND TEMPERATURE DEPENDENCY FOR CU AND PD. ON GOLD

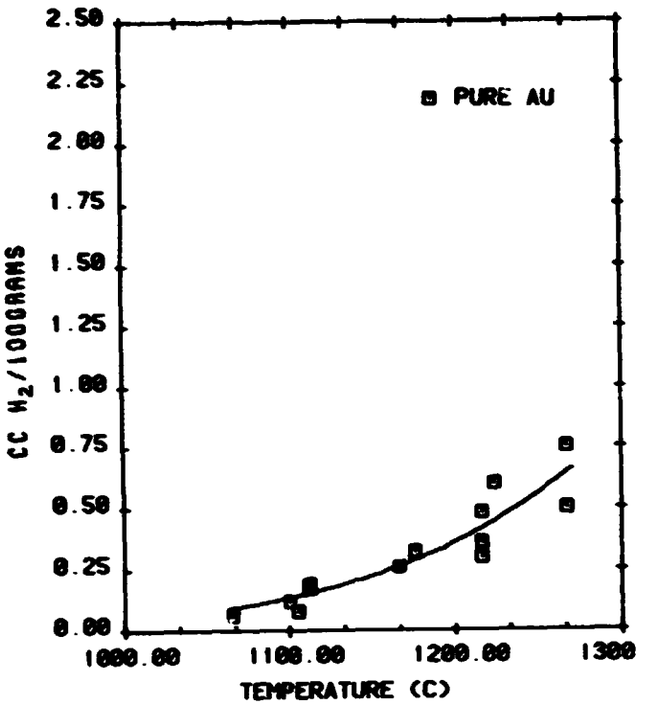

FIG.2: HYDROGEN SOLUBILITY IN PURE GOLD

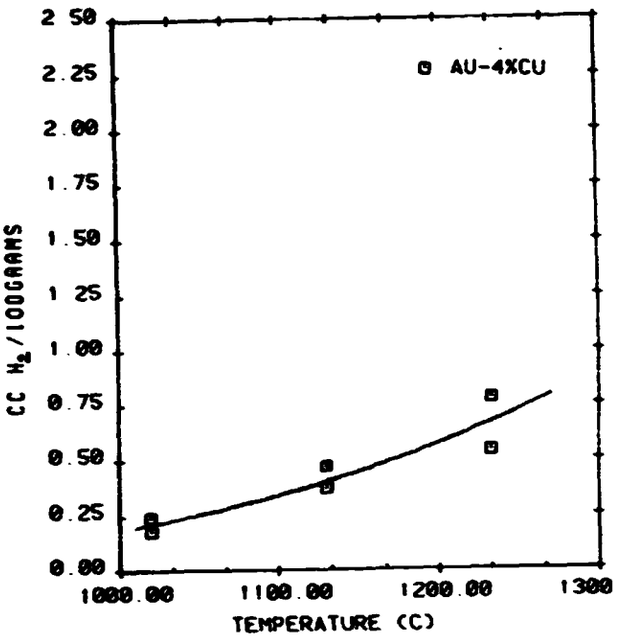

FIG.3: HYDROGEN SOLUBILITY IN Au-4%Cu

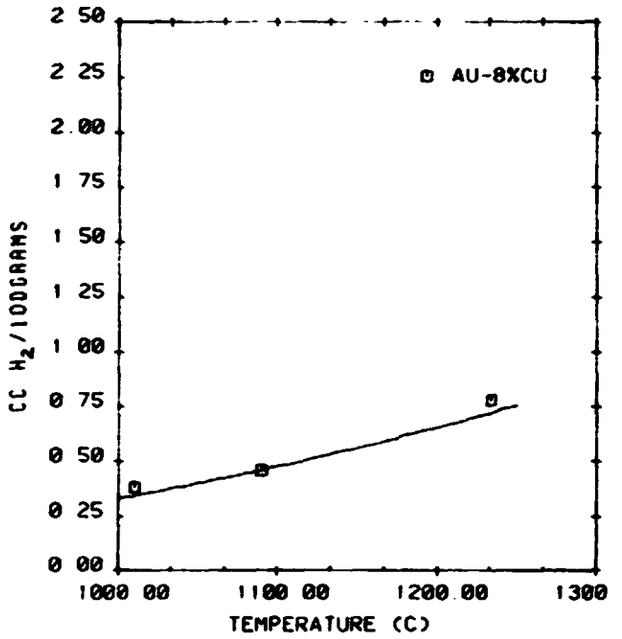

FIG.4: HYDROGEN SOLUBILITY IN Au-8%Cu

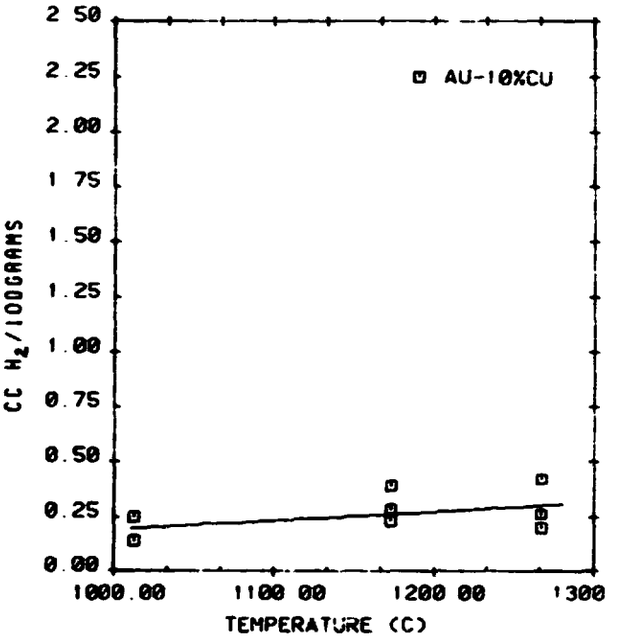

FIG.5: HYDROGEN SOLUBILITY IN Au-10%Cu

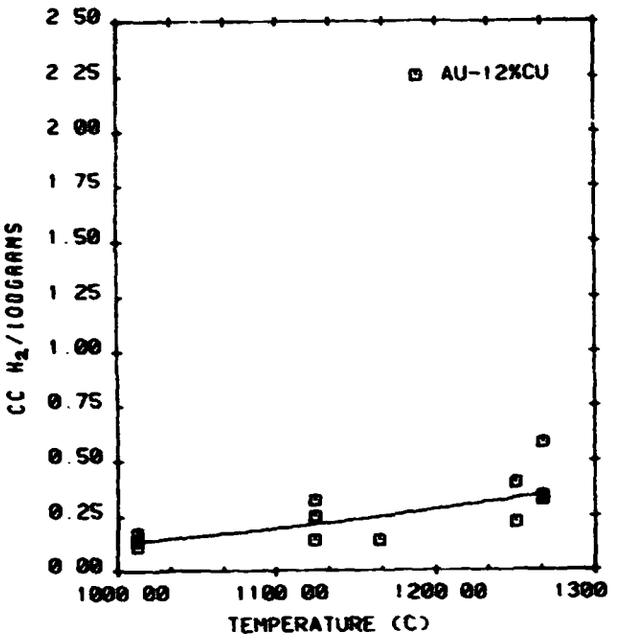

FIG.6: HYDROGEN SOLUBILITY IN Au-12%Cu

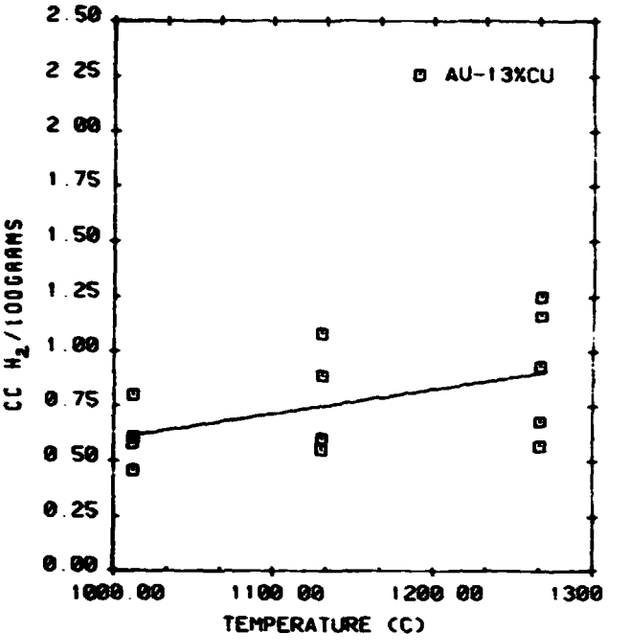

FIG.7: HYDROGEN SOLUBILITY IN Au-13%Cu

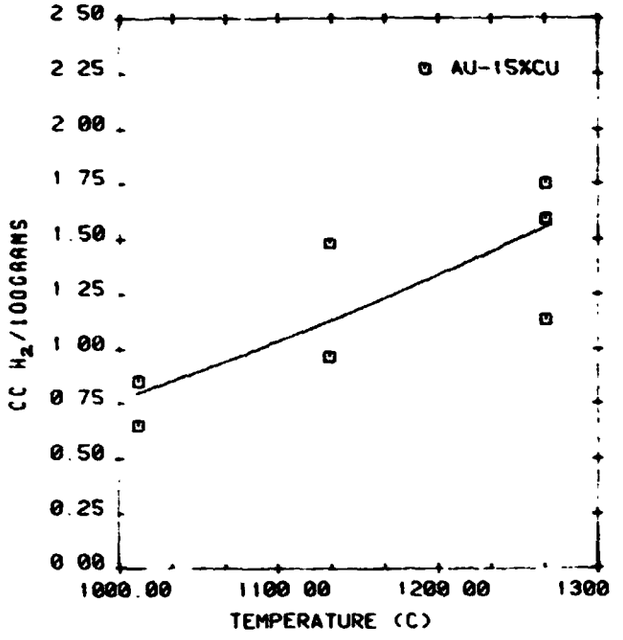

FIG.8: HYDROGEN SOLUBILITY IN Au-15%Cu

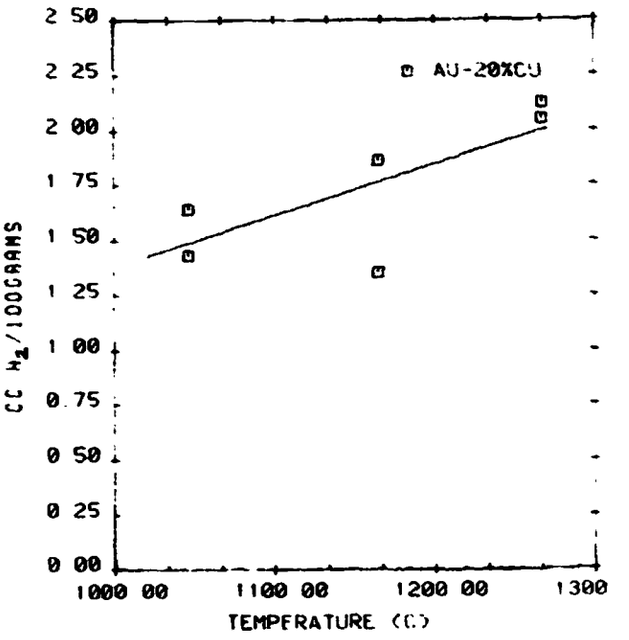

FIG.9: HYDROGEN SOLUBILITY IN Au-20%Cu

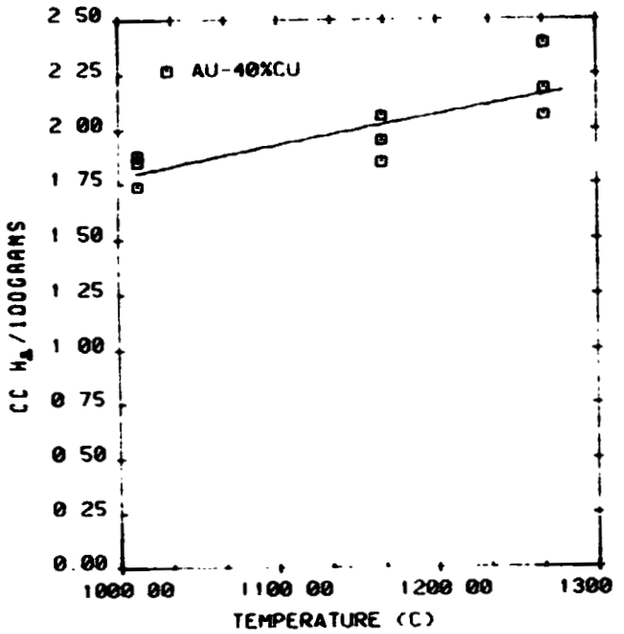

FIG.10: HYDROGEN SOLUBILITY IN AU-40%CU

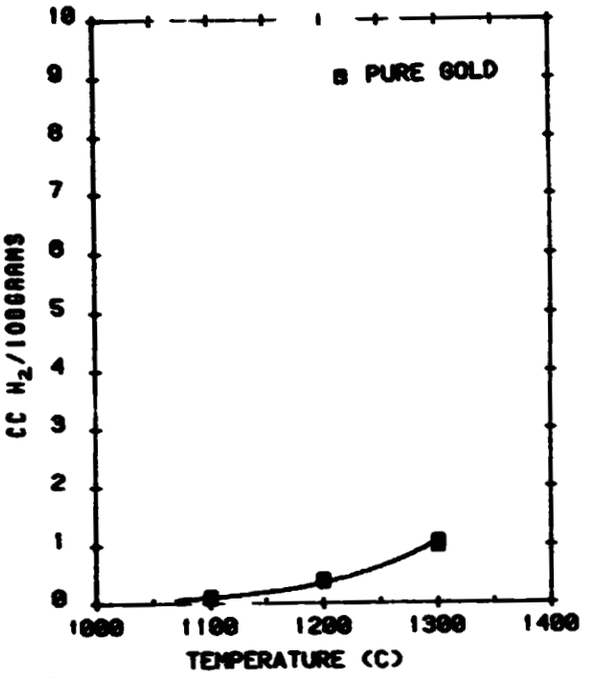

FIG.11: HYDROGEN SOLUBILITY IN PURE GOLD

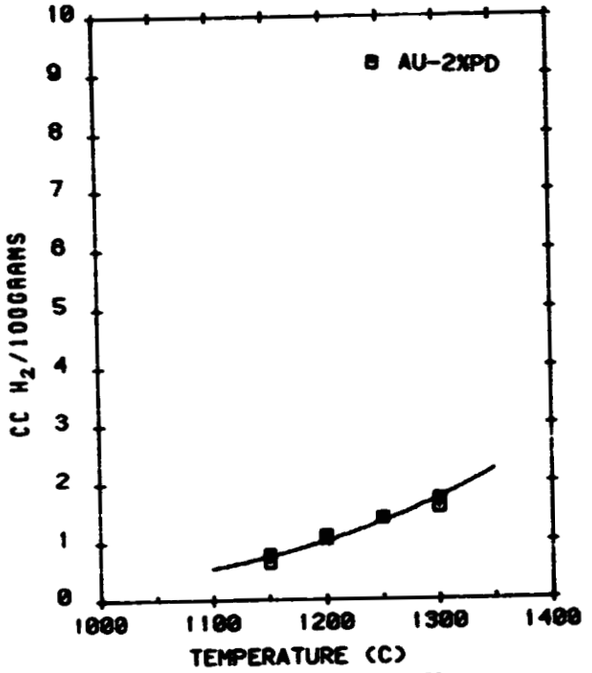

FIG.12: HYDROGEN SOLUBILITY IN AU-2%PD

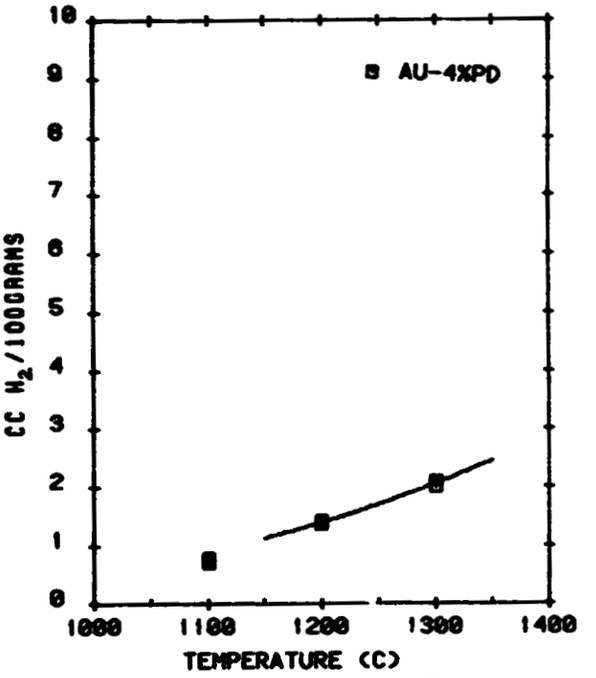

FIG.13: HYDROGEN SOLUBILITY IN AU-4%PD

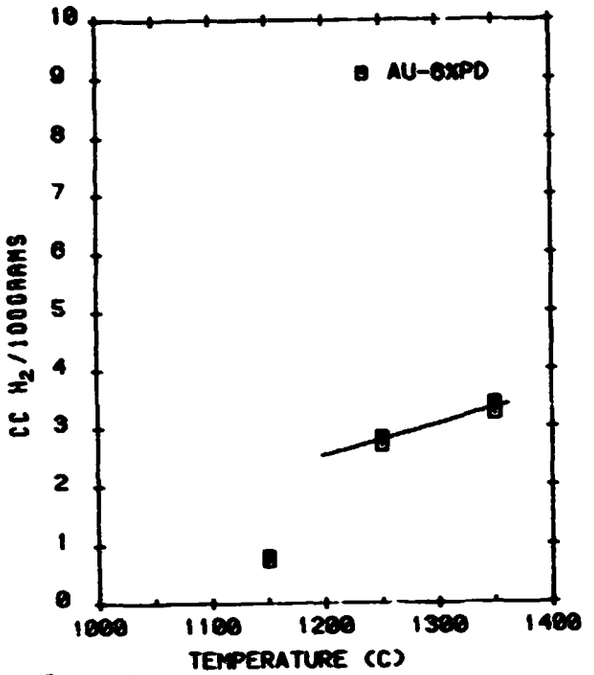

FIG.14: HYDROGEN SOLUBILITY IN Au-6Pd

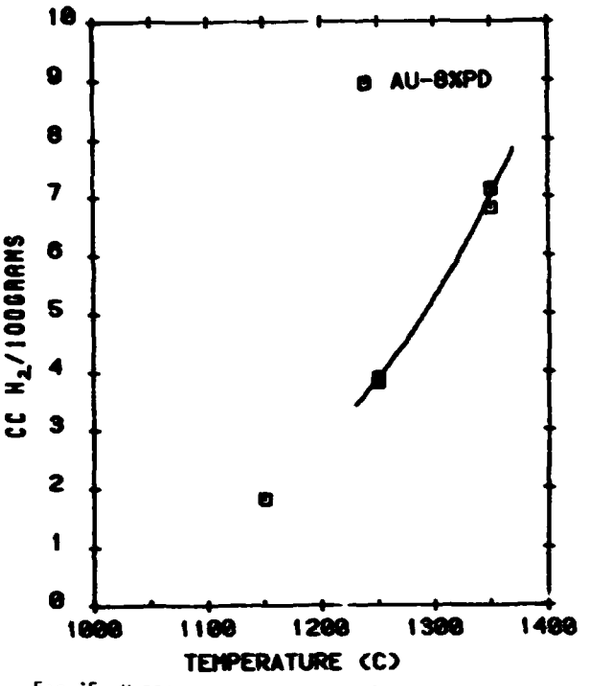

FIG.15: HYDROGEN SOLUBILITY IN Au-8Pd

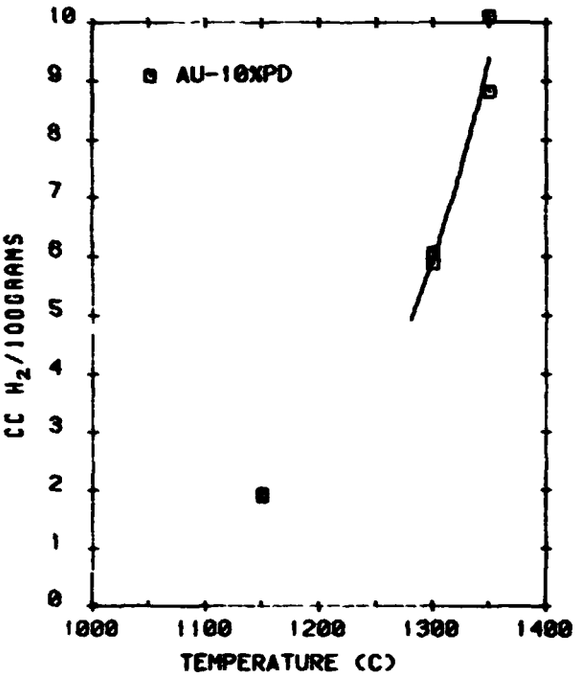

FIG.16: HYDROGEN SOLUBILITY IN Au-10Pd

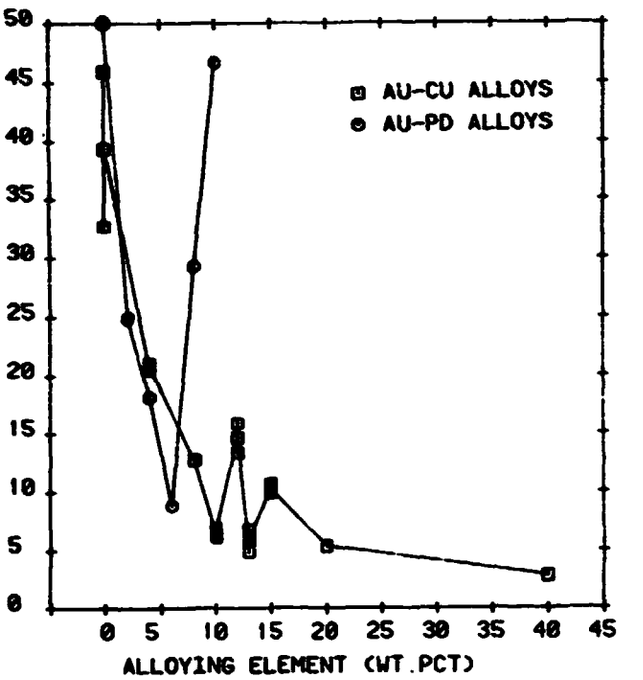

FIG.17: VARIATION OF STANDARD HEAT OF SOLUTION FOR HYDROGEN IN Au-Cu AND Au-Pd ALLOYS.

PAPER III

H. SHAHANI, R. JÖNSSON, S. WALLIN

ON THE DESIGN OF HIGH PRESSURE CASTING EQUIPMENT AND RAPID HEATING FURNACES USED IN METALLIC FOAM EXPERIMENTS

SEPTEMBER 1983

ON THE DESIGN OF HIGH PRESSURE CASTING EQUIPMENT AND RAPID HEATING FURNACES USED IN METALLIC FOAM EXPERIMENTS

Hamid Shahani

Dept. of Casting of Metals
The Royal Inst. of Technology
S-100 44 Stockholm
Sweden

Rolf Jönsson, Sven Wallin

Swedish Space Corporation
Tritonvägen 27
S-171 54 Solna
Sweden

September 1983

1. ABSTRACT

The design of high pressure casting and rapid heating furnaces are discussed. These furnaces were used for studying the nucleation and growth of pores and also to study the possibility of producing metallic foams in reduced gravity.

2. INTRODUCTION

Particle composites are difficult to produce from melts. Due to variation in the density of two phases, they either float or sediment during the production process. Thus, it leads to uneven distribution of the particles in the matrix. In order to avoid segregation of the particles, it has been proposed to use a micro-gravity environment. One of the most difficult composite to produce from melts is metallic foam, i.e metals containing numerous small gaseous pores.

In order to investigate the nucleation and growth of pores and also to produce metallic foams directly from melts, aluminium base alloys were supersaturated with respect to hydrogen on earth and remelted in reduced gravity and under reduced pressure.

Reduced gravity was achieved by two methods. In the first, a material science module was flown within the framework of the Swedish sounding rocket program, PIRAT (Pointed Infra-Red Astronomical Telescope). The payload was launched on the 30th of September 1981 using a Nike-Black Brant V C rocket. A peak altitude of 270 Km was attained. The duration of the micro-g flight was 410 seconds giving average acceleration levels of $0.3\text{-}2\times10^{-3}$ g. Reduced gravity in the second case was achieved on board a Lockheed F104 aircraft, flown in a parabolic trajectory. Reduced acceleration levels of 0.03-0.1 G were achieved for about 50-60 seconds.

To accomodate the constraints imposed by the flight conditions remelting furnaces were specially designed to overcome the limitations of weight, power supply and duration of the experiment.

3. THE HIGH PRESSURE CASTING FURNACE

Hydrogen solubility in melts is a function of the melt properties, temperature and hydrogen pressure. By rapid cooling, dissolved hydrogen can be arrested within the small pores in the sample. To produce samples with the required hydrogen supersaturation, a furnace was required wherein high pressure could be regulated and where facility existed for rapid quenching.

The electro magnetic levitation technique was chosen. With such a technique, the samples could be reacted with the gas at high temperature while desired pressure could be applied and due to good stirring, required time for dissolving hydrogen in the sample could be minimized. By turning the furnace off, sample could be ejected into a water-cooled copper mould and thus be quenched.

Gas treated samples had to be at least about 10 grams with diameter of 18 mm and height of 15 mm before machining. These limitations were imposed by the flight conditions. Figure 1 shows a schematic drawing of the levitation equipment built for this purpose using a 15 kHz induction furnace. It consists of a quartz tube with the inner diameter 46 mm, the wall thickness 2.5 mm and the height 400mm. A copper tube with five turns (Ø=6mm) functioned as the induction coil.

The lower section of the furnace housed a graphite crucible and a water-cooled copper mould. The quartz tube was sealed at the top and the sample was inserted from the bottom with the help of a pneumatic device. The water-cooled copper mould was soldered to the bottom section. A stomatite cylinder was used as heat and electric insulator and was inserted between the crucible and the mould. A graphite table was placed in the crucible just above the outlet. The table supported the melt in the center of the induction-field where the lifting force was at its minimum.

The wall thickness of the crucible was critical. Thick walls reduce the levitation force and thin walls lift the sample out of the induction field. The thickness in the present work was about 3 mm, which was found optimal in this application. The position of the table was also crucial. It was imperative that it should be placed exactly where the induction field balanced the gravity field. This, in turn, was influenced by the mass and the alloy composition. The latter, was due to change of the electrical resistance of the sample and the related effect on the eddy currents.

3.1 EXPERIMENTAL PROCEDURE

The candidate alloys, Al, Al-4%Ti and Al-10%Fe were cast into a water cooled copper mould with the diameter 18 mm and the height 20 mm. They were subsequently machined to a height of 15 mm and washed with aceton.

Clean specimens were placed on the graphite table inside the crucible. The reaction chamber was then closed, evacuated and refilled with hydrogen to a predetermined pressure. The pressure of hydrogen was varied between 0.5 to 5 atm. With this technique, different quantities of hydrogen could be dissolved within the sample. Once the sample had melted the process was continued for further six minutes before the furnace was switched off. The melt was ejected through the channel under the table and via the outlet hole into the copper mould beneath the crucible. To enhance the formation of smaller pores, the ambient pressure during quenching, was increased to 6 atm by addition of argon. The melt temperature was measured by a pyrometer and was about 1000°C for all the runs. The total solidification time in the mould was between 5-7 seconds dependent on the alloys. After casting the samples were stored in liquid nitrogen except during machining to proper dimensions. The steuctur of the pores fomed in this work are discussed in reference 1.

4. THE RAPID HEATING FURNACES

The power package in the material science module was built of 28 silver-zinc cells of 5 Ah capacity which gave a nominal voltage 36 V at a current load of 11 amp. This allowed about 400 W capacity for each furnace during the heating sequence. For the heating elements under the existing conditions, a novel solution was resorted to. A filament was extracted from a halogen projector lamp, Philips 7787,36V,400W. This element had the appropriate dimension and the power capacity to meet the required heating rate. To prevent rapid vaporization and prolong the life of the filament, argon or helium atmosphere was employed. The applied voltage was also restricted to 30 volts. The life time of the filaments was now well above the duration of the experiment. The current through the filament was about 10 amperes at 30 volts giving a power output of about 300 W. To prevent short circuiting of the filament by the melted sample a thin boron nitride cap was inserted between the sample and filament. Boron nitride is an electrical insulator with good thermal propertie. The samples should be melted within 15 seconds. Equation 1 depicts the appropriate mass that could be melted within the limited time and power for pure aluminium;

$$m\cdot(C_p^s \Delta T^s + L_m^{\ell} + C_p^{\ell} \Delta T^{\ell}) = P\cdot t \qquad (1)$$

m	mass of the sample (gram)
ΔT^s	change of temperature in the solid phase, 640 (c)
ΔT^{ℓ}	melt over heat, 50 (C)
C_p^s ,C_p^{ℓ}	the specific heat of solid and liquid aluminium 0.215 and 0.26 (cal/g/K)
L_m	heat of fusion of aluminium 95 (cal/g)
t	total heating and melting time, 15 sec
P	power delivered to the sample, 240 (W) (calculated with 80% efficiency)

m=3-4 grams , volume =2.5-3 cm

The shape and dimension of the samples were based on the design of the filament and allowed mass as calculated above. Figure 2 shows the furnace assembly consisting of the filament, the boron nitride cap and the sample. The furnace and sample were assembled by attaching the sample directly to the mounting plate by a screw, figure 3. The boron nitride cap was then placed in the cavity of the sample and the heating filament was subsequently lowered into the cap. Each furnace had a height of 50 mm and diameter of 60 mm. The temperature was monitored by chromel-alumel thermocouple inserted into the sample through a drilled hole, figures 2,4. Three of these furnaces were incorporated in a cannister shown in the figure 4. System pressure was monitored by an IC pressure transducer mounted on a PC-board at the bottom of the cannister. Four cannister were incorporated in the module for the eventual flight.

4.1 ACTIVATION OF THE FURNACES

Acceleration during the flight was monitored by accelerometers (G-sensors). When entering into the low g level part of the flight, the G-sensors started the control electronics for the furnaces in the cannisters. When the first sample had reached a predetermined temperature, the power was switched off after a programmed delay (3-6 seconds) and the next furnace was then switched on. This procedure was repeated for all the furnaces. Depending on the gas and pressure used in the cannister it took 20-40 seconds for the samples to solidify.

4. EQUIPMENT FOR VIDEO OBSERVATION

The experiments were repeated on board a Lockheed aircraft with similar equipment. The processes were monitored by a motor driven camera. Illumination of the samples was provided by six incandescent lamps (24v, 10W). The melting,

expansion and solidification of the samples were photographed at a rate of three frames per seconds. The equipment is shown in figure 5. Totally nine flights were performed and 27 samples were processed. The results of this investigation are presented in reference 2.

5. ACKNOWLEDGEMENT

We would like to thank Prof. Hasse Fredriksson for his valuable advises in developing the equipments. This project was financed by the Swedish Board for Space Activities.

6. REFERENCES

1- H. Shahani, H. Fredriksson, On the Mechanism of Precipitation of Pores in Melts, this thesis.

2- H. Shahani, H Fredriksson, Proceeding of the 4th European Symposium on Material Science under Microgravity, (ESA SP-191-June 1983), p.71-78

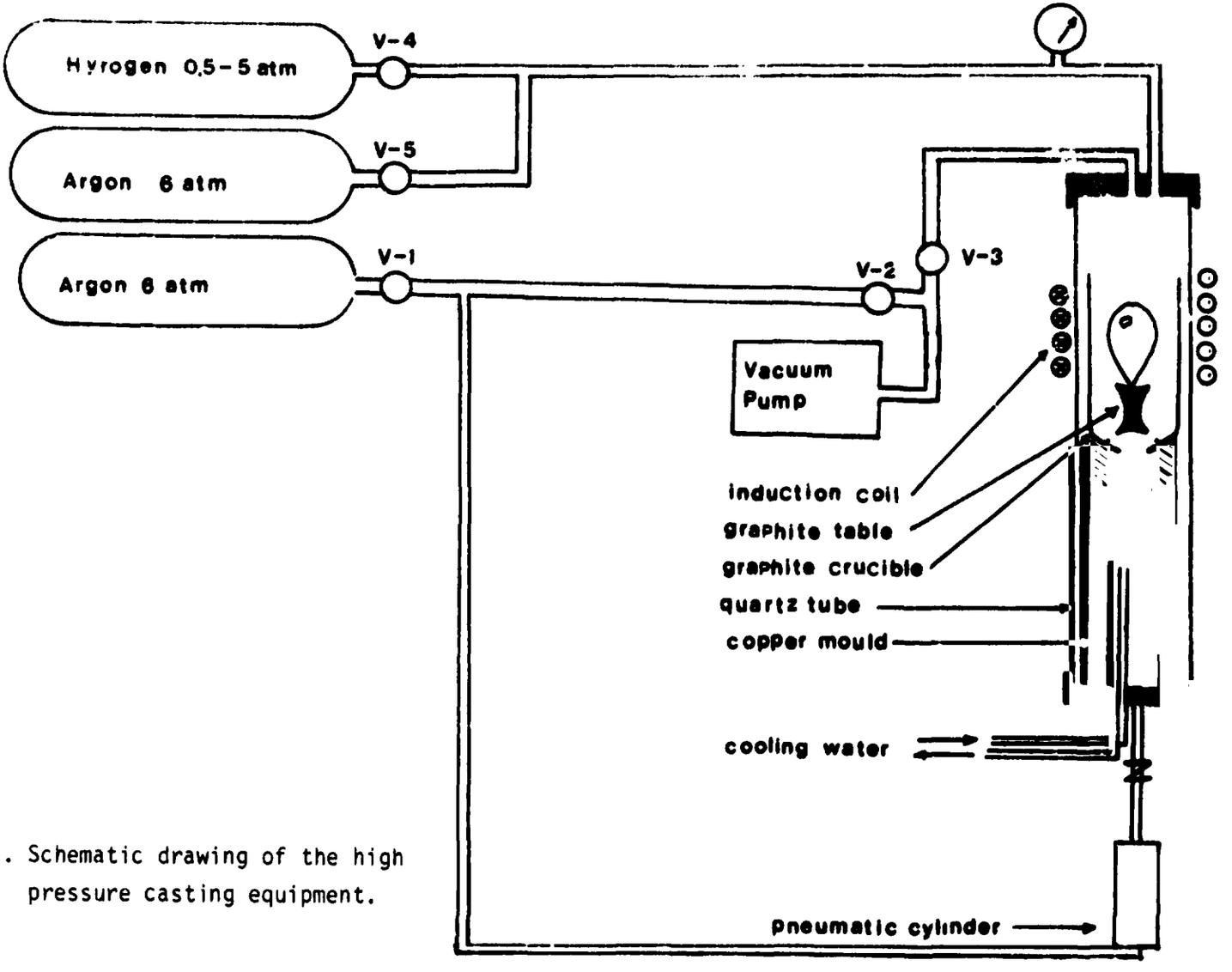

Figure 1. Schematic drawing of the high pressure casting equipment.

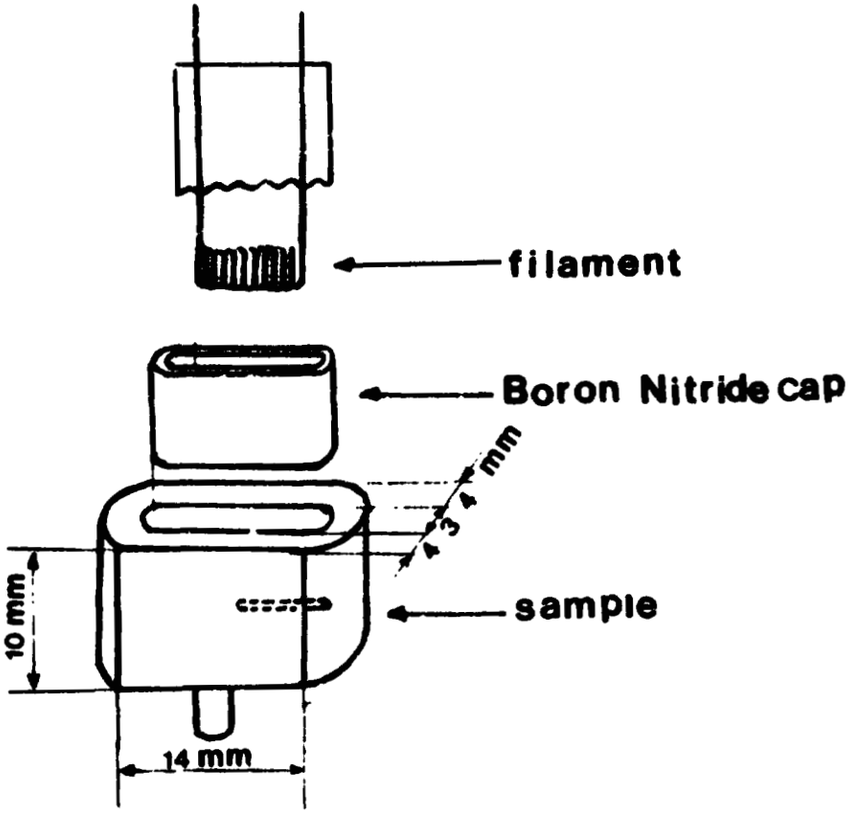

Figure 2. Schematic drawing of the sample, cap and filament.

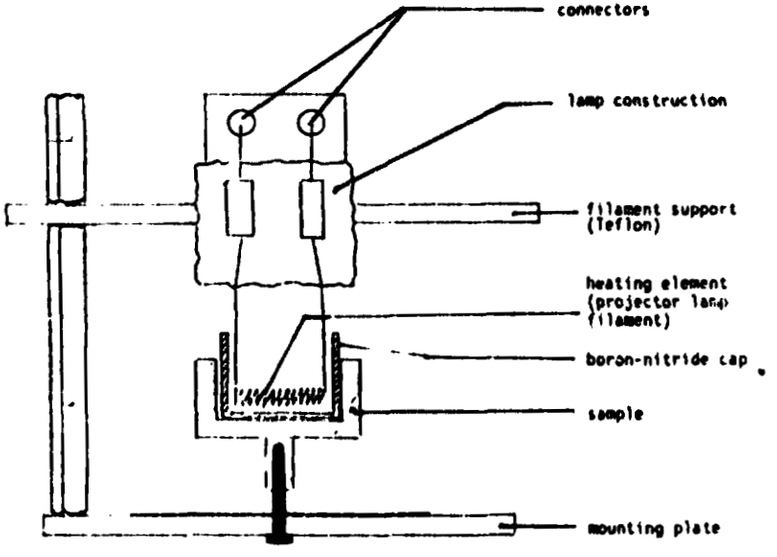

Figure 3. Rapid heating furnance assembly.

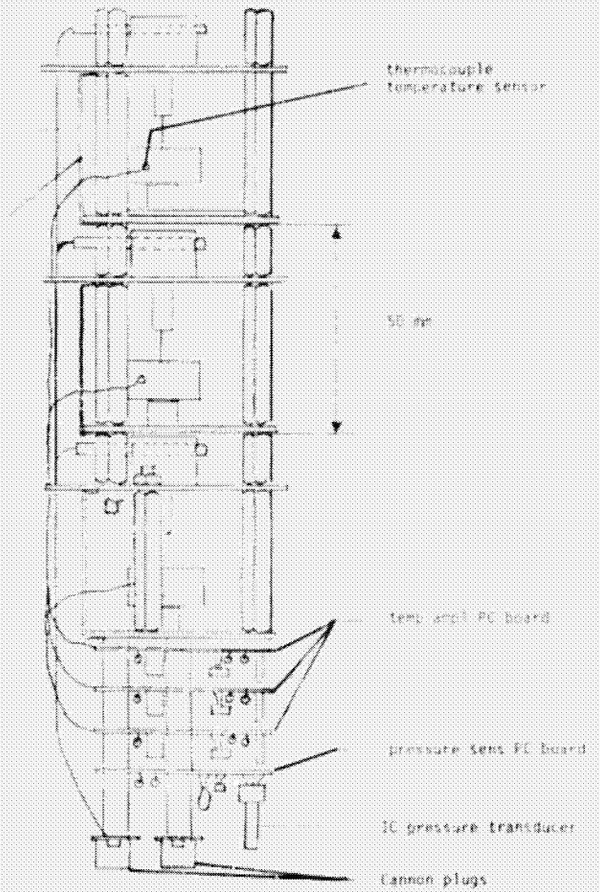

Figure 4. Complete assembly of furnances and electronics.

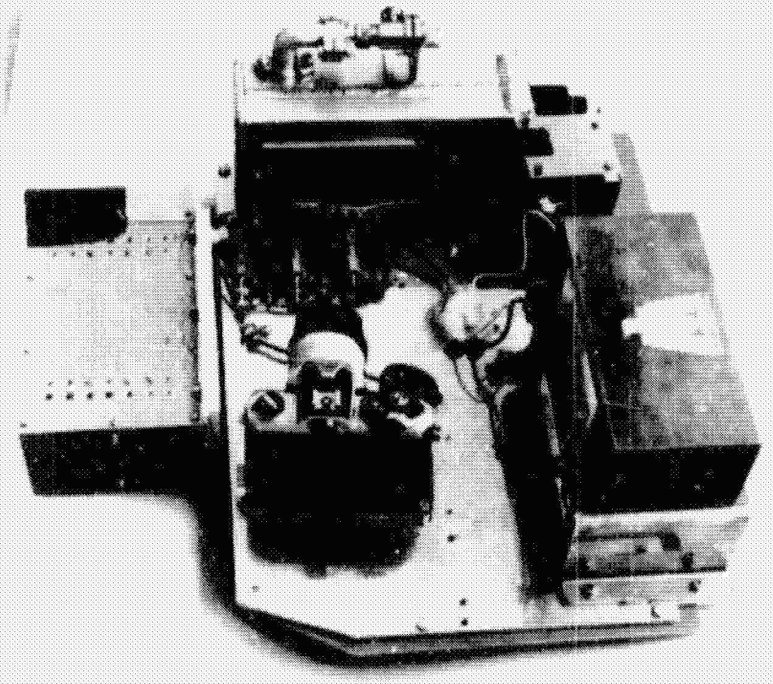

Figure 5. Cannister with remelting equipments and camera unit used in the aircraft experiments.

PAPER IV

H. SHAHANI, H. FREDRIKSSON

ON THE MECHANISM OF PRECIPITATION OF PORES IN MELTS

JANUARY 1984

ON THE MECHANISM OF PRECIPITATION OF PORES IN MELTS

Hamid Shahani Hasse Fredriksson

Dept. of Casting of Metals
The Royal Institute of Technology
S-10044 Stockholm
Sweden
January 1984

1. ABSTRACT

Precipitation of rounded pores in aluminium, Al-4%Ti and Al-10%Fe has been studied. Samples were equilibrated with hydrogen at 1000^{o}C and subsequently quenched at an ambient pressure of 6 atm. During quenching, due to increasing hydrogen pressure in the melt, pores were formed. A model for nucleation and growth of these pores in pure metals has been presented. In accordance to this model, existence of foreign particles in the melt is necessary for pore formation and pore size increases with the initial hydrogen content. The measured size of the pores in pure aluminium are in a good agreement with computed values.

2. INTRODUCTION

Pores are usually formed in cast metals during cooling and solidification processe. In general, the various types of pores can be related to the gas content of the melt prior to casting and they can be classified into three groups:

A) Rounded Pores;

When the gas content of a melt is greater than its gas solubility these pores may precipitate in the melt. They are mostly spherical and due to the buoyancy forces, usually located in the upper section of castings.

B) Elongated Pores;

When the initial gas content is below the gas solubility of the melt, at the ambient pressure and solidification temperature, this type of pores nucleate at the solidification front and grow in an eutectic-like reaction (1-4).

C) Shrinkage Pores;

They form in parts of the melt that solidify last and are often termed as shrinkage pores. They are formed due to the pressure drop caused by the solidification shrinkage and their shape is influenced by the dendrite structure (4-7).

In the present investigation, formation of rounded pores has been studied. Aluminium alloys were equilibrated at 1000 °C with hydrogen at various pressures. After equilibration, the specimens were quenched at an ambient pressure of 6 atm. This treatment enhances formation of smaller pores (8-16). These pores were metallographically examined and in the case of pure aluminium, theoretically analysed.

In a follow up investigation (17), samples produced by the above method were remelted at the reduced ambient pressures and reduced gravity. This treatment enabled the pores to expand and resulted in a metallic foam. Reduced gravity was achieved by either using a sounding rocket or an

aircraft flying in a parabolic trajectory.

3. EXPERIMENTAL WORK

Samples of pure Al, Al-4%Ti and Al-10%Fe, weighing about 12 grams each, were electromagnetically levitated at 1000 ^{o}C for about 6 minutes in a hydrogen atmosphere. The levitation equipment is shown in figure 1 and is described in detail in references (17,18). The investigation was carried under hydrogen pressures of 0.5, 1, 3 and 5 atm. At the termination of each run, the furnace was switched off and the sample was quenched in a water-cooled copper mould located beneath the crucible. The mould diameter and height were 18 and 20 mm respectively. During the quenching step, the ambient pressure in the reaction chamber was increased to 6 atm by applying argon. Cooling rate of the melts during quenching was about 50-70 ^{o}K/sec.

4. EXPERIMENTAL RESULTS

The density of the samples was measured by immersing them in the water. The total volume of the pores, V_p, was then computed by equation 1:

$$\%V_p=(1-\frac{\rho}{\rho_o})x100 \qquad (1)$$

where ρ_o and ρ are densities of the sample in the pore-free state and the treated state respectively. Samples were subsequently sectioned into two halves along the vertical axis and prepared for metallographic investigations. The area fraction of porosity, the average and also the largest size of the pores for each case were measured using a False Color TV Analyser. The average number of the pores was calculated from the measured pore size and total volume of porosity. Examination of the samples indicated that pore size distribution in the castings were not uniform. Small pores (20-50um) tended to concentrate at the periphery, while larger pores tended to accumulate along the center.

Figures 2a-c, show micro-graphs taken from the central area of samples treated at 5 atm hydrogen. In the case of pure aluminium pores were mostly spherical while in Al-4%Ti and Al-10%Fe alloys they were irregular and influenced in shape by primary Ti(β) and Fe(θ), figures 3a-c. A trace of aluminiumoxide could be detected at the periphery of the pores, figure 3a.

Hydrogen content of the samples was between 1 to 4 ppm. The measurements, as presented in table I, indicate that the hydrogen content, as well as porosity and size of the pores increased with the pressure of hydrogen during gas treatment. These values were higher for the investigated alloys than the respective ones in pure aluminium.

5. THEORETICAL ANALYSIS

Hydrogen dissolves in melts as atoms (19);

$$H_2(g) \longrightarrow 2\underline{H} \qquad (2)$$

Chemical potential of hydrogen in the gas phase and in the melt at the equilibrium must be equal. The effect of external pressure on the system (20) can be considered as:

$$2(\mu^o_H + RT \ln X_H - \bar{V}_H(P_t - P_o)) = \mu^o_{H_2} + RT \ln(P_{H_2}/P_o) \qquad (3)$$

where:

- $\mu^o_{H_2}$ = standard chemical potential of hydrogen in the gas phase (J/mole)
- μ^o_H = standard chemical potential of hydrogen in the melt (J/mole)
- X_H = hydrogen concentration in the melt (mole fraction)
- P_o = standard pressure of hydrogen (1E5 N/m^2=1 atm)
- P_{H_2} = equilibrium pressure of hydrogen during gas treatment (N/m^2)
- P_t = total pressure in the system, equal to P_{H_2} during gas treatment at 1000 C (N/m^2)

$\bar{V}_H$ = partial molar volume of hydrogen in the melt (m^3/mole)

T = melt temperature (K)

R = gas constant, 8.314 (J/mole/K)

This gives:

$$X_H=(P_{H_2}/P_o)^{\frac{1}{2}} \exp((\mu^o_{H_2}-2\mu^o_H)/2RT) \exp(\bar{V}_H(P_t-P_o)/RT) \quad (4)$$

Equation 4 can be rewritten as:

$$X_H=(P_{H_2}/P_o)^{\frac{1}{2}}A \exp(-B/T) \exp(\bar{V}_H(P_t-P_o)/RT) \quad (5)$$

Equation 5, reflects the solubility of hydrogen in the melt as a function of pressure and temperature. The partial molar volume of hydrogen in aluminium, $\bar{V}_H$, is not determined. In the present analysis, it is assumed that $\bar{V}_H$ and its variation with the temperature is the same as the molar volume of aluminium, V_m^{Al}. This is because the solubility of hydrogen in the aluminium melt , max. 2×10^{-4} mole fraction is very small. Equation 5 then becomes;

$$X_H=(P_{H_2}/P_o)^{\frac{1}{2}}A \exp(-B/T) \exp(V_m^{Al}(P_t-P_o)/RT) \quad (6)$$

The molar volume of aluminium, used in equation 6, as a function of temperature (21) is calculated by:

$$\rho_{Al} = 2646.2-0.28T \qquad (Kg/m^3) \qquad (7)$$

$$V_m^{Al} = 27\times10^{-3}/\rho_{Al} \qquad (m^3/mole) \qquad (8)$$

The constants A and B in equation 6, can be determined experimentally. Their values, for the case of hydrogen solubility in pure liquid aluminium (22,23) are equal to 1.42×10^{-2} (mole fraction) and 6178 (K) respectively. For Al-4%Ti and Al-10%Fe, A and B have also been determined (23). The dissolved hydrogen content in pure aluminium, table I, were 1.5 to 3 times less compared with the calculated values.

Hydrogen equilibrium pressure in the melt, P_{H_2}, during quenching as a function of melt temperature can be calculated with equation 6. The total pressure in the system P_t, is equal to the pressure of argon during quenching. Equation 6 may be rewritten as:

$$P_{H_2} = \frac{P_o X_H^2 \exp(\frac{2B}{T})}{A^2 \exp(\frac{2V_m^{AT}(p_t-p_o)}{RT})} \qquad (9)$$

Eqilibrium pressure of hydrogen in the pure aluminium melt, as a function of temperature is plotted in Fig.4. This pressure, at its solidification temperature, varies between 10 to 25 atm, depending on the initial gas content.

The pressure balance for a bubble in mechanical equilibrium with a liquid phase gives the required pressure of hydrogen in the melt for homogeneous nucleation;

$$r_b = \frac{2Y}{P_b-P_a} \qquad (10)$$

where:

r = radius of the bubble (m)
Y = surface tension between liquid and gas (N/m)
P_b= pressure inside the bubble (N/m^2)
P_a= ambient pressure (N/m^2)

The work expended for the formation of a bubble of size r_b,(24) is described by:

$$W=4\pi r_b^2 Y-4\pi r_b^3(P_b-P_a)/3 \qquad (J) \qquad (11)$$

Substituting equation 10 into equation 11 gives;

$$W=16\pi Y^3/3/(P_b-P_a)^2 \qquad (J) \qquad (12)$$

Mechanical and chemical equilibrium co-exist at the nucleation of a bubble. Accordingly P_b, becomes equal to P_{H_2}. Equation 12 can be thus rewritten as:

$$W^* = 16\pi\gamma^3/3/(P_{H_2} - P_a)^2 \qquad (J) \qquad (13)$$

Where W* is the activation energy for nucleation (24) equal to 60kT; k, is the Boltzman's constant. P_{H_2}, as a function of melt temperature for different values of surface tension is calculated then, figure 5. For aluminium with surface tension (25) of 0.914(N/m), homogeneous nucleation occures at hydrogen pressures of about 40000 atm, see Fig. 5. For pore nucleation to take place at hydrogen pressures of 10 to 25 atm, the surface tension must be below 0.01 (N/m). It is therefore concluded that all the "rounded pores", observed in the present investigation must have been formed by heterogeneous nucleation.

In a melt, there usually are particles; such as oxides, which can cause heterogenous nucleation of the pores. The mechanism of this nucleation is normally treated by considering the gap formed on a flat substrate, which is shown in figure 6. In a spherical substrate, the size of particles as well as the difference in surface tensions influence the spread of the gas around the particle. In order to simplify the problem, we have assumed that $\gamma^{L/P}/\gamma^{L/g} = n$, where $\gamma^{L/P}$ and $\gamma^{L/g}$ are surface tension of liquid-particle and liquid-gas, respectively. If n is greater than 1, (26) the bubble will spread around the particle and the condition described by figure 7 will be obtained. Activation energy for the pore nucleation can now be written as;

$$W^* = 4\pi(r_b^{*2} - nr_p^2)\gamma^{L/g} - \frac{4}{3}\pi(r_b^{*3} - r_p^3)(P_{H_2} - P_a) \qquad (14)$$

where:

r_b^* = critical bubble radius (m)
r_p = particle radius (m)
$n = \gamma^{L/P}/\gamma^{L/g}$

Substituting r_b^* and W*=60kT into equation 14 yields

$$W^* = \frac{16\pi(\gamma^{L/g})^3}{3(P_{H_2} - P_a)^2} - 4\pi nr_p^2\,\gamma^{L/g} + \frac{4\pi r_p^3}{3}(P_{H_2} - P_a) \qquad (15)$$

From this the pressure of hydrogen, P_{H_2}, required for heterogeneous nucleation as function of the particle size, r_p can be calculated at Pa=6 atm , figure 8. With the presence of the particle sizes larger than 2 μm in the melt, the required hydrogen pressure for the nucleation reduces to about 10 atm. With this pressure the critical melt temperature for nucleation, T*, is determined depending on the initial hydrogen content, its values ranging between 680-750 ^{o}C. The critical size of the pores is then evaluated to 12 μm at P_{H_2}=10 atm.

With progressive cooling, the nucleated bubble grows by diffusion of hydrogen from the surrounding supersaturated liquid. The growth process, using Fick's first law, is described by;

$$\frac{dn_H}{dt} = \frac{8\pi}{3RT}(3P_a r_b^2 + 4Yr_b)\frac{dr}{dt} = \frac{4\pi r_b^2 D_H}{V_m^{Al}} \cdot \frac{X_H^o - X_H^P}{r_b} \qquad (16)$$

where X_H^o and X_H^P are concentrations of hydrogen in bulk liquid and at the liquid-bubble interface, respectively. The former, X_H^o, is the measured hydrogen content, and the latter X_H^P obtained from equation 6. When r >12 μm, $P_b \cong P_a$, and equation 6 becomes;

$$X_H^P = \left(\frac{P_a}{P_o}\right)^{1/2} A \exp\left(\frac{-B}{T}\right) \exp\left(\frac{V_m^{Al}(P_a - P_o)}{RT}\right) \qquad (17)$$

Inserting the hydrogen diffusivity (27), $D_H = 3.8\times10^{-6}$ (m^2/sec), and the change of variable; dr/dt=dr/dT. dT/dt=-50. dr/dT, equation (17) is then integrated to;

$$\int_{r_b^*}^{r_f} \frac{-100(3P_a + 4Y)}{3R}\, dr = \int_{T^*}^{933} \frac{D_H(X_H^o - X_H^P)}{V_m^{Al}}\, T dT \qquad (18)$$

From equation 18, the pore size, r_f, as a function of critical temperature and initial hydrogen content can be determined, Fig. 9.

Area percent and total volume of porosity for the other investigated alloys also increased with the hydrogen content and were greater than in the pure aluminium cases. This can be related to the dendritic solidification, existance of primary phases in the melt during pore nucleation, and also greater hydrogen solubility in these melts. However, due to the change in the melt composition during solidification, the pressure of hydrogen can not be evaluated.

6. CONCLUDING REMARKS

In this paper, we have presented a model for formation and growth of the pores in the melt. This model indicates that the presence of particles in the melt, for formation of pores is necessary. These particles are mostly aluminium oxide. More ever, the size of the pore increases with the higher hydrogen content. The computed size of the pores are in a good agreement with the experimental results. The hydrogen content of the samples was about one to five times less than those calculated during hydrogen treatment. This has been ascribed to insufficient quenching and the high diffusivity of hydrogen during handling and preparation for gas analysis treatments. Pore size is inversely proportional to the cooling rate and it reduces with higher cooling rate.

7. ACKNOWLEDGEMENT

This work was a base study on the producing of metallic foam in reduced gravity, sponsored by the Swedish Board for Space Activities.

8. REFERENCES

1- D. Burns and J. Beech, Chemical metallurgy of iron & steel 229,1973, London, The Iron and Steel Institute.

2- I. Svensson and H. Fredriksson, Solidification Technology in the foundary and cast house. The Metal Society, Warwick 15-17 Sep. 1980 p376-380

3- D. B. Burns, J. Beech: "Growth of Blowholes During solidification of Iron-Base Alloys", Chemical Metallurgy of Iron and Steel, 1971

4- H. Fredriksson, I. Svensson, Metallurgical Transactions B, vol. 7B, Dec. 1976 p. 599-605

5- T. S. Piwonka FOUNDARY, Aug. 1966 p. 66-69

6- T. S. Piwonka and M. C. Flemings,Trans. Metals. Society of AIME Vol. 236, Aug. 1966, p. 1157-66

7- H. Shahani, The effect of hydrogen on the shrinkage porosity in aluminium base alloys, this thesis.

8- D. Hanson J. of Metals 1935, p 103-123

9- D. R. Kononow iron& Steel, Oct. 1957 p. 489-491

10- W. P. Desnizky, ibid. February 1958 p. 51-52

11- S. Z. Uman, etal. TRANS. A.F.S., V 66, p 129-134, 1958

12- K. S. S. Murthy ibid, V 91, p 281-286 (1971)

13- M. Sugiyama AFS Cast Metals Research Journal, June 1969 p 59-62

14- S. Lipson TRANSACTIONS A.F.S.,Vol 73 p.194-203,1965

15- J. M. Middleton, The British Foundaryman, Nov. 1962, p.443-448

16- J. T. Berry, Modern Casting, January 1961, p. 63-74

17- H. Shahani and H. Fredriksson, Material Scince under Microgravity, Madrid, Spain. 5-8 April 1983. / ESA SP-191-June 1983), p. 71-78

18- H. Shahani, R. Jönsson, On the design of high pressure casting and rapid heating furnaces, this thesis

19- R. D. Pehlke Trans. of the Metal Soc. of AIME vol. 227

20- R. A. Swalin, Thermodynamics of solids, John Wiley & sons, New York, 1962, p. 143-149

21- W. J. Coy, R. S. Mateer, Trans. Q. ASM, 1965, 58, 99.

22- W. R. Opie Transactions AIME vol 188 p 1237 J. of Metals

1950

23- H. Shahani, Solubility of hydrogen in aluminium alloys, this thesis.

24-J. C. Brice:The growth of crystals from liquids, North-Holland Publication., Amsterdam,1973

25- B. C. Allen, Liquid Metals, S. Z. Beer, Dekker;1972

26- J. A. Champion, B. J. Keene Journal of Material Science 4 (1969) 39-49

27- W. Eichenauer, Z. Metallkde, Bd65 (1974) H.10

TABLE I

pressure of hydrogen during gas treatment (atm.)	hydrogen content (ppm) measured	calculated	measured density (g/cm)	total volume of porosity (%)	average area fraction of porosity (%)	measured pore diameter (um)	number of pores per mm of the sample
			PURE ALUMINIUM				
0.5	2.1	2.9	2.66-2.70	0.0-1.5	0.2	40-60	130-450
1	2.5	4.1	2.59-2.69	0.4-4.1	0.9	50-60	60-350
3	2.7	7.1	2.58-2.69	0.4-4.4	0.6	125-150	10-25
5	3.4	9.2	2.58-2.65	1.9-4.4	1.1	150-200	10-15
			AL-4% TI				
0.5	2.1	4.7	2.65-2.70	1.1-2.9	1.6	70-80	60-110
1	3.3	6.7	2.61-2.64	3.3-4.4	2.3	60-80	160-290
3	3.5	11.6	2.54-2.63	3.7-7.0	4.8	100-125	60-70
5	3.6	15.0	2.55-2.60	4.8-6.6	5.2	100-150	40-90
			Al-10% Fe				
0.5	1.1	3.0	2.74-2.86	1.4-5.5	2.2	80-140	40-50
1	2.8	4.3	2.79-2.81	3.1-3.8	3.7	80-110	55-110
3	4.2	7.4	2.71-2.80	3.4-6.6	7.0	150-175	20-25
5	3.0	9.6	2.67-2.69	7.2-7.9	8.3	150-200	20-40

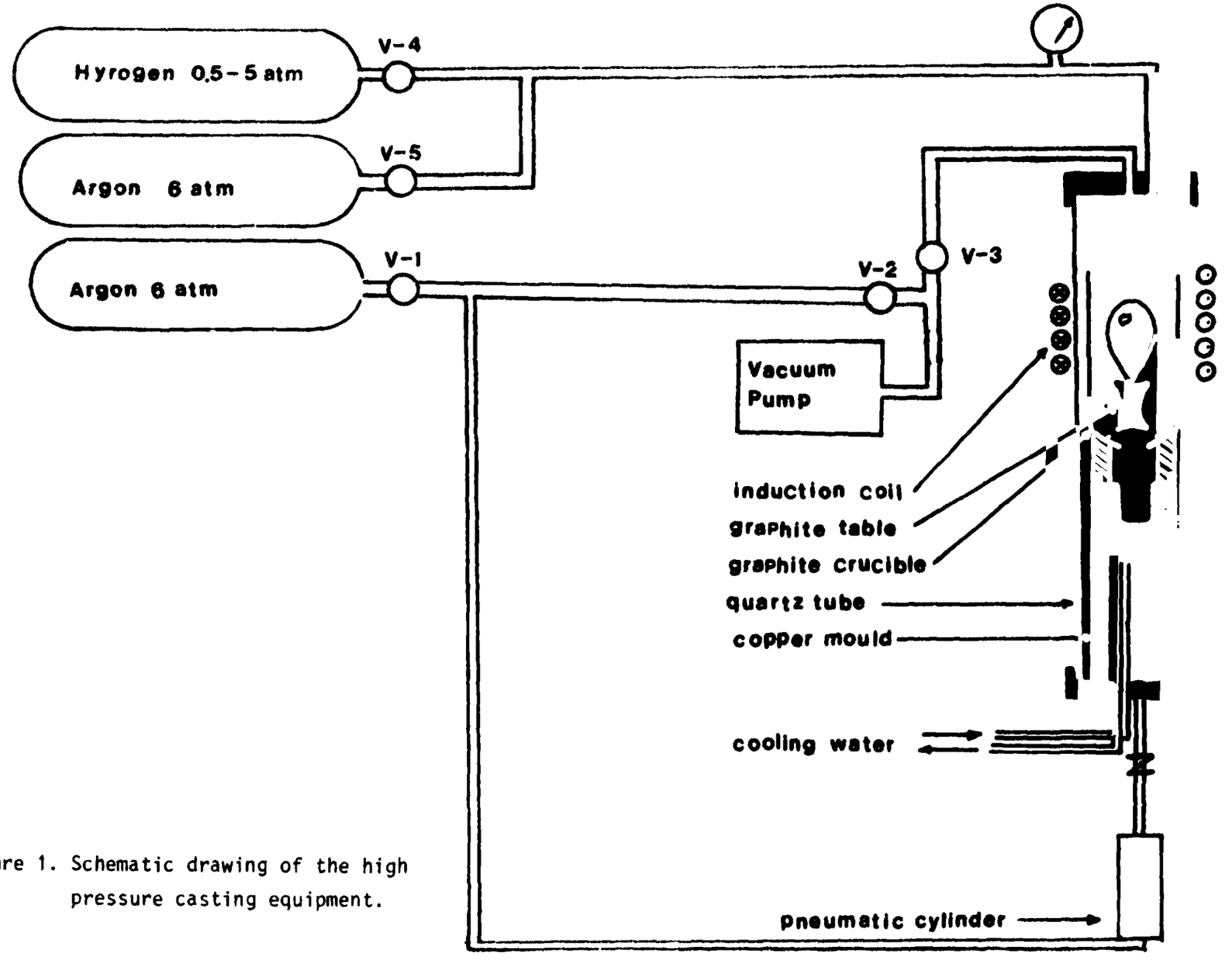

Figure 1. Schematic drawing of the high pressure casting equipment.

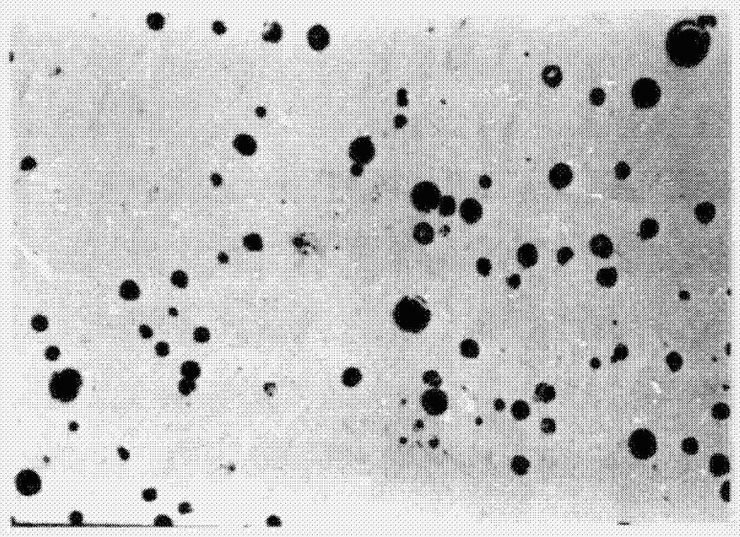

Figure 2a. Pure Al treated at 5 atm hydrogen.

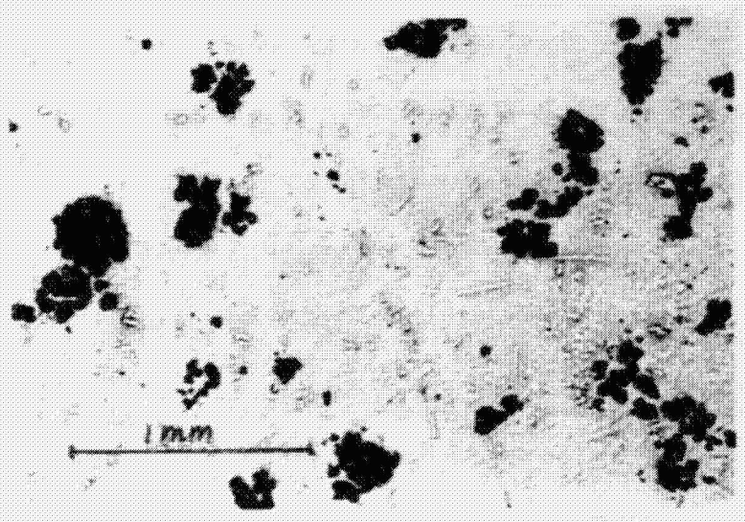

Figure 2b. Al-4 Ti treated at 5 atm hydrogen.

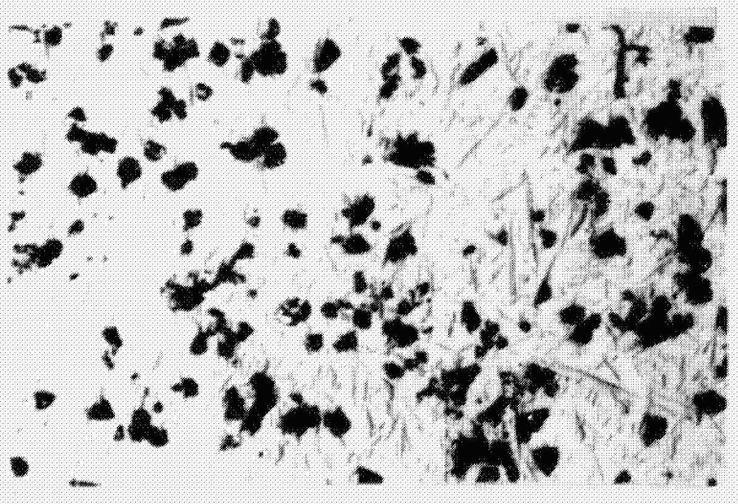

Figure 2c. Al-10 Fe treated at 5 atm hydrogen.

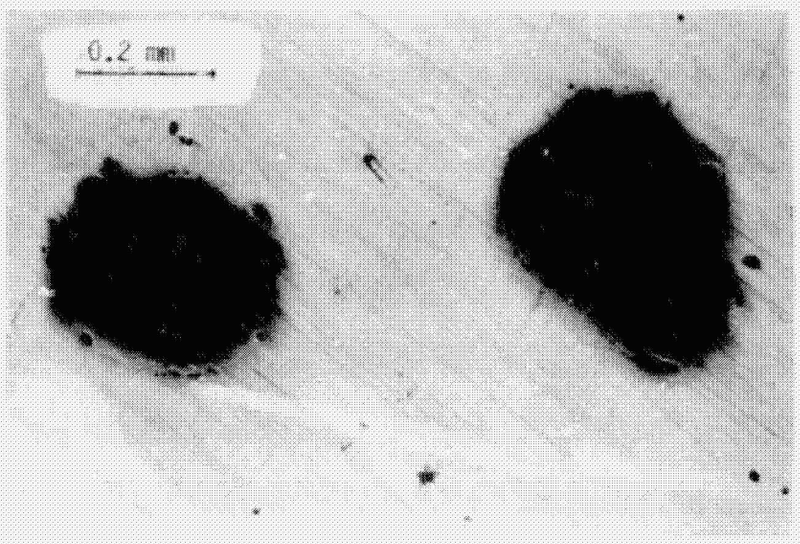

Figure 3a. Pure Al.

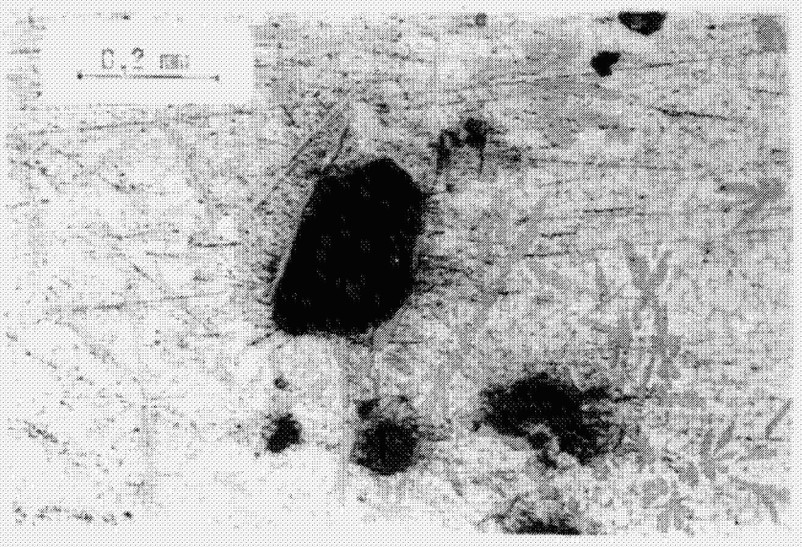

Figure 3b. Al-4%Ti.

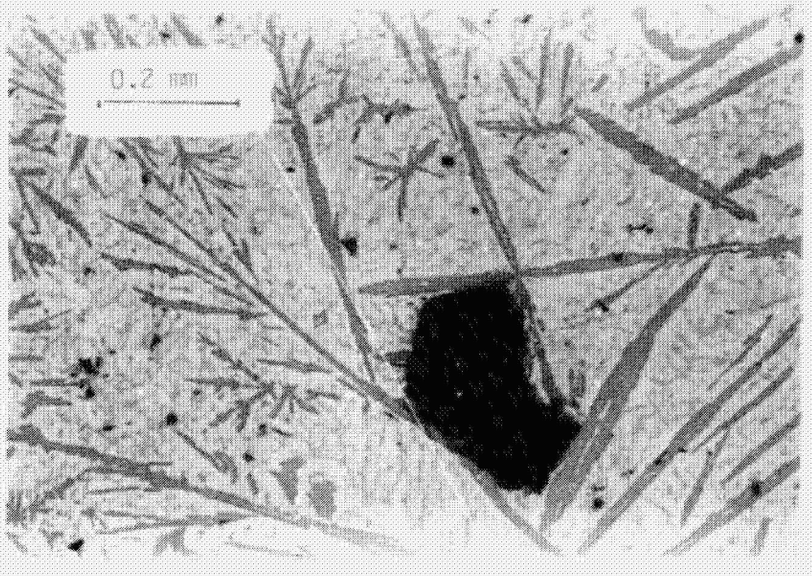

Figure 3c. Al-10%Fe.

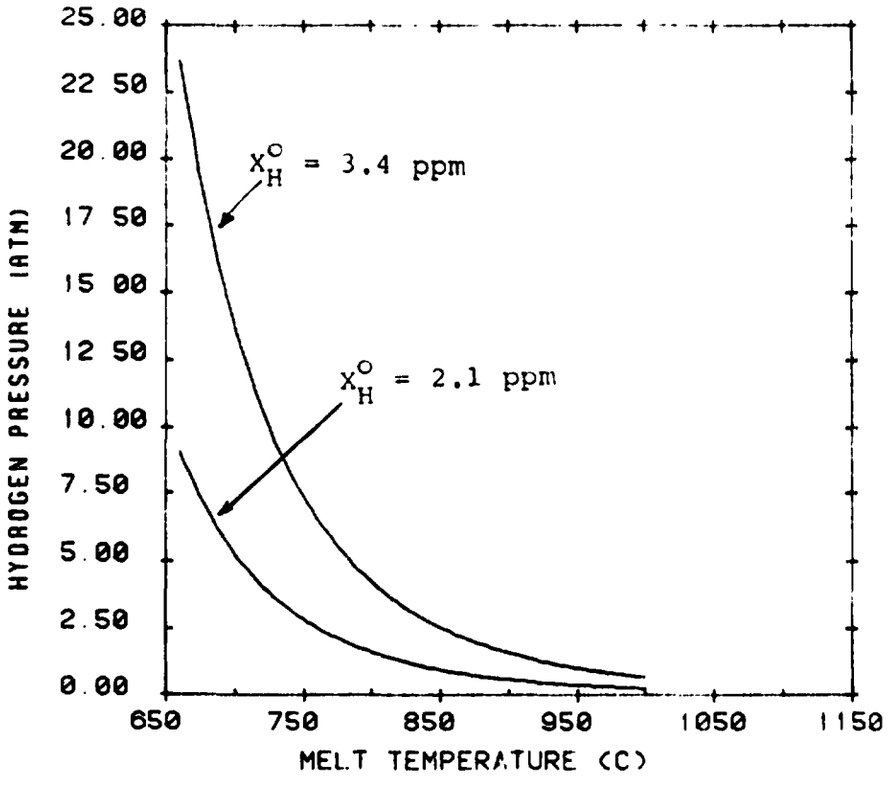

Figure 4. Pressure of hydrogen in the melt during cooling.

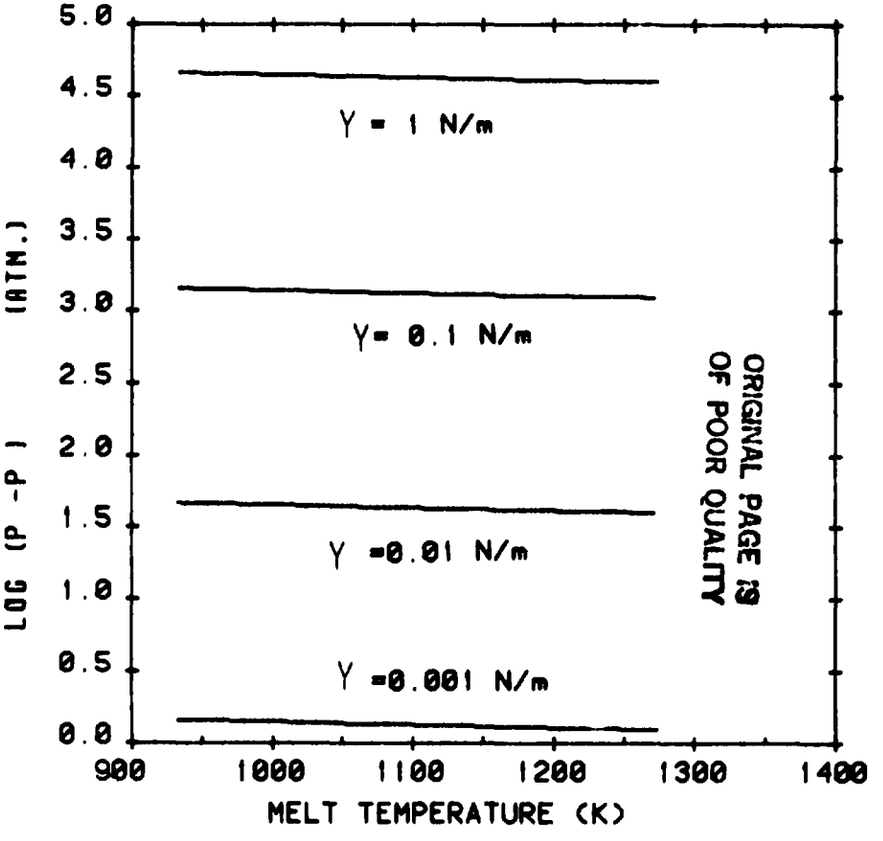

Figure 5. Required pressure of hydrogen for nucleation with varying surface-tensions.

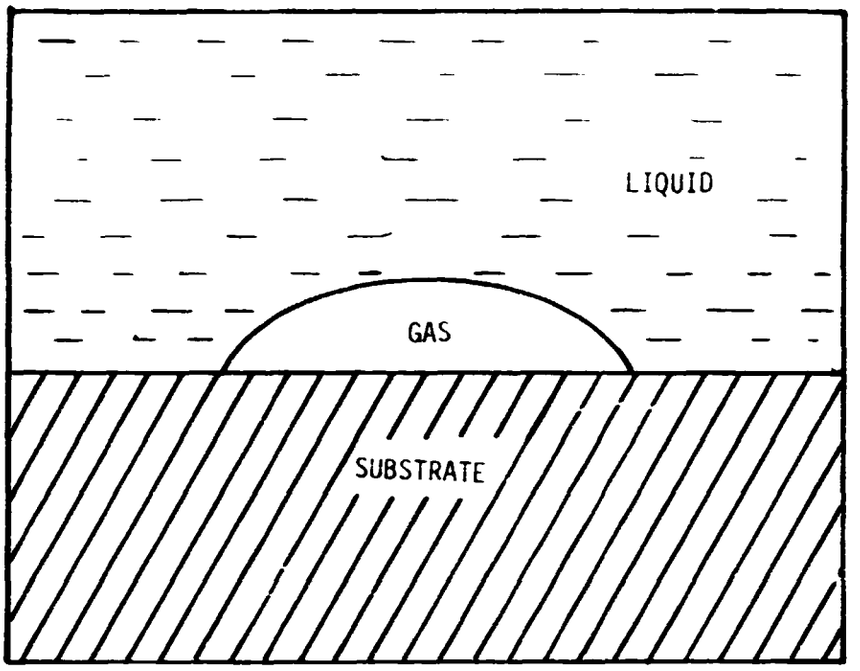

Figure 6. Heterogeneous nucleation on a flat substrate

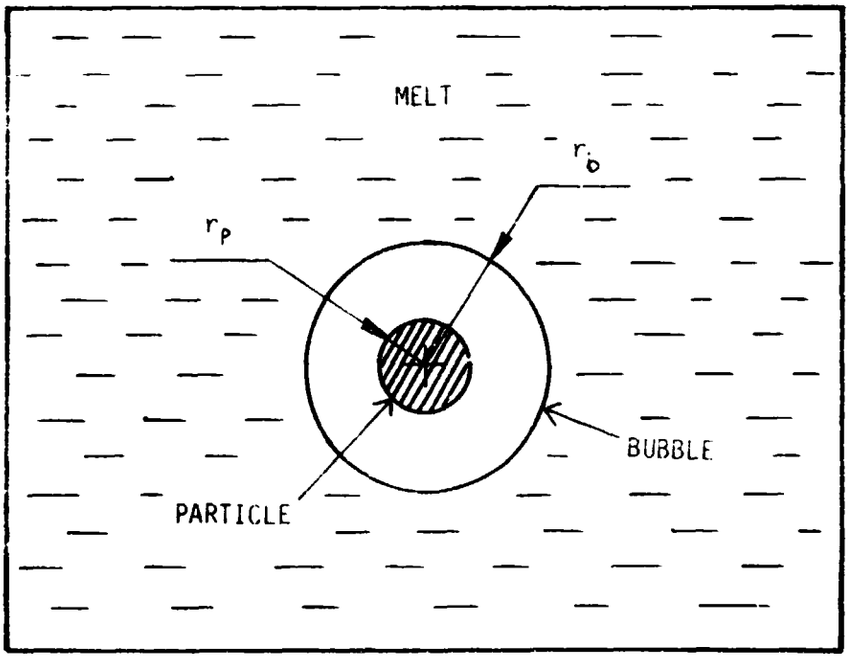

Figure 7. Heterogeneous nucleation on a spherical particle

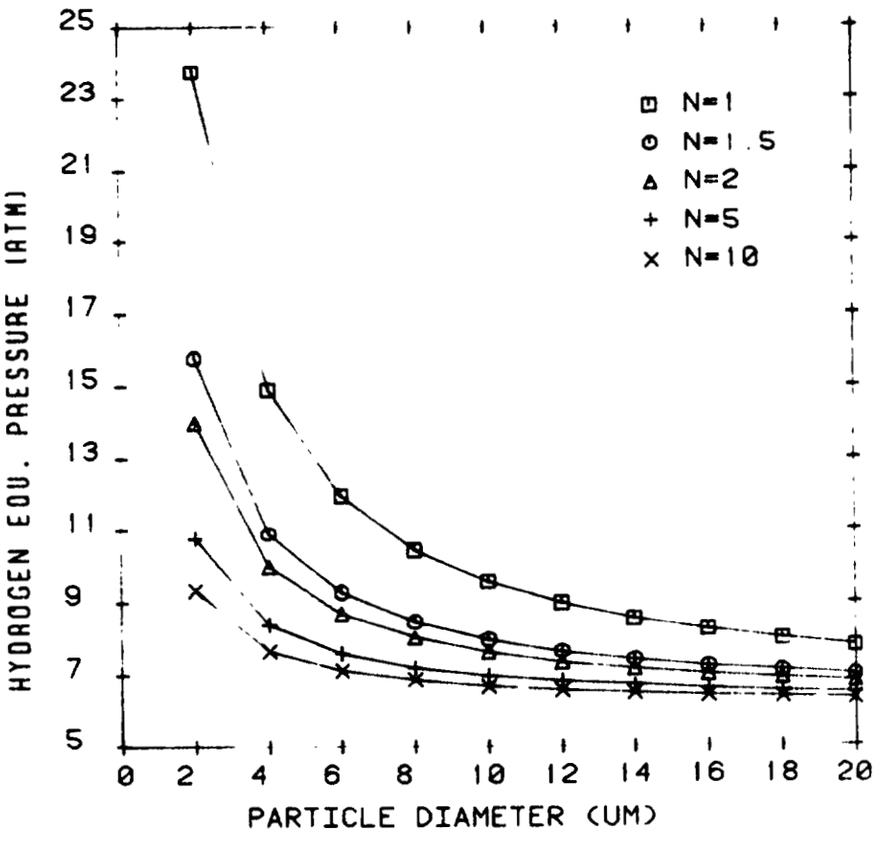

Figure . Required pressure of hydrogen for nucleation of pores with particles

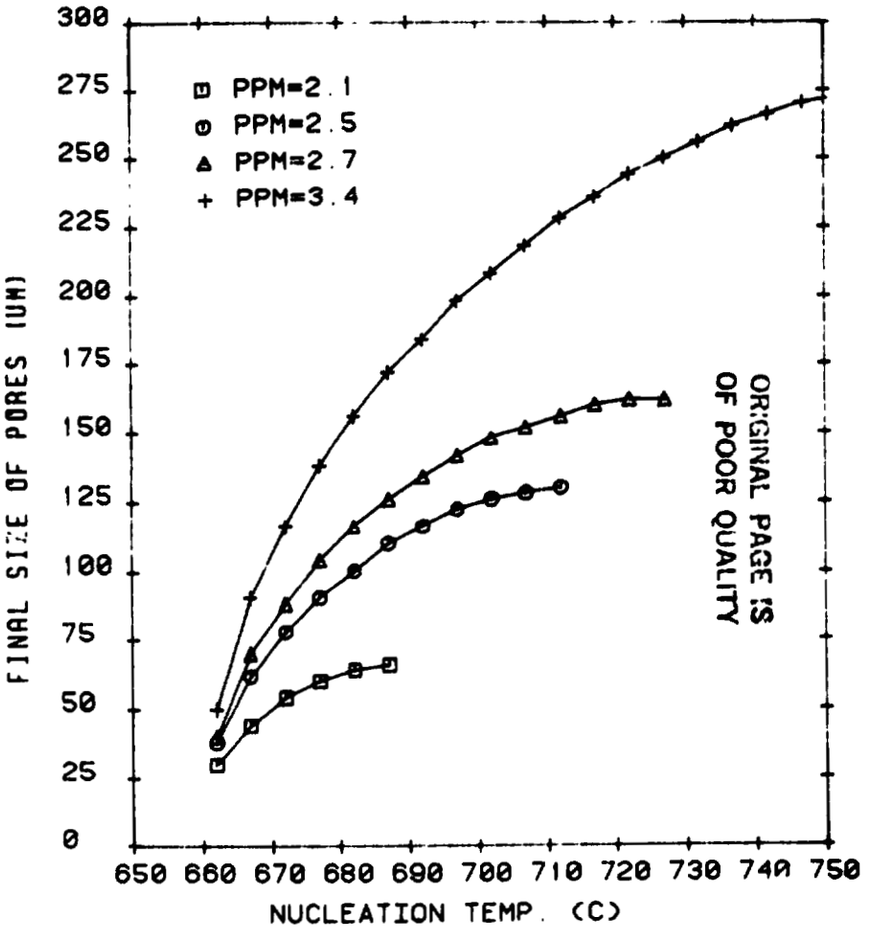

Figure . Calculated size of the pores as a function of critical temperature of the melt.

PAPER V

H. SHAHANI, H. FREDRIKSSON

PRECIPITATION OF GAS PORES IN METALLIC MELTS
DURING COOLING UNDER MICROGRAVITY

PROCEEDINGS OF THE 4TH EUROPEAN SYMPOSIUM ON
MATERIAL SCIENCE UNDER MICROGRAVITY
(ESA SP-191-JUNE 1983) P. 71-78

PRECIPITATION OF GAS PORES IN METALLIC MELTS DURING COOLING UNDER MICROGRAVITY

H. Shahani & H. Fredriksson

Royal Institute of Technology, The Department of Casting of Metals, Stockholm, Sweden

ABSTRACT

In the Swedish rocket program for Material Science research a series of experiments in pore formation in Al-base alloys have been performed. The alloys were melted under high pressure H_2-atmosphere on earth and remelted at low pressure in space. Due to the pressure difference pores were formed. The nucleation and growth of the pores were analysed as a function of the pressure difference and also as a function of the alloy composition. The results of the experiment will be discussed in the paper. The growth of pores will be theoretically discussed.

Keywords: Metallic Foam, Hydrogen, Microgravity

1. INTRODUCTION

Particle composites are difficult to produce from the melt. The particles often have another density than the liquid. Due to this they will flotate or sedimentate during the production process. One thus gets an uneven distribution of the particles in the matrix. In order to avoid movement of the particles it has been proposed to use a microgravity environment.

One of the most difficult composites to produce from a melt is metal foams, metals containing a lot of small gaspores. In order to investigate the possibility to produce metal foams directly from the melt a series of experiments with aluminium alloys supersaturated with hydrogen were performed in space. The alloys were produced on earth at a high pressure of hydrogen and after that remelted at a reduced helium pressure in a microgravity environment. The experiments were performed in a rocket campaign and in an aircraft with a parabolic path.

2. EXPERIMENTAL WORK

Three different alloys were investigated, namely pure Al, Al with 4% Ti and Al with 10% Fe. The addition of Ti and Fe was made in order to investigate the effect of a second phase in the liquid on the pore growth. The solubility of hydrogen (ref. 1, 2) in the three alloys is presented in fig. 1 at a hydrogen pressure of one atmosphere. The

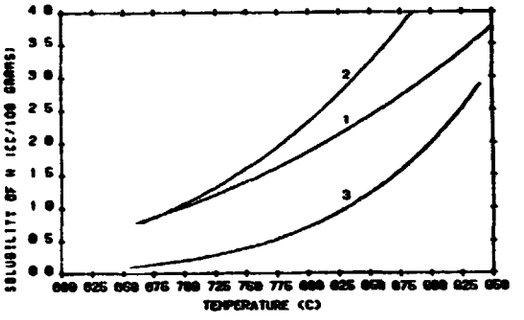

Figure 1. The solubility of hydrogen in pure Al (1), in Al, 4% Ti (2) and in Al, 10% Fe (3)

Figure shows that the solubility is about 10 times higher in the liquid than in the solid at the melting point. Sievert's law tells us that the solubility increases with the square root of pressure. It will thus be possible to get a high hydrogen content in an alloy by melting it at a high hydrogen pressure and at a high temperature. It will be possible to store hydrogen in the alloy by rapid quenching of a melt treated under those conditions.

To produce the samples an equipment, schematically shown in fig. 2, was constructed.

The sample, which was cast in a copper mould (dimensions diameter 18 mm and height 20 mm), was placed on the graphite table in the crucible. The crucible was mounted on a water cooled copper mould by a cylindrical insulator.

(a) At the beginning all the valves shown in fig. 2 were closed. The valve (1) was opened and argon with 6 atm pressure closed the quartz tube with a pneumatic device.

(b) Valve (3) was opened and the chamber was evacu-

Proceedings of the 4th European Symposium on Materials Sciences under Microgravity, *Madrid, Spain, 5-8 April* 1983 (*ESA SP-191 June* 1983).

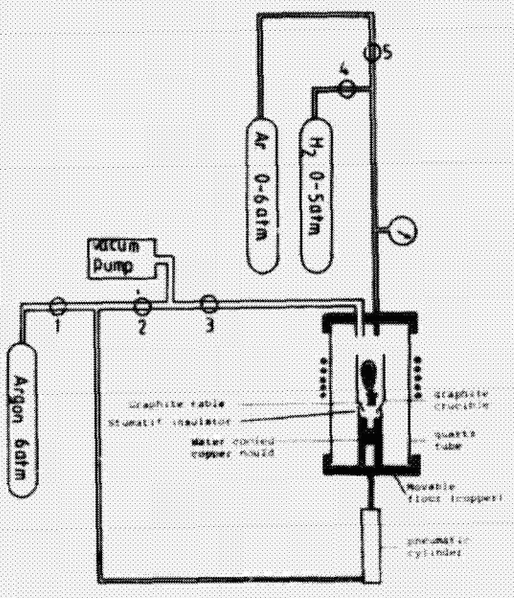

Figure 2. Equipment for producing hydrogen supersaturated samples

ated for 3-4 minutes. The valve (3) was closed again.

(c) Valve (4) was opened to let the hydrogen fill the chamber to the desired pressure. After adjusting the pressure this valve was closed again.

(d) The induction furnace was switched on and the melting process started after 3-4 minutes. The sample was heated to ca 1000° C and kept at this temperature for 6 minutes. This was enough for the hydrogen to react with the melt, since the sample was partly levitated, fig. 3, and that the melt was heavily stirred and kept at a high temperature. During this process the pressure usually increased slightly in the chamber. By controlling the valve (3), the pressure could be adjusted.

(e) After the dissolving reaction had taken place valve (5) was opened and argon at 6 atm pressure was applied to the melt in order to prevent hydrogen from leaving the sample. The furnace was switched off and the levitated melt was dropped through the hole in the bottom of the graphite crucible into the copper mould. A measurement showed that it took 5-7 seconds for the sample to solidify.

For the remelting of the sample in space an equipment, shown in fig. 4, was constructed. The sample size and form are shown in the figure. The sample was placed on a lampfilament. The filament was extracted from a 400 Watt halogen lamp. The sample and the filament were electrically isolated from each other by a boron nitride cap. This type of furnace was developed in order to have a solid skin around the sample as long as possible to prevent a loss of hydrogen during the remelting process.

Figure. 3 Levitation melting in the equiment shown in fig. 2

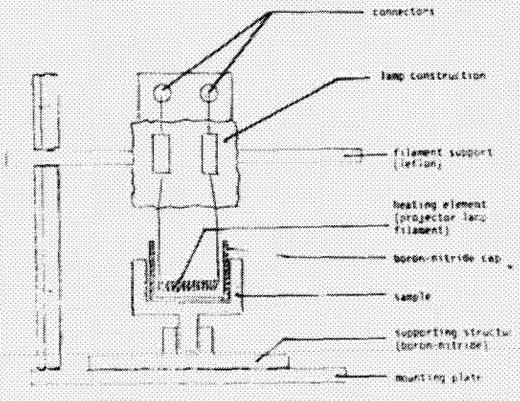

Figure. 4 Drawing of sample and space melting equiment

Three melting equipments of the type shown in fig. 4 were placed in a cannister. fig. 5. Two different types of cannisters were built. One for the aircraft experiment and one for the rocket experiment, fig. 6. The chamber was evacuated and filled with Ar or He to a predetermined pressure before the experiments. A pressure transducer measured the pressure inside the cannister. In the aircraft experiment a motor driven camera was added. The process was photographed each 0,3 seconds.

The temperature of each sample was measured by a Chromel-Alumel thermocoax, which would send the singnals to the unit control of the same furnace. The furnace switched off after a predetermined delay and the next furnace switched on automatically.

3. RESULTS

3.1 Original samples

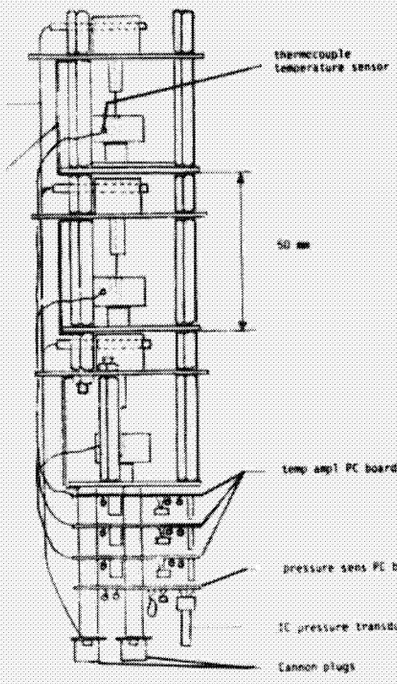

Figure 5. Cannister with remelting equipments used in the rocket experiments

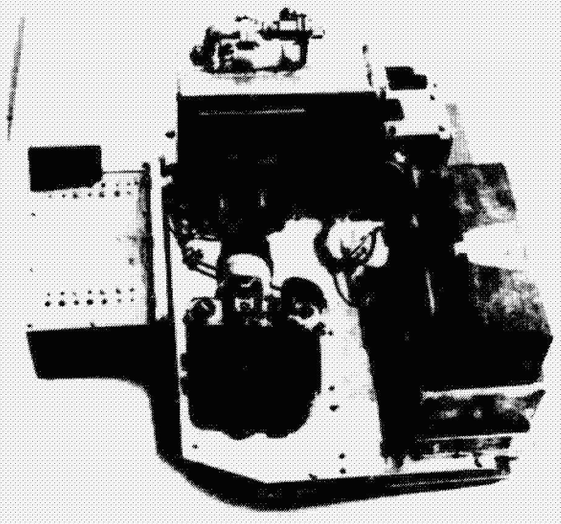

Figure 6. Cannister with remelting equipments and camera unit used in the aircraft experiments

The alloys were melted under a pressure of 0,5, 1,0, 3,0 and 5,0 atm hydrogen. The pressure was increased with Ar to 6 atm just before quenching. The samples were machined to the proper dimensions. The side of each sample was metallographically prepared and analysed. Fig. 7, 8 and 9 show the microstructure in each alloy. All the figures are taken from samples produced under a hydrogen pressure of 5 atm. Fig. 7 shows that the sample of pure aluminium contains a lot of small rounded pores. Fig. 8 showes that the alloy with 4% Ti also contains rounded pores. The figure also shows that the structure contains crystals of Al_3Ti.

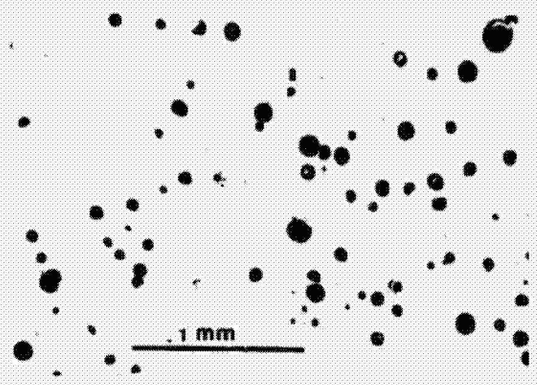

Figure 7. Microstructure in a pure Al sample treated at a pressure of 5 atm H_2

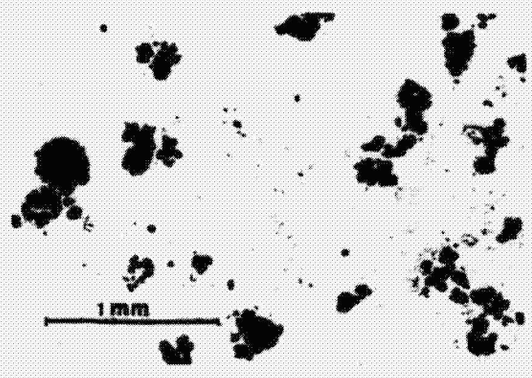

Figure 8. Microstructure in a sample with 4% Ti, treated at a pressure of 5 atm

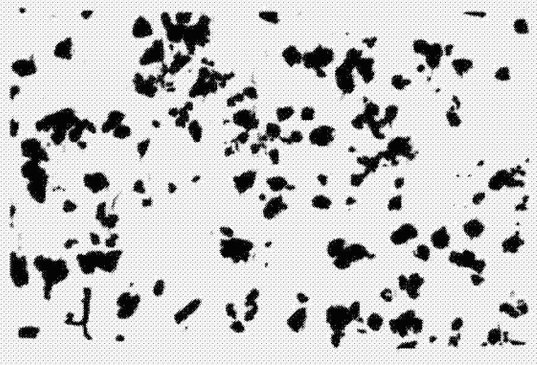

Figure 9. Microstructure in a sample with 10% Fe. treated at a pressure of 5 atm

Many of those crystals nave contacts with very small pores. This structure might have been formed in the following way. During the quenching gas pores have started to grow in the liquid. After this a precipitation of Al_3Ti has started. New pores have then been formed in contact with the Al_3Ti crystals. Fig. 9 shows the structure in the alloy with 10% Fe. The structure consists of Al_3Fe crystals with a plate-like morphology. Gas pores are

situated between the plates. This structure has probably been formed by a precipitation of Al_3Fe-crystals followed by a gas pore precipitation.

For each alloy and for each hydrogen pressure a series of samples were produced. In one sample from each series the pore size and number were evaluated. The density of the sample as well as the hydrogen content were also evaluated. All those data will be presented together with the flight data.

3.2 Aircraft samples

Twentyseven experiments were performed. The samples were processed during the parabolic flight according to the time-temperature curve shown in fig. 10. The samples were melted under different He pressures (0,1, 0,4 and 1,0).

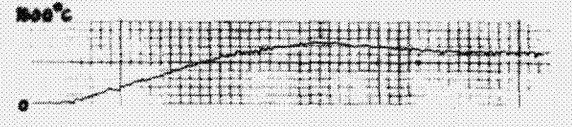

Figure 10. The temperature-time curve for sample EE5

The camera started to take pictures after nine seconds. Fig. 11 gives an example of the melting and expansion process of one sample. After the flight all the samples were photographed from six different directions, and fig. 12 and 13 show one sample before and after the flight process.

All the samples were then cut and metallographically prepared. Fig. 14, 15 and 16 show a cross section of three different samples, one from each alloy.

The area fraction of pores was measured, the number and the size were evaluated. The density of each sample was also determined. All the evaluated data is presented in table 1.

3.3 Rocket flight

Nine successful experiments were performed. All the samples were treated and evaluated in the same way as in the aircraft experiments. Table 1 shows the results (they are marked with &).

One of the samples (number 8) was only partly remelted in space, fig 17 showes a cross section of this sample. The melting border is shown in the upper part of the figure. The figure shows that the small pores are expanding at the melting of the alloy.

4. DISCUSSION

The alloys were melted under a high hydrogen pressure on earth and after that rapidly solidified in a copper mould. When the melt was quenched in the copper mould a solid skin formed immediately. During the solidification process solubility of hydrogen decreases sharply, as can be seen from fig. 1. Due to this pores are formed. However, the solid skin and the rapid cooling lead to entrappment of pores and the samples are supersaturated with hydrogen.

A comparison of the solubility of hydrogen at high pressure and high temperature, fig. 1 and the amount of hydrogen kept in the samples, table 1, shows that some hydrogen must have left the samples during the quenching process. However, the amount of hydrogen kept in the samples is higher than the equilibrium value of the remelting pressure.

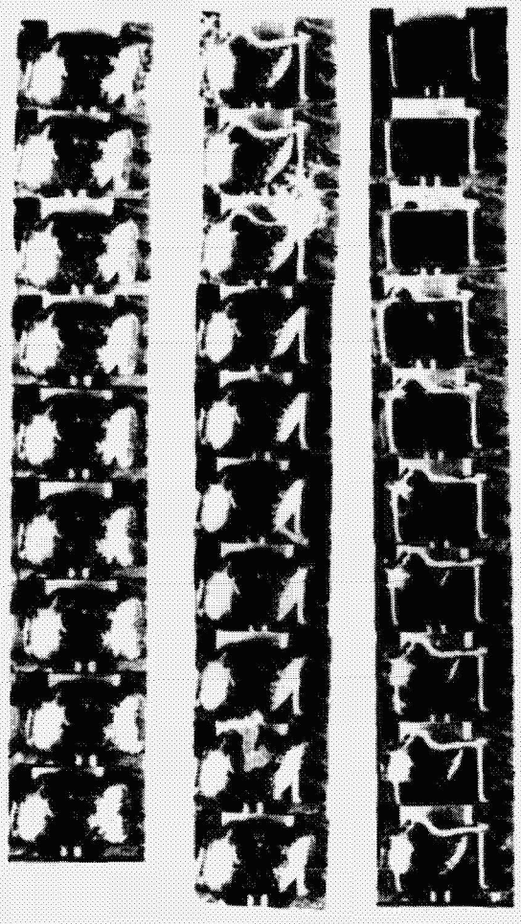

Figure 11. Melting and expansion of the sample EE5

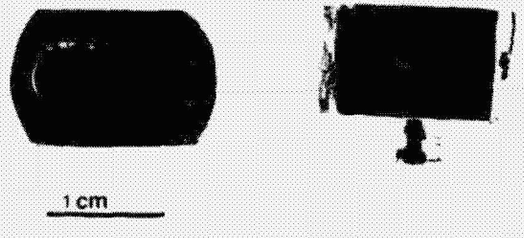

Figure 12. Top and side view of sample EE5 before remelting

The samples are thus supersaturated with hydrogen, when remelting in space. The samples contain a lot of small pores. Those pores will grow and the sample will expand during the remelting process until equilibrium is reached.

The number of pores as a function of pore size and

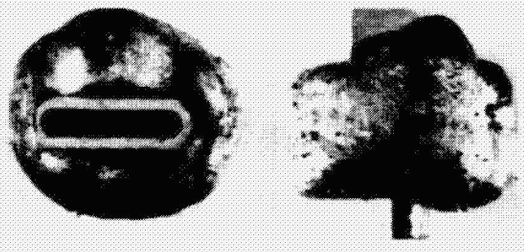

Figure 13. Top and side view of sample EE5 after remelting P_{H2} = 1 atm, Al 4% Ti, P_{He} = 0.1

Figure 14. Metal foam of pure Al(N). Remelting pressure 1.2 atm. Supersaturation pressure 0.2 atm. R.R.D. = 19 . Pores are spherical

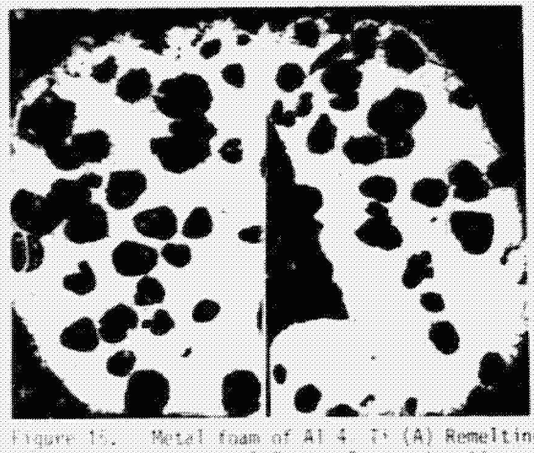

Figure 15. Metal foam of Al 4 Ti (A) Remelting pressure 0.2 atm. Supersaturation pressure 0.2 atm. R.R.D. = . Pores are affected by second phase

hydrogen content and remelting pressure can be calculated by the following equation:

$$\frac{P_o \cdot V_o}{T_o} = \left(P_a + \frac{2\sigma}{R}\right)^{1/2} \cdot \frac{V_{eq}^o}{T_a} \sqrt{P_a + \frac{2\sigma}{R}} + \frac{N \cdot \frac{4}{3}\pi R^3 \left(P_a + \frac{2\sigma}{R}\right)}{T_a} \quad (1)$$

where

P_o = equilibrium pressure (1 atm)
V_o = amount of hydrogen stored in the super saturated sample given by table 1 (cc H2/gram)
T_o = equilibrium temperature (273°K)
P_a = remelting pressure (0.1 - 0.4 - 1 atm)
σ = surface tension 0.914 N/m
R = radius of the pores (cm)
V_{eq}^o = solubility of hydrogen at the remelting temperature given by fig. 1
T_a = solidification temperature (933 °K)
N = number of pores per gram

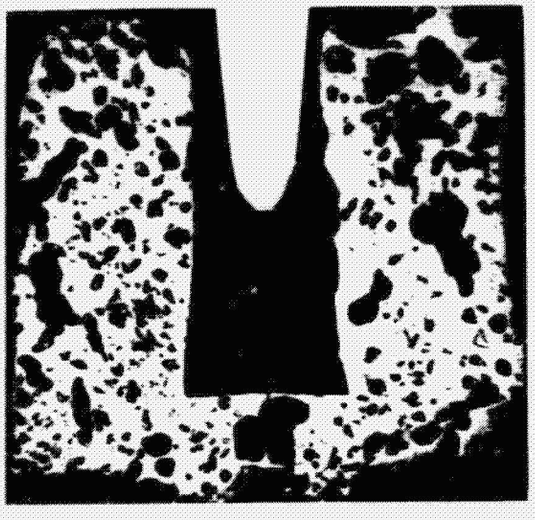

Figure 16. Metal foam of Al 10 Fe (E). Remelting pressure 0.2 atm. Supersaturation pressure 1 atm. R.R.D. 24 . Pores are affected by second phase

Figure 18 and 19 show the number of pores per gram as a function of the radius of pores with P_a equal to 0.1 and 1 atm. with hydrogen content varying from 1.5 to 3 cc /100 gr. The data presented in table 1 is also given in the figures.

Equation 1 can also be used to calculate the density of the sample, as a function of P_a and V_o. The calculated density is changed to Relative Reduction of Density (R.R.D.) and given in figures 20-22 for three different values of P_a (p_a = 0.1-0.4-1 atm). The figures show that the density will decrease with decreasing remelting pressure (P_a), decreasing radius and increasing solved hydrogen.

The figures can be used to compare the experimentally measured density with the theoretically measured. A comparison shows that the theoretical R. R. D. is higher than the experimental one. The comparison also shows that one has come closest to the theoretical density in the sample containing small and large amounts of pores such as the samples alloyed with titanium. The reason for this might be as follows:

Both in the aircraft and in the rocket some gravity is left during the experiments. In the aircraft the

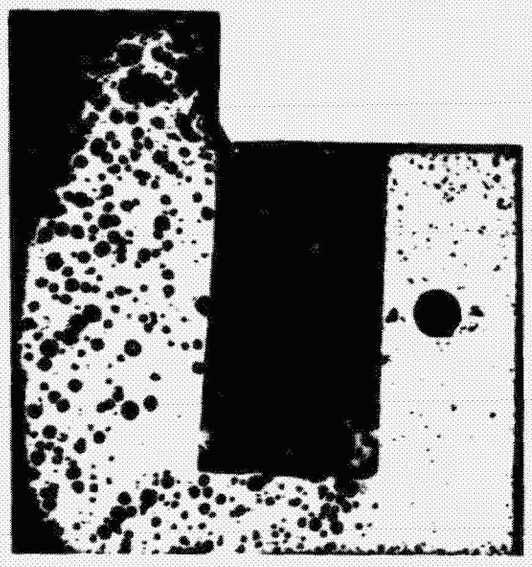

Figure 17. The expansion process during remelting in space for sample (B). The big hole at the right side of the sample is for adjustment of thermo-couple.

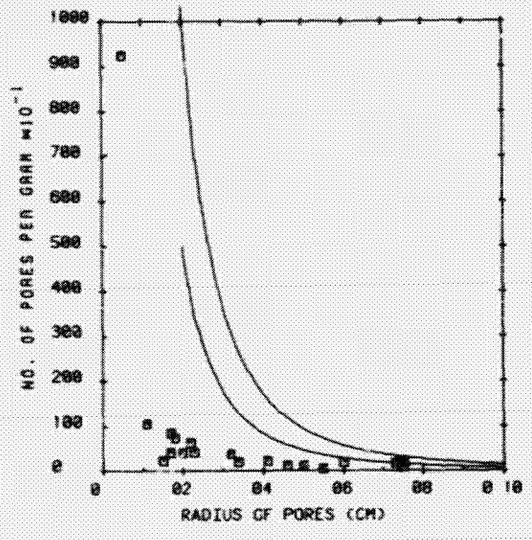

Figure 18. Number of pores per gram as a function of the pore radius (cm) with P_a=0,1 atm and V_0= 1,5-3 cc/gr

gravity was 10^{-2} cm/s^2 and in the rocket ca 10^{-3} cm/s^2. This gravity will give a floatation of the pores. Stokes equation gives the movement of the pores as function of the gravity and pore size. For pores in an Al-melt one gets the following relation:

$$V \quad 10^{-1} R^2 \text{ (m/sec)} \qquad (2)$$

Calculation shows that there is a considerable movement of pores. The larger pores move faster than the smaller ones so they will collide and float together. This coalescence process will partly explain why the number of pores is smaller in the remelted samples than in the starting samples. The coalescence process will partly be influenced by the movement of the particles due to the gravity. It is also possible that the pores collide during the expansion process.

Integration of Stoke's law gives the distance for the pores to move within the available time. In our case the solidification of the samples was within 30 seconds, pores larger than 500 μm can move out from the sample. This is a pore size which is bigger than the size observed in the sample of pure Al.

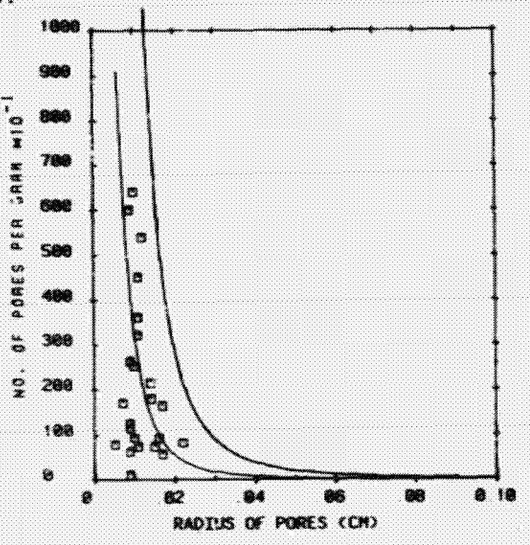

Figure 19. Number of pores per gram as a function of the pore radius (cm) with P_a=1 atm and V_0=1,5-3 cc/gr

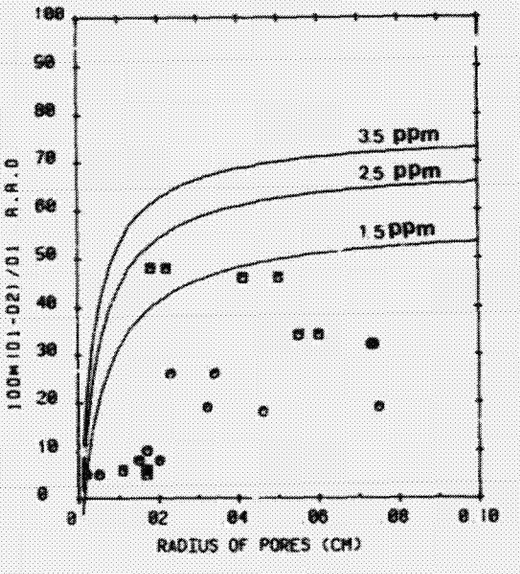

Figure 20. Variation of Relative Reduction of Density as function of pore radius P_a=0,1 atm and V_0=1,5-3,5 ppm

However, the movement of pores is influenced by the particles in the liquid and both Al_3Ti and Al_3Fe influence the coalescence process. Both the coalescence and the movement will decrease as a result of foreign particles. In the experiments

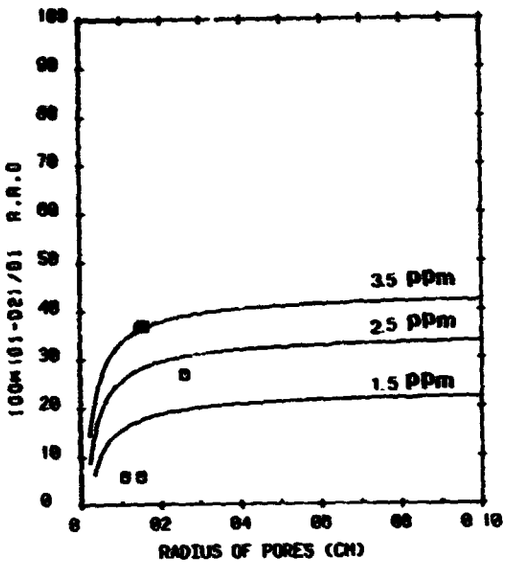

Figure 21. Variation of Relative Reduction of Density as a function of pore radius at P_a=0,4 atm and V_0= 1,5-3,5 ppm

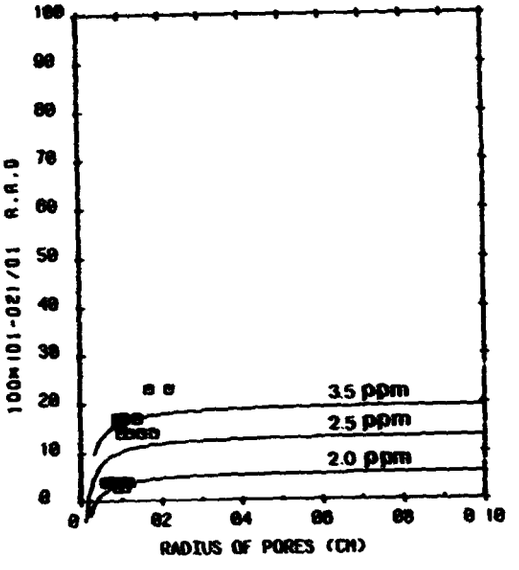

Figure 22. Variation of Relative Reduction of Density as a function of pore radius at P_a=1 atm and V_0=2-3,5 ppm

Table 1.

Sample	Alloy	H-treatment (atm)	H content (cc/100g)	Density D_1 (g/cc)	Remelting pressure	Density D_2 (g/cc)	R.R.D	R(cm)	No./g	R(cm)	No /g
A N	Al	0.2	2	2.61	0.2	2.12	19		1100		
A J	Al	0.5	2.1	2.63	1	2.55	3		4850		
BB1	Al	0.5	2.1	2.70	0.1	2.57	5	0.017	407		
BB2	Al	0.5	2.1	2.70	1	2.6	4	0.009	1260	0.009	630
AA2	Al	1	2.5	2.70	0.1	2.56	6	0.011	1040	0.017	850
AA5	Al	1	2.5	2.7	1	2.62	3	0.011	740	0.009	1150
A M	Al	3	2.7	2.58	0.2	2.39	7		-		
CC2	Al	3	2.7	2.69	0.1	2.55	5	0.005	9250	0.002	3100
CC5	Al	3	2.7	2.69	1	2.59	4	0.005	800	0.007	1700
DD1	Al	5	3.4	2.65	1	2.55	4	0.017	1650		
A A	48Ti	0.2	-	2.65	0.2	2.07	22		2800		
A B	48Ti	0.5	2.1	2.65	1	2.29	14		4900		
GG2	48Ti	0.5	2.1	2.70	0.1	1.39	48	0.022	630	0.018	740
GG5	48Ti	0.5	2.1	2.70	0.4	1.70	37	0.016	1260	0.015	1200
GG1	48Ti	0.5	2.1	2.70	1	2.27	16	0.009	6000	0.010	6400
EE5	48Ti	1	3.3	2.62	0.1	1.42	46	0.050	110	0.041	220
EE3	48Ti	1	3.3	2.62	0.4	2.47	6	0.015	560	0.011	670
EE2	48Ti	1	3.3	2.62	1	2.17	17	0.011	3600	0.011	4500
A O	48Ti	3	3.5	2.58	0.2	1.46	43		1100		
FF3	48Ti	3	3.5	2.63	0.1	1.94	26	0.023	410	0.034	185
FF1	48Ti	3	3.5	2.63	0.4	1.92	27	0.026	330	0.026	480
FF5	48Ti	3	3.5	2.63	1	2.53	4	0.009	1100	0.010	930
HH2	48Ti	5	3.6	2.60	0.1	2.39	8	0.020	410	0.015	220
HH4	48Ti	5	3.6	2.60	1	1.99	23	0.017	580	0.022	820
A H	10%Fe	0.5	1.1	2.74	1	2.53	8		7000		
II2	10%Fe	0.5	1.1	2.86	0.1	1.89	34	0.0[illegible]	185	0.055	37
II3	10%Fe	0.5	1.1	2.86	1	2.46	14	0.010	3220	0.012	5400
KK3	10%Fe	1	2.8	2.81	0.1	2.26	19	0.075	74	0.032	380
KK2	10%Fe	1	2.8	2.81	1	2.34	17	0.014	2150	0.014	1800
A E	10%Fe	1	2.8	2.79	0.2	2.12	24		1900		
A F	10%Fe	3	4.2	2.71	0.2	1.90	30		1850		
LL2	10%Fe	3	4.2	2.80	0.1	1.90	32	0.074	185	0.073	174
LL4	10%Fe	3	4.2	2.80	1	2.33	17	0.009	2040	0.010	2520
MM5	10%Fe	5		2.67	0.1	2.25	16	0.046	110		
MM2	10%Fe	5		2.67	1	2.31	14	0.015	740	0.015	930

the gravity vector is not constant and this will decrease the possibility for the pores to leave the sample.

5. CONCLUDING REMARKS

It has been shown that it will be possible to produce metal foams in space. Due to the low solubility of hydrogen in Al the density was in this case only reduced by a factor of two. This can be overcome by using metals with a higher solubility of gases.

6. ACKNOWLEDGEMENT

Grants were given by the Swedish delegation of space research. The furnaces were constructed by the Swedish Space corporation. We are grateful to Rolf Jönsson and Sven Walin for their help with the experiments. We are also grateful to D.F.R.F., NASA for the possibility of performing the aircraft experiments.

7. REFERENCES

1) W.R. Opie and N.J. Grant, Trans. A.I.M.M.E., 1950, vol. 188, p. 1237.

2) H. Shahani, Solubility of hydrogen in Al-4%Ti, Al10%Fe, To be published.

PAPER VI

H. SHAHANI

EFFECT OF HYDROGEN ON THE SHRINKAGE POROSITY OF ALUMINIUM-COPPER AND ALUMINIUM SILICON ALLOYS

JANUARY 1984

EFFECT OF HYDROGEN ON THE SHRINKAGE POROSITY OF ALUMINIUM COPPER AND ALUMINIUM SILICON ALLOYS

Hamid Shahani

Dept. of Casting of Metals
The Royal Institute of Technology
S-100 44 Stockholm
Sweden

January 1984

1. ABSTRACT

The effect of hydrogen content on shrinkage porosity of Al-Cu and Al-Si alloys was studied. A model for formation of shrinkage porosity is presented. Experiment and theory show that the amount of shrinkage porosity in castings is dependent on the gas content, pressure drop due to shrinkage and amount of foreign particles in the melt. Modifiers facilitate formation of these types of pores.

2. INTRODUCTION

Existance of porosity in metals, in general, reduces the mechanical properties of the products (1-2). It has been shown earlier that initial gas content of the melt (3-4), mode of solidification (5) and shrinkage caused by solidification (6-9) are among the parameters which may influence the porosity. Due to good mechanical and machining properties, aluminium-copper and aluminium-silicon alloys are widely used in industry. Hydrogen is the only soluble gas in aluminium alloys (10) and thus is the leading contributor to porosity in these alloys. In nearly all cases, the source of the hydrogen is some form of water. Water sources in foundaries are numerous but the main ones are moisture in the air, combustion products in gas burnner furnaces during melting, and holding and moisture absorbed on the surfaces of charge components. Water, in contact with aluminum melt, dissociates to hydrogen and oxygen according to the following reaction:

$$2\,Al + 3\,H_2O \;\;\text{=========}\;\; Al_2O_3 + 6\,\underline{H} \qquad (1)$$

Hydrogen dissolves in the melt as atoms and oxygen remains as dross. The reaction rate increases rapidly with temperature and is even more rapid when Mg is present (10). Hydrogen solubility in the melts decreases with lowering temperature and falls sharply from 0.7 ppm to 20 times less during solidification (11). When hydrogen content in the melt exceeds the solubility limit, with the presence of proper nucleants (12), pores form and grow. Pores can either form prior or during the solidification. The former are spherical and relatively large. The latter are small and irregular in shape and are known as shrinkage porosity (13). Their formation is influenced by the hydrogen enrichment and shrinkage pressure in the interdendritic area (14).

The present work was aimed at studying the effect of hydrogen on the shrinkage porosities in pure aluminium, Al-4.5%Cu and Al- 2%, 4%, 7% Si. Hydrogen content of the melts,

were varied by injecting argon saturated water and purging with argon. In the case of Al-4.5%Cu samples, AlLiH powder and hydrogen gas were also applied.

Alloying elements, temperature and modifiers influence melt properties such as surface tension, viscosity (29-31) and the solidification mechanisms. In aluminium alloys, silicon decreases the surface tension of pure aluminium from 0.9 (N/m) to 0.8 (N/m), while Cu has no influence (30,32,33). Modifiers such as sodium also decrease the surface tension (30). Increasing temperature reduces both the surface tension and viscosity of the alloys.

The effect of modifiers Na and Sr (15-28) on the porosity of Al-Si alloys was studied. They were added to the melt after gas treatment and prior to casting. In the case of Al-4.5%Cu, effect of aluminium oxide powder on pore nucleation was studied.

3. EXPERIMENTAL PROCEEDURE

Materials investigated in the present study were:

1- Pure aluminium (99.8%)
2- Al-2%Si
3- Al-4%Si
4- Al-7%Si,0.3%Mg
5- Al-4.5%Cu

Al-7%Si,0.3%Mg, SIS4244, was supplied by Ardal og Sunndal Verk a.s Norway. Alloys of 2%, 4% Si were made by adding pure aluminium (99.8%) to alloy SIS4244. Al-4.5%Cu was made by adding electrolytic copper to pure Al. Alloys were melted in a graphite crucible at temperatures about 100 C above their respective liquidus temperatures. Hydrogen content of the melts was varied by the equipment shown in Figure 1, as follows:

1- Injecting water saturated argon at different time

intervals, with 22 mm Hg partial pressure of water in in the gas mixture

2- Purging the melt with argon.

3- Injecting directly hydrogen and AlLiH4, for Al-4.5%Cu (AlLiH decomposes easily and generates hydrogen)

Hydrogen flam was formed around the lance after 10 minutes injecting watersaturated argon. It indicated that melt was saturated with hydrogen. In the case of Al-Si alloys, 250 ppm Sr and 100 ppm Na were also added to the melt after gas treatment and prior to casting. For Al-4.5%Cu, 0.5 wt.pct aluminium oxide powder was sprayed into the melt after 20 minutes of gas treatment with water satrated argon. Table 1 summarizes the treatments performed on the samples. Treated melts were cast in a mould as shown in figure 2. The top and bottom sections of the mould as well as the chill were made of cast iron. The side walls and the raiser were of asbestos.

4. EXPERIMENTAL RESULTS

The hydrogen analysis of the samples is presented in Table 1 and indicates that:

Hydrogen content of the samples Z1 to Z3 (Al-4.5% Cu), treated with argon, AlLiH and hydrogen was unaffected and remained at 0.18 ppm. Hydrogen content increased for the samples Z4-Z8 treated with the argon saturated water.

These results can be explained by the dissolving mecnanism of hydrogen in melts. Hydrogen dissolves in the melts as atoms (32). The dissociation rate of the molecular hydrogen to atomic at the treatment temperature (750°C) is exteremly low (35). Thus, change of hydrogen content was not achieved and it behaved as an inert gas, argon. In the other hand, the standard free energy change for reaction 1 is very high (1_) and the values for the activity quotient $a_{H} \cdot a_{H_2O}$ is so high that for practical purposes it implies the complete conversion to hydrogen for all traces of water vapour contacting the metal. The resulting atomic hydrogen is readily soluble in the melt

up to its solubility.

In order to study the effect of extra solid particles on the poreformation, Al_2O_3 powder was added to sample Z8. The hydrogen content, compared to the similar gas treated sample Z7, reduced from from 0.43 ppm to 0.35 ppm. Variation of hydrogen content in Al-4.5%Cu samples as a function of reaction time is presented in figure 3.

Variation of hydrogen content in aluminium and Al-Si alloys are presented in figures 4-7. Hydrogen content in these samples also increased wiht the reaction time. In oroer to study the effect of modifiers, 250 ppm Sr or 100ppm Na were added at the end of gas treatment. The addition of Sr and Na to the melt prior to the casting, however reduced the gas content.

The area fraction of porosity in the samples was measured by a False Colour TV Analyser. Average values of porosity, measured in 4x7 mm^2 field from the chill to the raiser (horizontal central plane) are presented in figures 8-37. Most of the samples had a "sink" on the upper surface, around the center. Existence of "sink" in the castings indicates that feeding was not sufficient (37). Samples had higher values of porosity in these areas but low porosity closer to the chill (38). Fine interdendritic shrinkage pores, 20-100 um, were uniformly dispersed in the castings. Figures 38-40 show examples taken from samples A1 (pure Al), B1 (Al-2%Si) and Z1 (Al-4.5%Cu). Pores of 100-500 um were also observed around the center of the castings, figures 41-44.

For equal hydrogen content, the average values of porosity in the samples increased with the silicon content, samples A2, B3, C3, D6. Addition of Al_2O_3, Sr and Na did not change the shape of the pores. Comparing the equal gas content samples, D3-D8, B2-B4, C1-C4 indicate that these additive increased the porosity values.

5. DISCUSSION

The porosity in the samples was dependent on the hydrogen content, duration of gas treatment, and addition of modifiers such as Na or Sr or Al_2O_3.

Aluminium oxide particles which form during the gas treatment according to equation 1, contribute as nucleation sites for bubbles. The greater the amount of Al_2O_3, the greater is the availability of nucleus sites. As soon as the melt becomes supersaturated with hydrogen, bubble formation is facilitated by the large number of nucleation sites that are available. This in turn results in greater porosity.

Modifiers also facilitate the nucleation of pores either by reducing the surface tension or acting as nucleants. In these samples the hydrogen content was lower than expected from treatment time, while pores were formed more frequently, figures 12,13,17,21,28,29.

A theoretical model which can describe the size and the volume fraction of the pores, may predict the quality of the products. Such a model should consider mechanism of pore nucleation and is developed as below:

Pore formation is influenced by gas content of the melt, pressure in the liquid phase, and the surface tension. The size of the pores is determined by the volume of the liquid confined between the denderite arms.

Figures 38-44 indicate that the samples undergo a dendritic solidification. However, the length of the mushy zone for pure aluminium is smaller than that for the alloyed ones. During dendritic growth, due to much lower solubility of hydrogen in the solid phase (11), it enriches in the melt. Due to the high diffusivity of hydrogen (38), it is possible to use the lever rule. Hydrogen content in the melt can thus be written as :

$$X_H^L = X_H^o / f_L \qquad (2)$$

where:

X_H^L hydrogen content in the melt (mole fraction)
X_H^o initial hydrogen content (mole fraction)
f_L melt fraction

Figure 45 shows the enrichment of hydrogen in the melt as a function of fraction solid for the lowest and highest measured hydrogen contents. The average solubility of hydrogen at one atmosphere and for Al at the melting point is also shown on the same figure. The hydrogen content of the melt exceeds the equilibrium solubility value when more than 60% solidification has taken place. The required supersaturation for nucleation may be disregarded by assuming that the pores are formed hetrogenously (12). The balance of pressures in a bubble can be represented by:

$$P_{H_2} - P_L = \frac{2Y}{r} \qquad (3)$$

P_{H_2} pressure in the bubble (N/m^2)
P_L pressure in the liquid (N/m^2)
Y surface tension, for pure Al (0.914 N/m)
r radius of the pore (m)

The hydrogen pressure, P_{H_2} can be calculated from the initial hydrogen content, solid fraction, and Sievert's law;

$$P_{H_2} = \left(\frac{X_H^o}{f_L K}\right)^2 \qquad \text{(atm.)} \quad (4)$$

where k is Sieverts constant, for pure Al (0.7 ppm/atm). Due to the solidification shrinkage, pressure in the liquid, P_L, decreases. The pressure drop in the liquid in the mushy zone is calculated previously (14):

$$P_a - P_L = \frac{32\mu\beta\theta^2 L^2}{r^4} \cdot \frac{t^2}{\pi h^2 n} \qquad (N/m^2) \quad (5)$$

where:

μ = viscosity (1.3E-3 kg/m/sec)

β = corrected shrinkage coefficient (0.0675)

θ = solidification rate (1.82E-3 m/sec)

L = length of the casting from raiser (m)

t = trotosity factor (2)

r = radius of the pores (m)

h = half of the height of the mould (0.01 m)

λ = denderite arm spacing (100 μm)

n = number of chanels per m during solidification equal to $1/\lambda^2$ about $1E8/m^2$

P_a = ambient pressure (1 atm.)

Inserting $r = f_L . \lambda /2$ in equation 5, results in:

$$P_L = P_a - \frac{32\mu\beta\theta^2 L^2 t^2 16}{f_L^4 \lambda^2 \pi h^2} \qquad (6)$$

Pressure in the liquid as a function of distance from raiser with different values of solid fraction are presented in figure 46. Figure indicates that pressure in the liquid drops rapidly with progress of solidification. The size of the shrinkage pores, r , is computed numerically by substituting P_{H_2} and P_L from equations 4 and 5 in equation :

$$\left(\frac{X_H^o \lambda}{2rK}\right)^2 + \frac{32\mu\beta\theta^2 L^2 t^2 \lambda^2}{r^4 \pi h^2} - P_a = \frac{2Y}{r} \qquad (7)$$

The results are presented in figure (47) as function of distance from raiser and hydrogen content. The size of the shrinkage pores increases from 10 μm to 60 μm, with the hydrogen content and distance from raiser. The size of the shrinkage pores is in a good agreement with the experimental measurements.

The present model does not describe the existance of random pores larger than 100 μm observed in some of the samples, figures 41-44. Formation of these pores may be explained as follows:

After a pore is formed, in accordance with the presented model, further growth of the pore takes place. This growth is

due to enrichment of hydrogen in the melt surronding the pore in the interdendritic regions. In the areas close to the chill or mould, melt solidifies faster and pores formed in these areas, are not able to expand (or grow). Thus, pressure inside the pores increases. However, if the solid phase is weak or the melt between the dendrite arms can be pushed away, the pores may expand due to the increasing pressure within t' pores. This can occur in the central parts of the casting which explains the formation of larger pores in these areas.

6. CONCLUSION

1- Shrinkage porosity in the samples are dependent on the duration of gas treatment and hydrogen content of the melt.

2- The pores were formed more frequently in the samples modified by Na or Sr. These samples had relatively lower hydrogen content.

3-Average values of porosity in the samples increased with the solidification rang induced by Si content.

4-The presented model indicates that the size of the shrinkage pores increases with the hydrogen content and pressure drop caused by shrinkage. Pressure drop increases with distance from raiser.

7. ACKNOWLEDGMENT

I would like to thank professor Hasse Fredriksson for his valuable advises and support during this work.This project was sponsored by Årdal og Sunndal Verk a.s ,Norway, which kindly helped me with hydrogen analysis.

8. REFERENCES

1- G. V. Kutumba, AFS Transactions vol.7, 1973 p.110-114

2- K. V. Prabhakar AFS Transactions vol.9, 1979 p.377-386

3- M. F.Jordan,G.D.Denyer Journal of the Inst.of Metals vol 91 1962-63 p 48-53

4- P. M. Thomas, Met.Trans.B Vol 9B Mar.1978 p 139-141

5- J. Cambell, The British Foundryman Apr.1969 p 147-158

6- J. Cambell, Trans. of Met. Soc. of AIME, vol 239, Feb.1967, p.138

7- J. Cambell, ibid, vol 245 Oct.1969 p.2325

8- J. Cambell, ibid, vol 242 Feb. 1968 p.264

9- H. Shahani, Precipitation of pores in melts, this thesis

10- F. O. Traenkner Modern Casting Dec.1981 p44-48

11- F. Weinberg, Metal Science Jun.1979 p335-340

12- H. Fredriksson, Metallurgical Transactions vol.7B Dec.1976 p.599

13- T. S. Piwonka Foundry Aug.1966 p 66-69

14- T. S. Piwonka, M. C. Flemings Trans. of the Metall.Soc. of AIME Vol.236 1966 p 1157-1165

15- A. Pacz, U.S.Patent No. 1,387,900 (13 Feb. 1920);Brit. patent No. 158,827 (26 Jan. 1921).

16- J . D. Edwards,F.C.Frary, U.S. Patent No. 1,410,461) 27 Nov. 1920)
R.S.Archer and J.D.Edwards,Brit.Patent No. 171,997(15 Nov.1921)

17- The British Aluminium Co.,Ltd., and A.G.C.Gwyer,Brit. patent No. 210,517 (31 Oct.1922)
The British Aluminium Co.,Ltd.,A.G.C.Gwyer
Brit. Patent No. 219,346(22 Jan.1923).

18- B. M. Thall and B. Chalmers J.Inst.Metals, 1950,77 p79-97

19- R. C. Plumb and J.E.Lewis Journal of Inst. of Metals Vol 86 1957-58 p393-400

20- P. Borgeaud, F.Dabel AFS Cast Metals Research Journal Sep. 1968 p. 151-158

21- G. G. Nair, S. S .Bhatngar AFS Cast Metals Research Journal Mar. 1968 p. 5-8

22- J.Sulzer Modern Casting Jan. 1961 p 38-43

23- C. B. Kim, R. W. Heine Journal of the Inst. of Metals Vol 92 1963-64 p 367-376

24- H. Fredriksson, M. Hillert, N. Lange Journal of the Inst. of

Metals Vol 101 1973 p 285-299
25- S. Bercovici, Giesserei 67 No.17.18. Aug 1980
26- S. M. D. Glenister, R. Elliott Metal Science Apr.1981 p 181
27- S. C. Flood, J. D. Hunt Metal Science July 1981 p 287-294
28- R. Redecker Giesserei 68 No.1.5 Jan.1981 p7-11
29- V. L. Davies, Journal of the Inst.of Metals vol 92 1963-64 p 208-210
30- F. D. Richardson, Transactions ISIJ,vol.14,1974 p 1-8
31- B. C. Allen, "Liquid Metals"S.Z. Bekker; 1972
32- F. D. Richardson Physical Chem. of Melts in Metallurgy 1974 Academic press London. 1963
33- W. Eichenauer, Z. Metallkunde Bd. 65 H.10, 1974 p.649-652
34- R. D. Phlke Trans. of the Metal Soc. of AIME vol. 227
35- W. R. Opie, Transactions AIME, vol 188 Oct.1950 Jornal of Metals p.1237
36- D . E. Talbot International Metallurgical Reviews vol 20 1975 p 166-184
37- J. Campbell AFS Cast Metals Research Journal Mar.1969,p 1-8
38- J. Campbell Trans. of the Metall.Soc. of AIME vol 242 Jul.1968 p 1464-5

TABLE 1, Treatment performed on the samples

sample		reaction time (minutes)	remark	Hydrogen content (ppm)
A1	Al	0		0.24
A2	Al	3		0.38
A3	Al	10		0.45
A4	Al	7	100ppm Na	0.20
A5	Al	7	100ppm Na(metallic)	0.30
A6	Al	7	250ppm Sr	0.23
B1	2%Si	0		0.19
B2	2%Si	3		0.32
B3	2%Si	7		0.32
B4	2%Si	7	250ppm Sr	0.27
C1	4%Si	0		0.35
C2	4%Si	3		0.40
C3	4%Si	6		0.38
C4	4%Si	7	250ppm Sr	0.25
D1	7%Si	0	15min flushed with argon	0.15
D2	7%Si	0		0.22
D3	7%Si	0	wet charge	0.30
D4	7%Si	2		0.24
D5	7%Si	5		0.39
D6	7%Si	7		0.38
D7	7%Si	10	100ppm Na	0.20
D8	7%Si	7	250ppm Sr	0.28
Z1	4.5%Cu	0	3 minutes argon flushed	0.18
Z2	4.5%Cu	0	0.5% AlH_3 added	0.18
Z3	4.5%Cu	2	flushed with hydrogen	0.17
Z4	4.5%Cu	2	P =240mmHg	0.26
Z5	4.5%Cu	5		0.31
Z6	4.5%Cu	10	Hydrogen flame formed	0.32
Z7	4.5%Cu	20	Hydrogen flame formed	0.43
Z8	4.5%Cu	20	Hydrogen flame formed 0.5% Al_2O_3 powder added	0.35

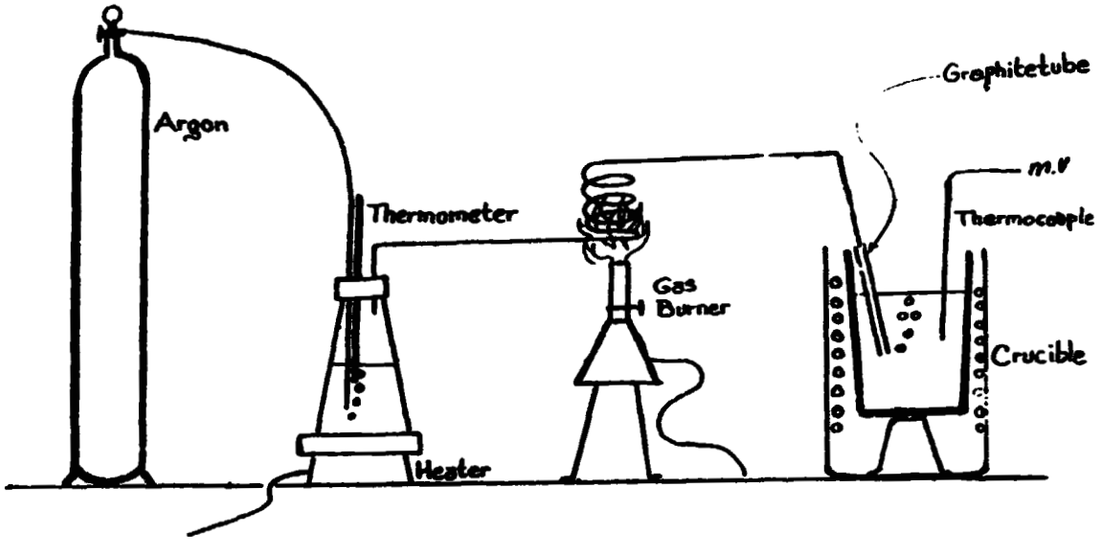

Figure 1. Schematic drawing of the melting and gas treatment apparatus.

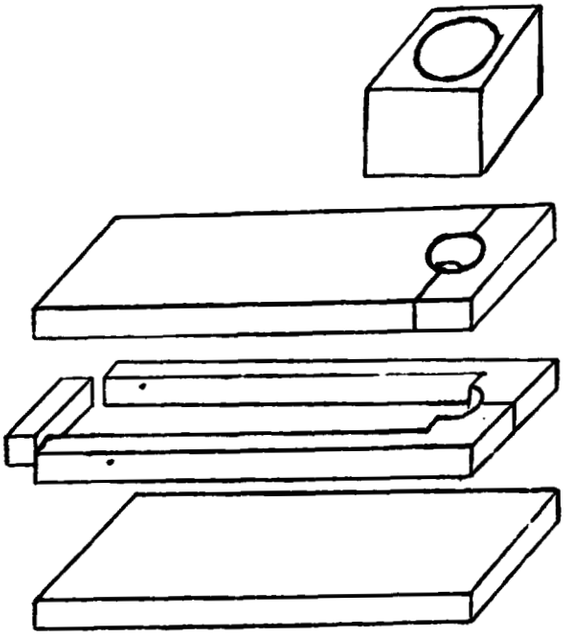

Figure 2. Schematic drawing of mold

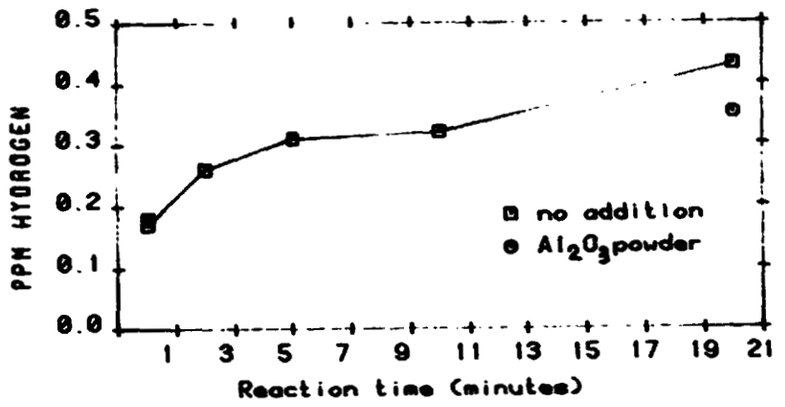

Figure 3. Variation of hydrogen content for Al-4.5%Cu.

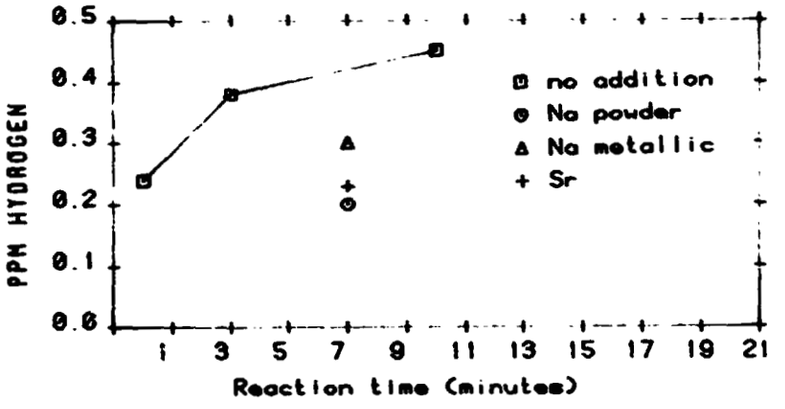

Figure 4. Variation of hydrogen content for pure Al.

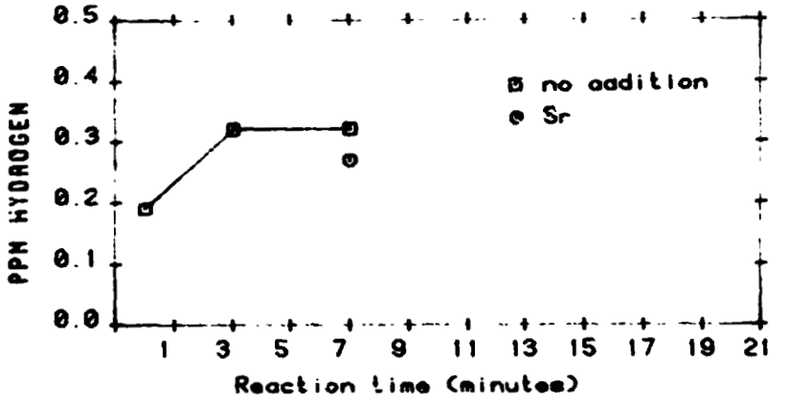

Figure 5. Variation of hydrogen content for Al-2%Si.

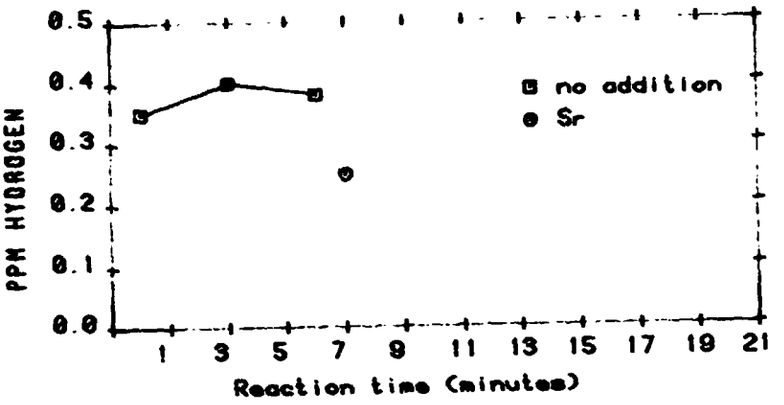

Figure 6. Variation of hydrogen content for Al-4%Si.

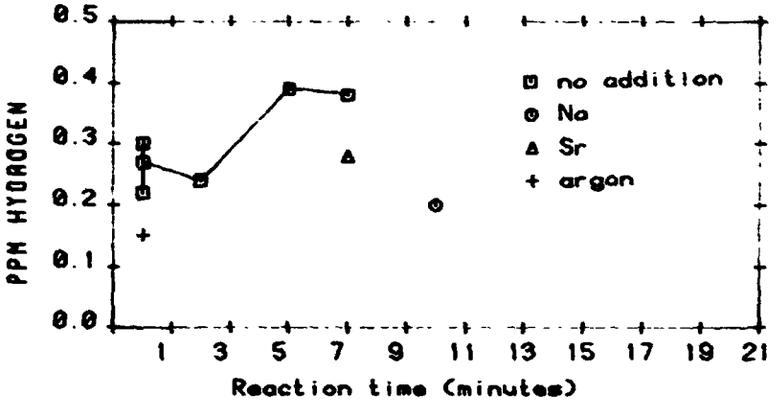

Figure 7. Variation of hydrogen content for Al-7%Si.

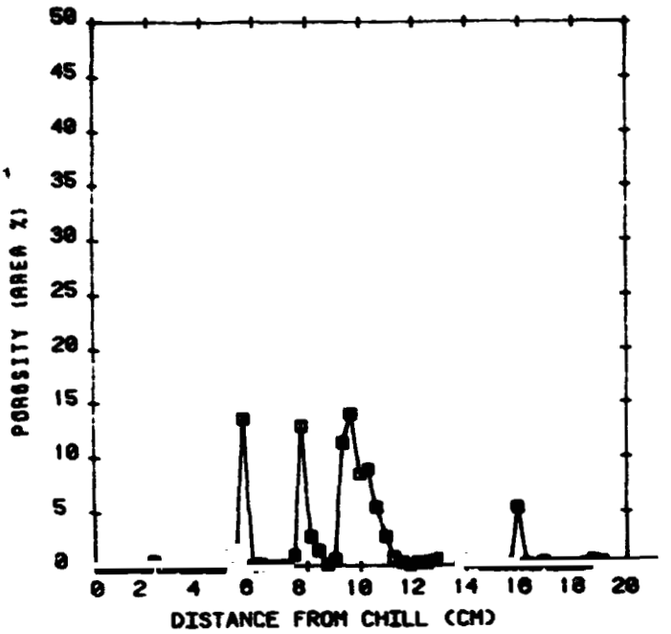

Figure 8. Variation of porosity in sample A1, pure Al.

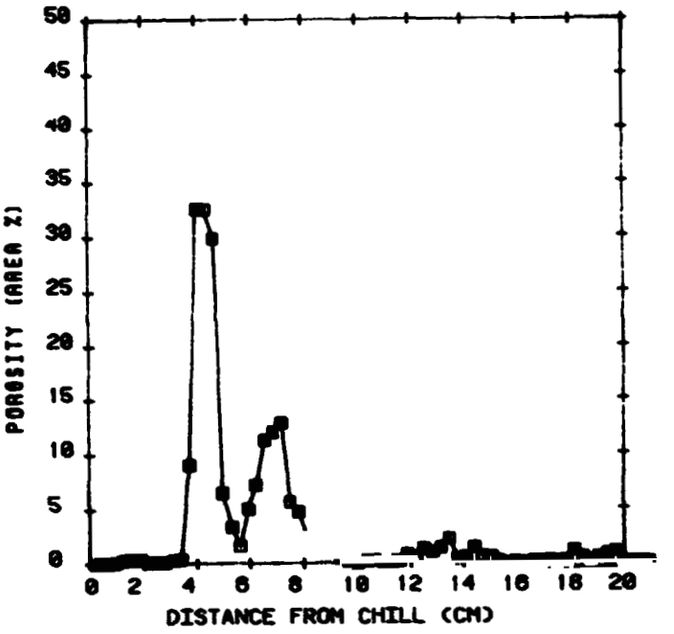

Figure 9. Variation of porosity in sample A2, pure Al.

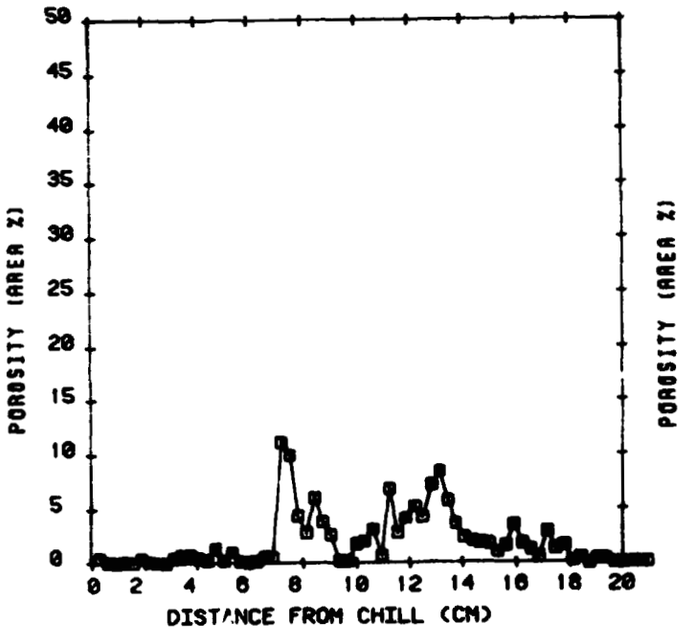

Figure 10. Variation of porosity in sample A3, pure Al.

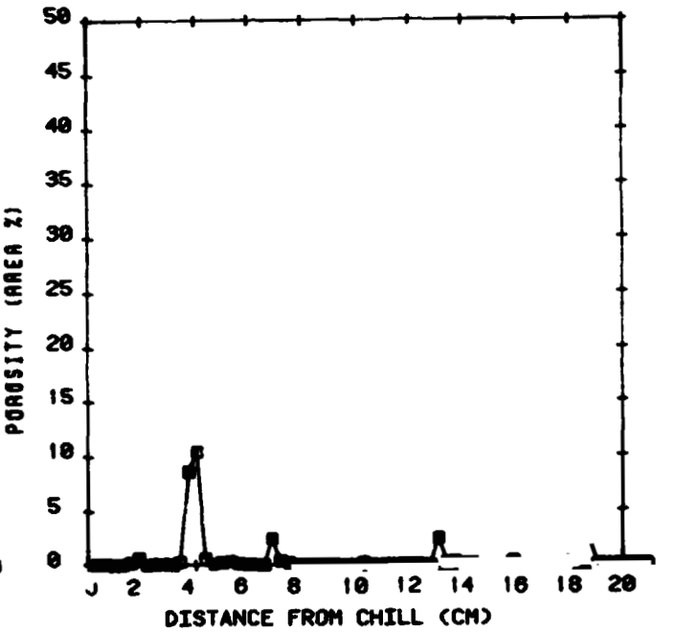

Figure 11. Variation of porosity in sample A4, pure Al.

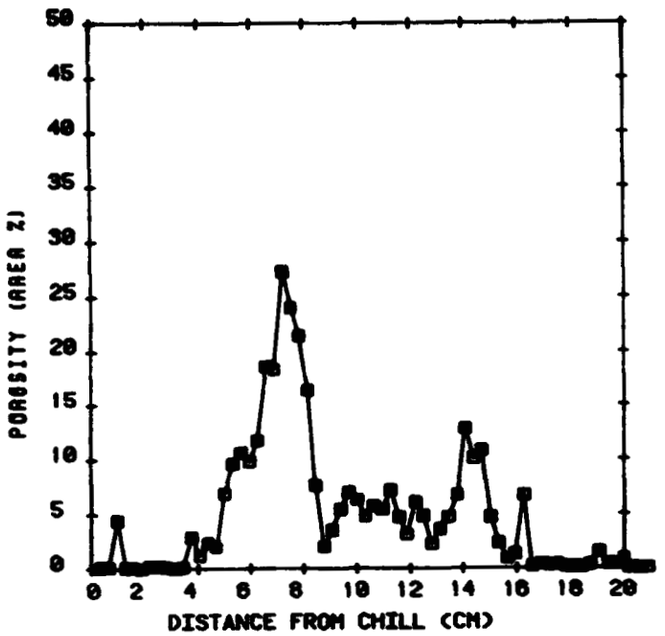

Figure 12. Variation of porosity in sample A5, pure Al.

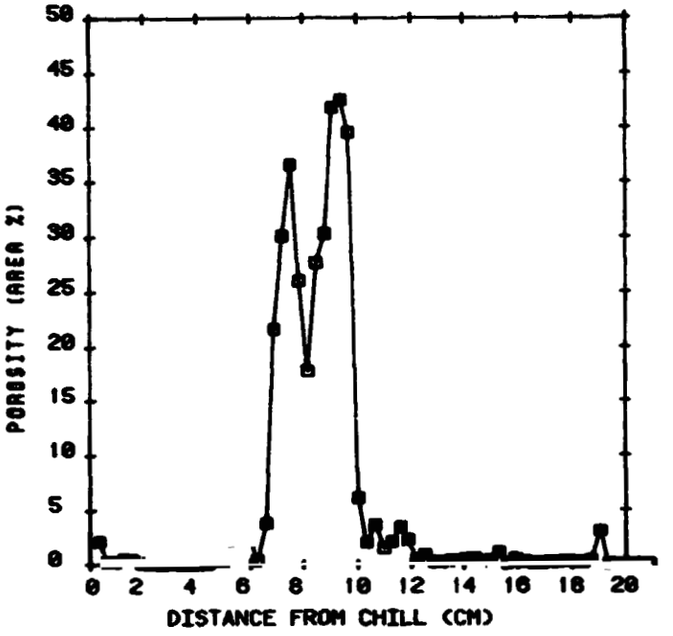

Figure 13. Variation of porosity in sample A6, pure Al.

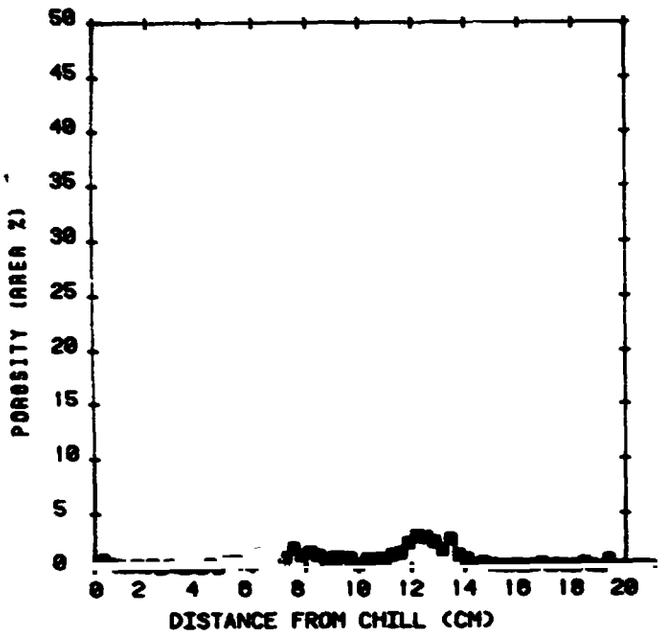

Figure 14. Variation of porosity in sample B1, 2%Si

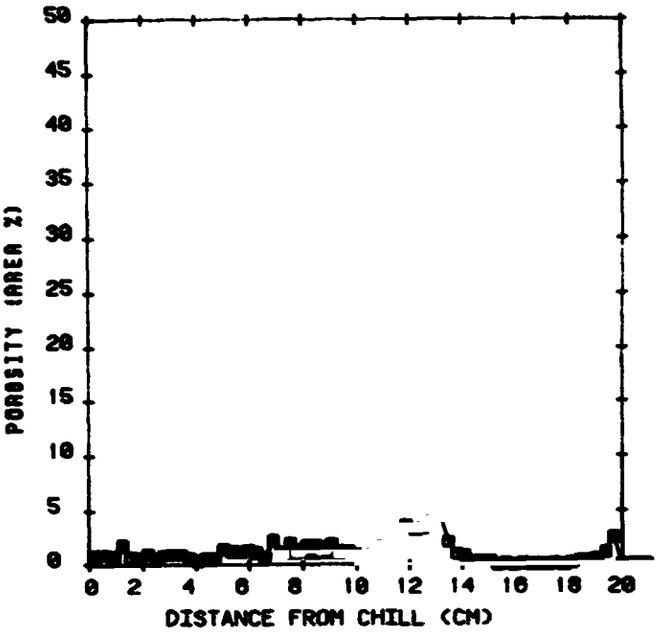

Figure 15. Variation of porosity in sample B2, 2%Si

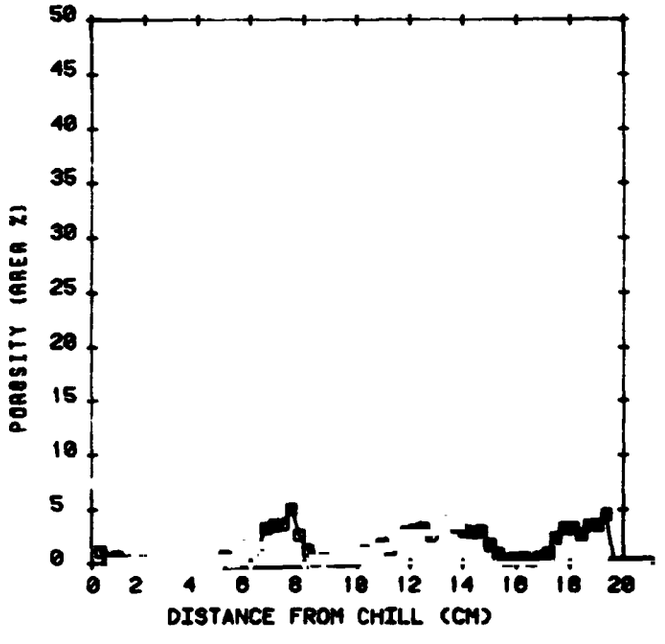

Figure 16. Variation of porosity in sample B3, 2%Si

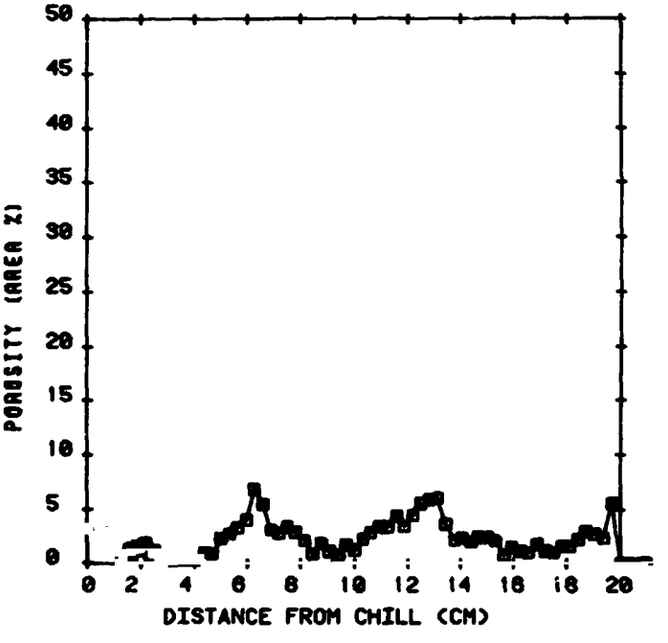

Figure 17. Variation of porosity in sample B4, 2%Si

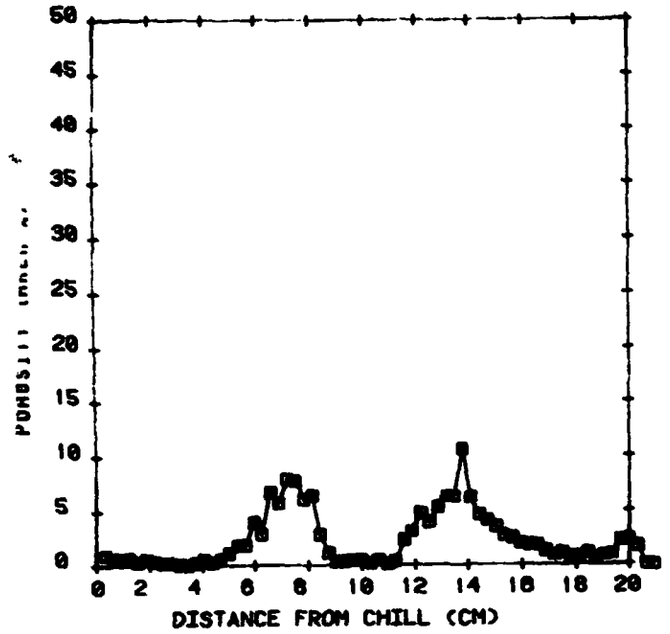

Figure 18. Variation of porosity in sample C1, 4%Si

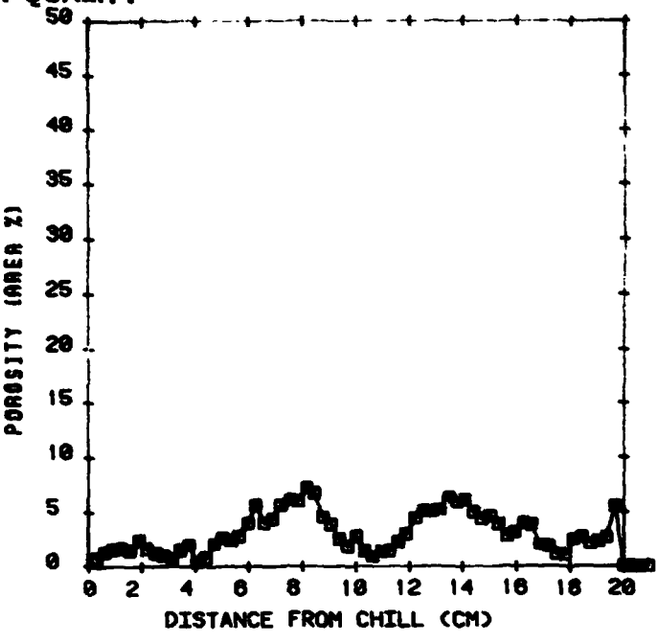

Figure 19. Variation of porosity in sample C2, 4%Si

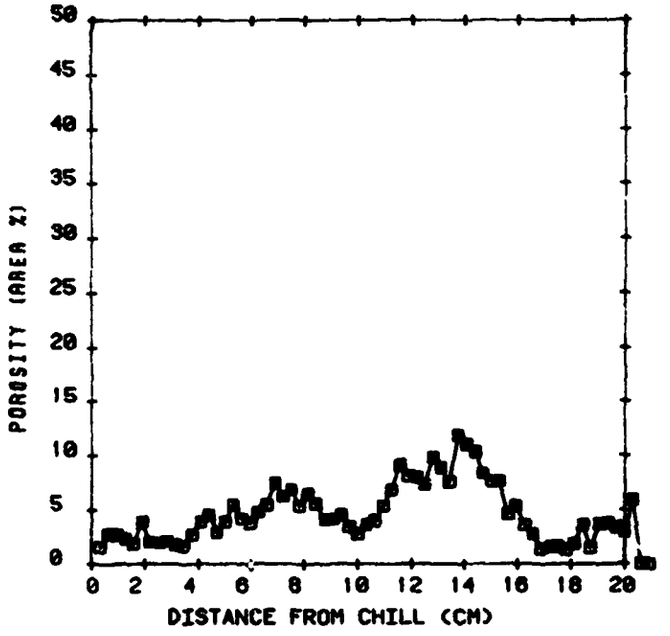

Figure 20. Variation of porosity in sample C3, 4%Si

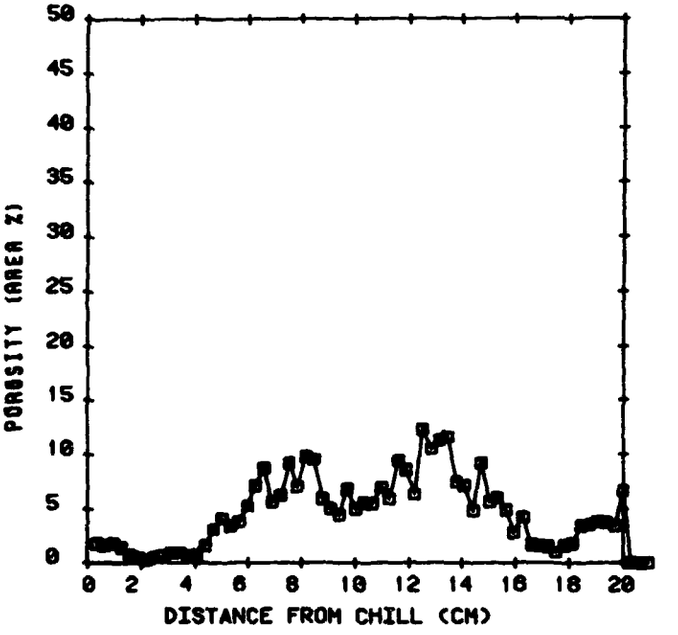

Figure 21. Variation of porosity in sample C4, 4%Si

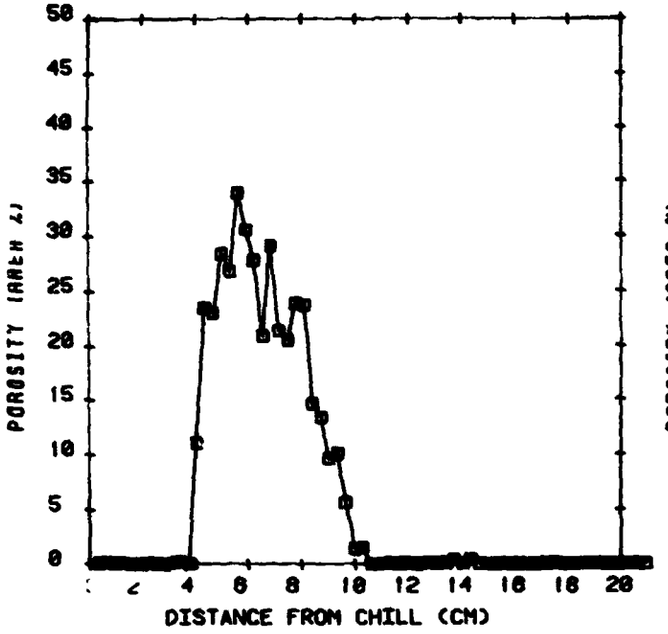

Figure 22. Variation of porosity in sample D1, 7%Si

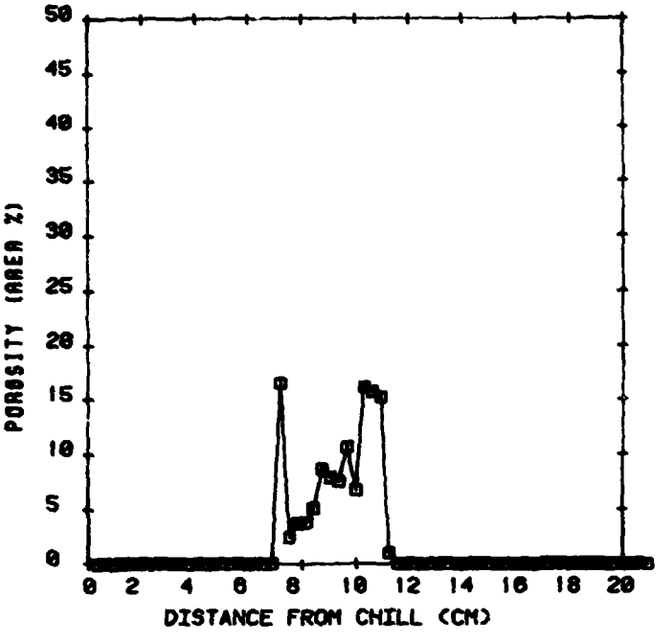

Figure 23. Variation of porosity in sample D2, 7%Si

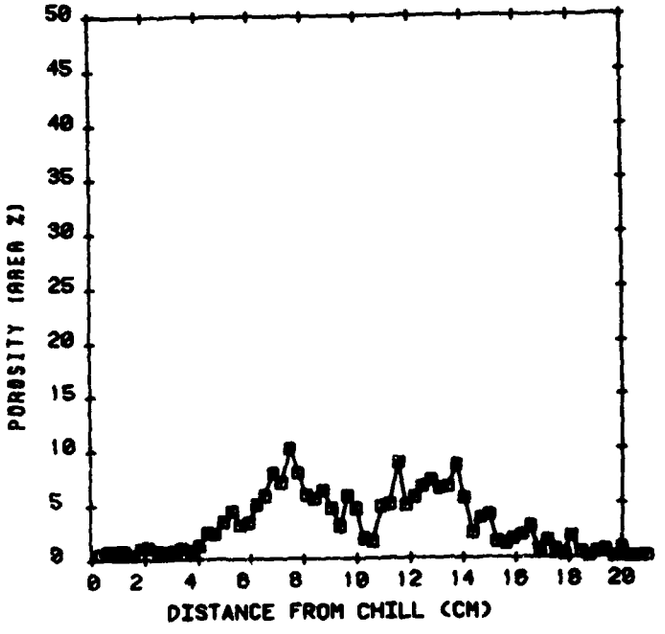

Figure 24. Variation of porosity in sample D3, 7%Si

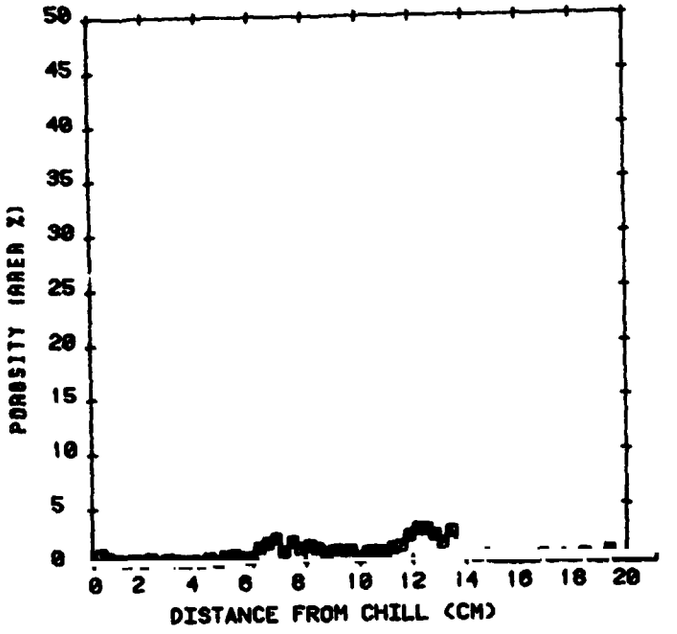

Figure 25. Variation of porosity in sample D4, 7%Si

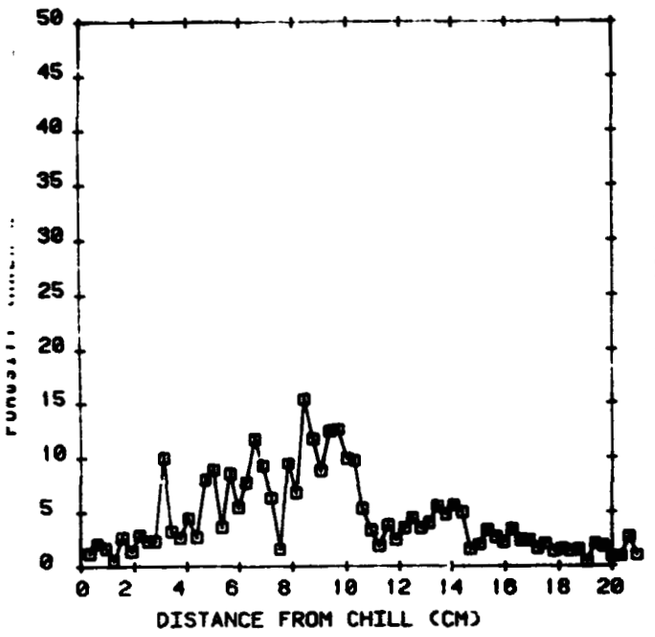

Figure 26. Variation of porosity in sample D5, 7%Si

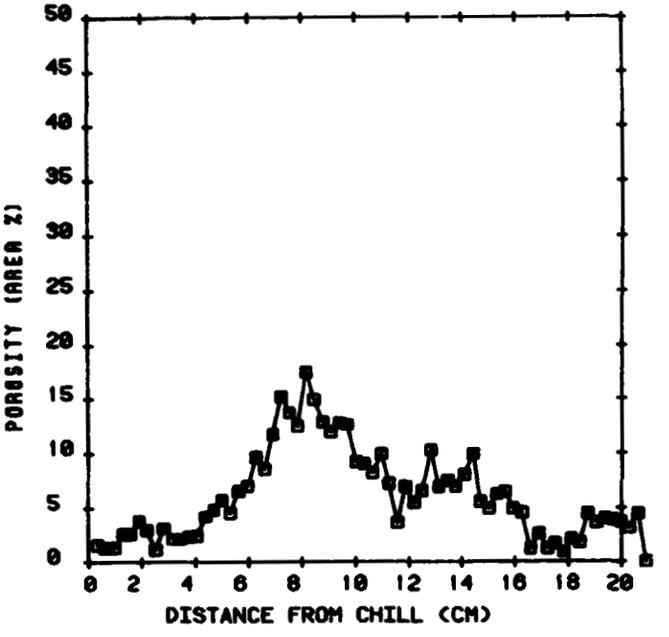

Figure 27. Variation of porosity in sample D6, 7%Si

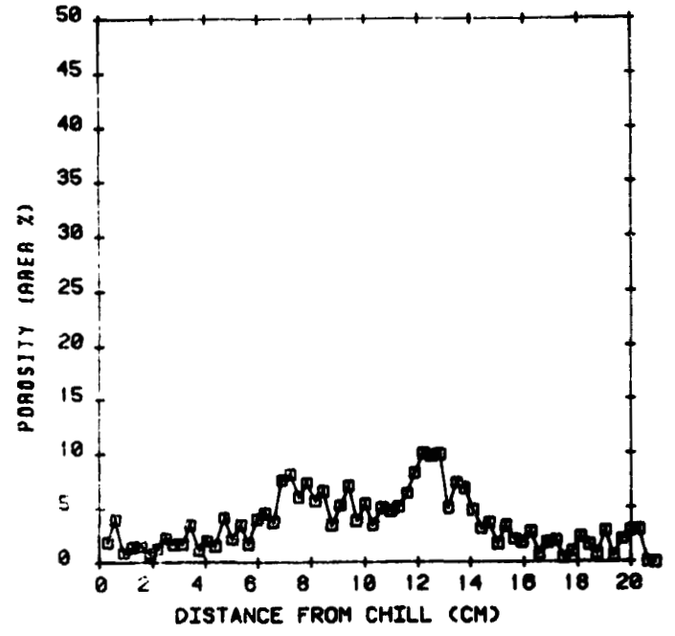

Figure 28. Variation of porosity in sample D7, 7%Si

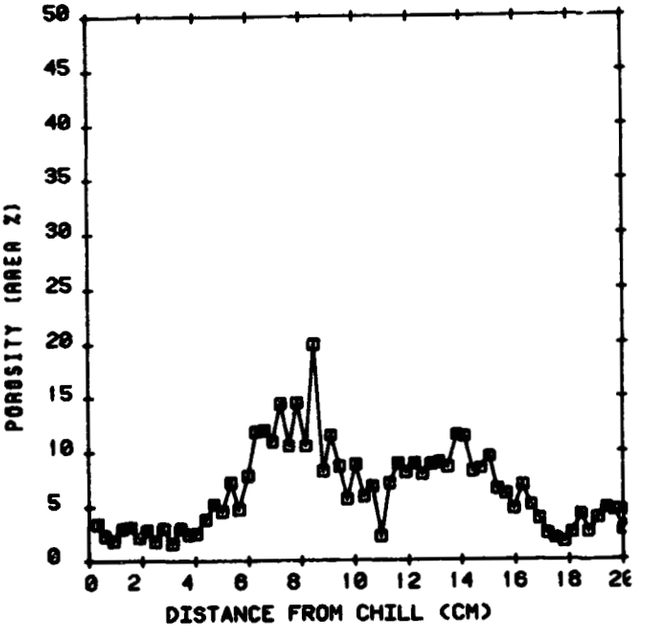

Figure 29. Variation of porosity in sample D8, 7%Si

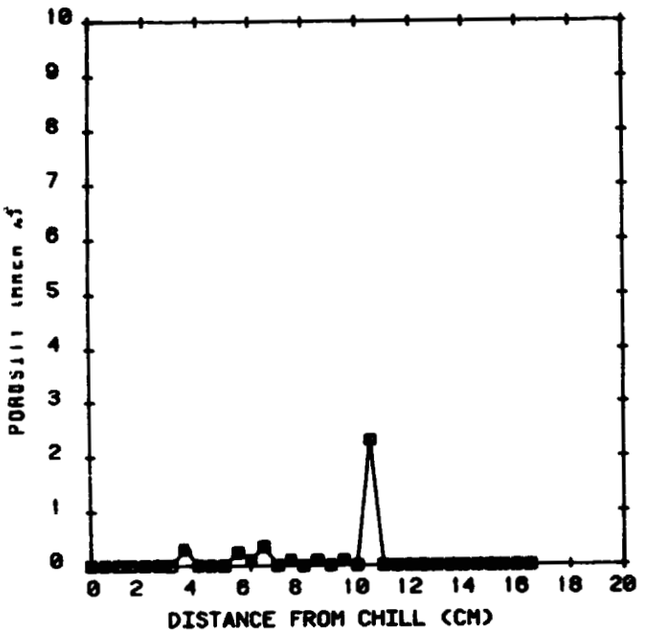

Figure 30. Variation of porosity in sample Z1, 4.5%Cu

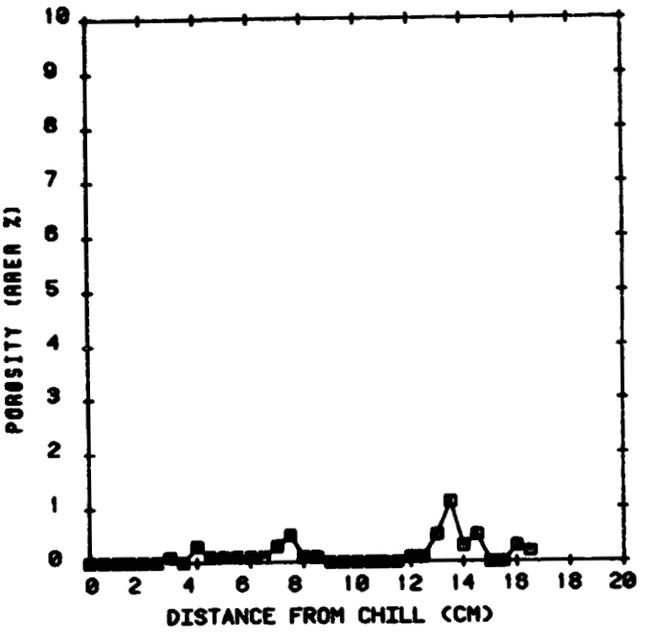

Figure 31. Variation of porosity in sample Z2, 4.5%Cu

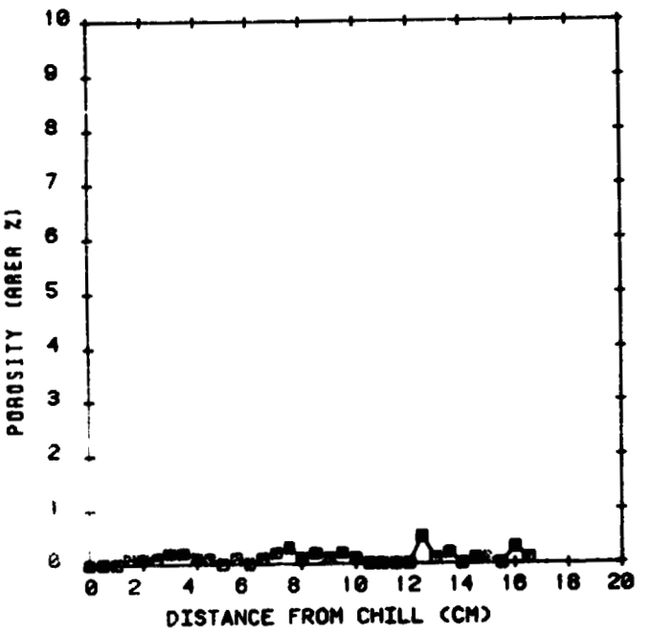

Figure 32. Variation of porosity in sample Z3, 4.5%Cu

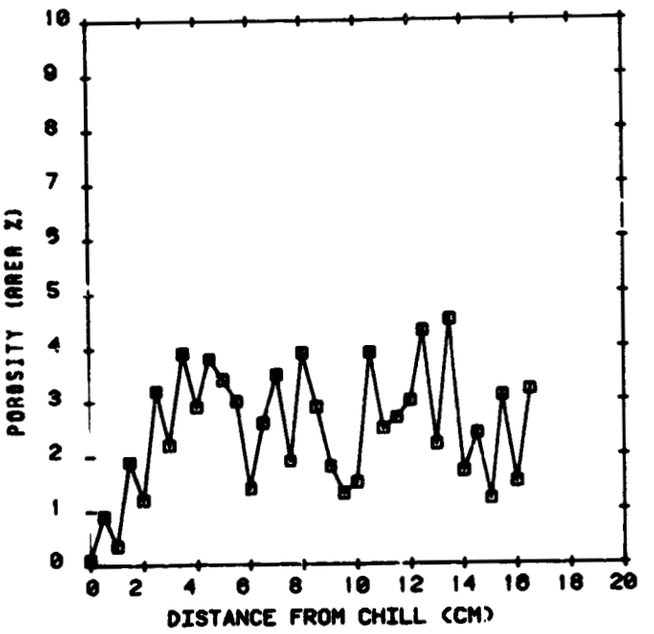

Figure 33. Variation of porosity in sample Z4, 4.5%Cu

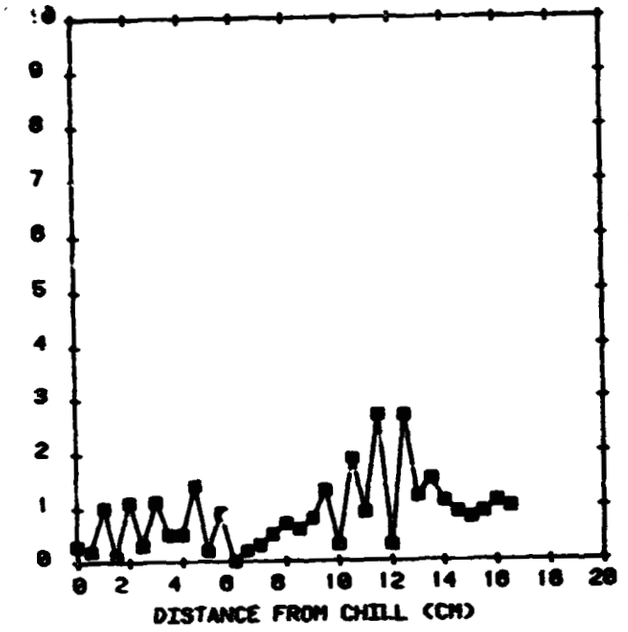

Figure 34. Variation of porosity in sample Z5, 4.5%Cu

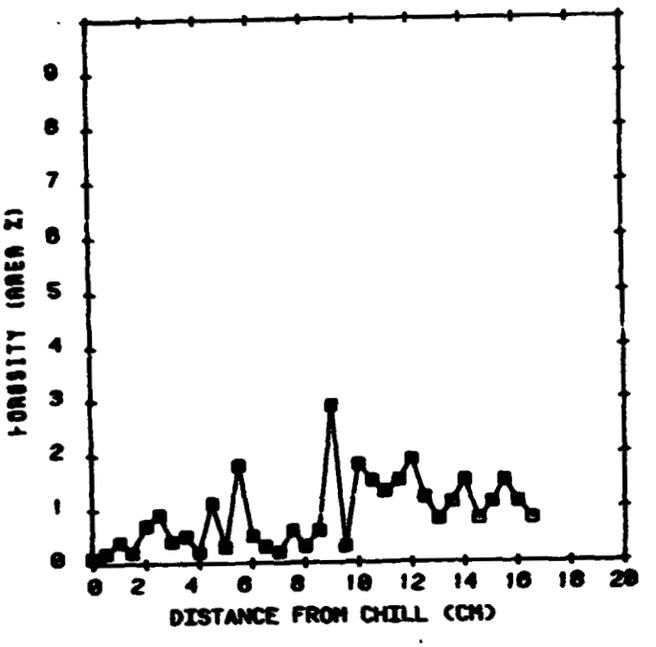

Figure 35. Variation of porosity in sample Z6, 4.5%Cu

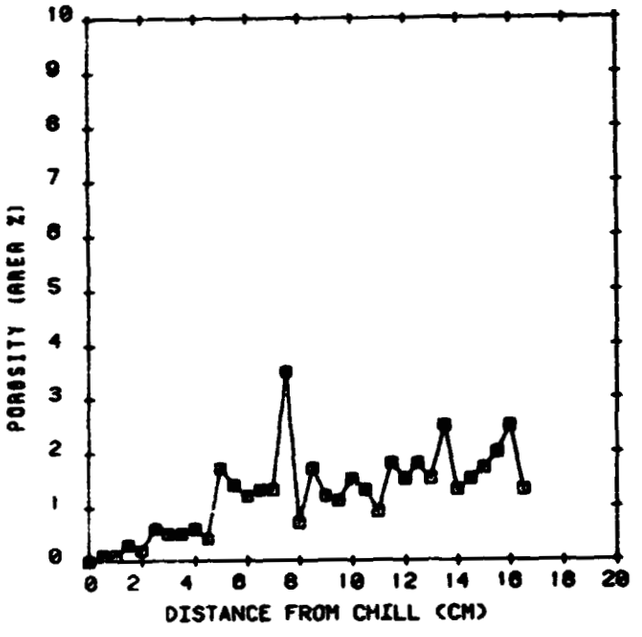

Figure 36. Variation of porosity in sample Z7, 4.5%Cu

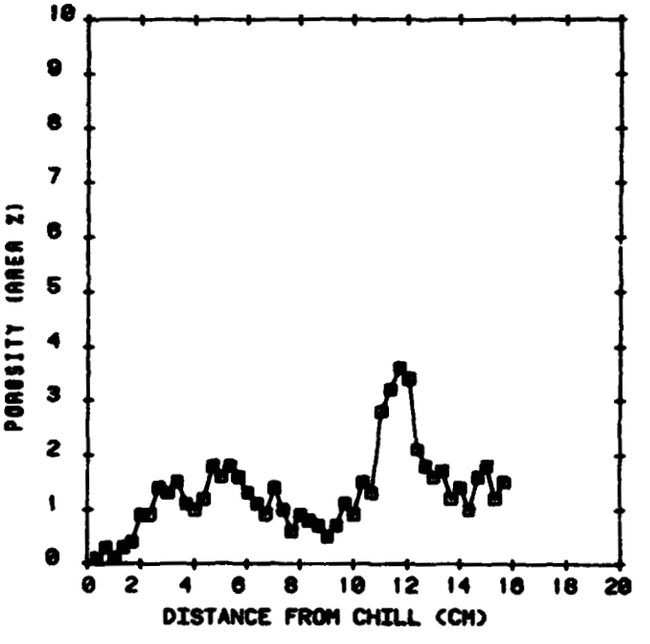

Figure 37. Variation of porosity in sample Z8, 4.5%Cu

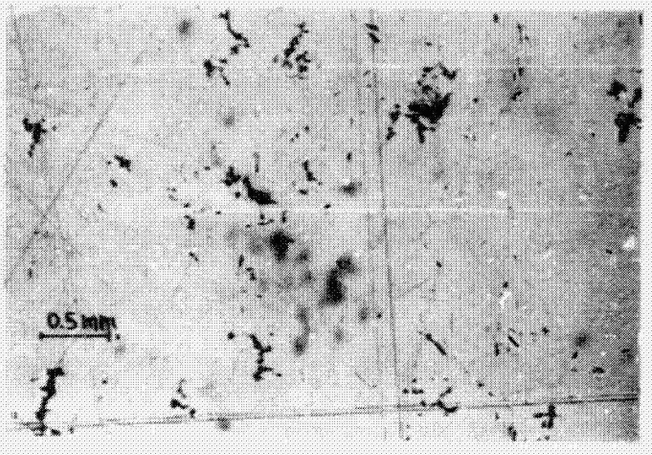

Figure 38. Sample B1.

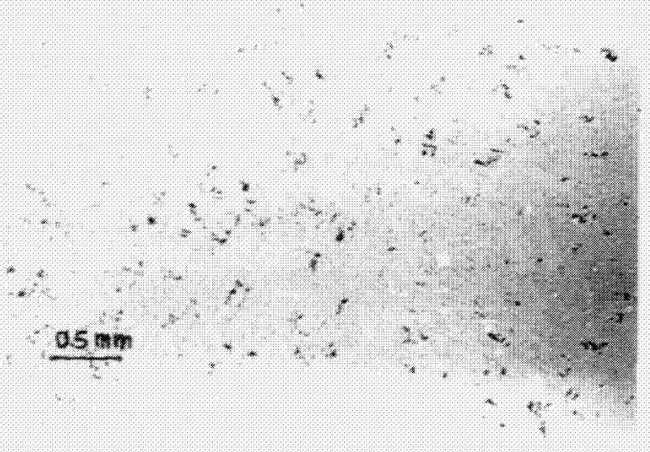

Figure 39. Sample Z1.

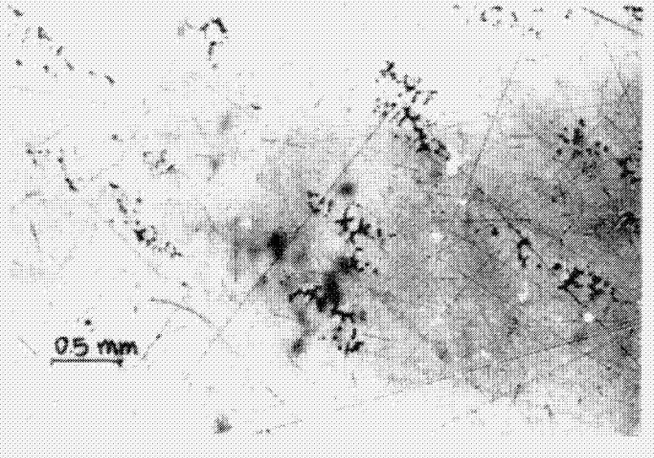

Figure 40. Sample A1.

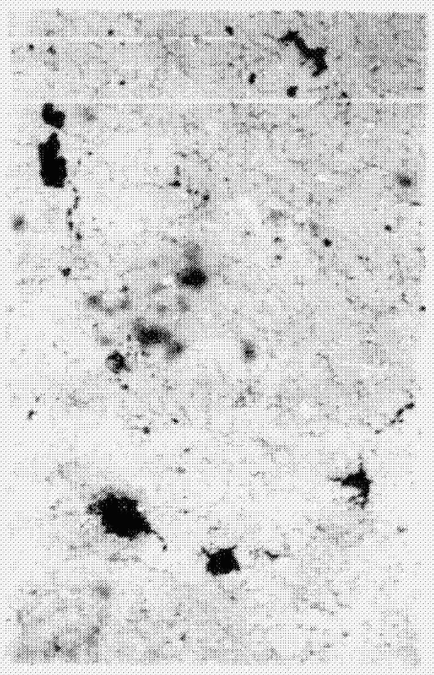

Figure 41. Sample C1.

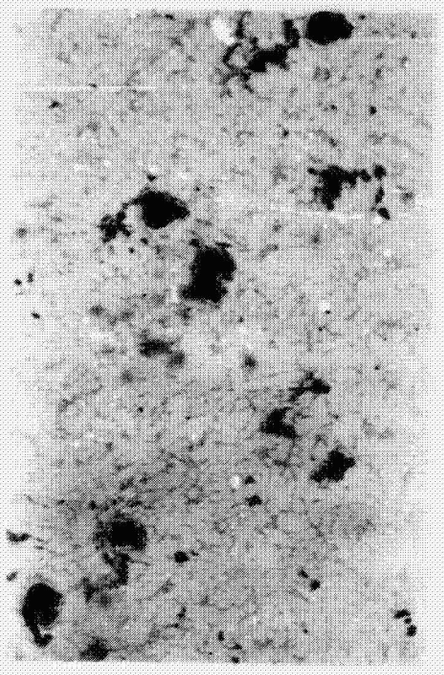

Figure 42. Sample C4.

Figure 44. Sample D6.

Figure 43. Sample Z7.

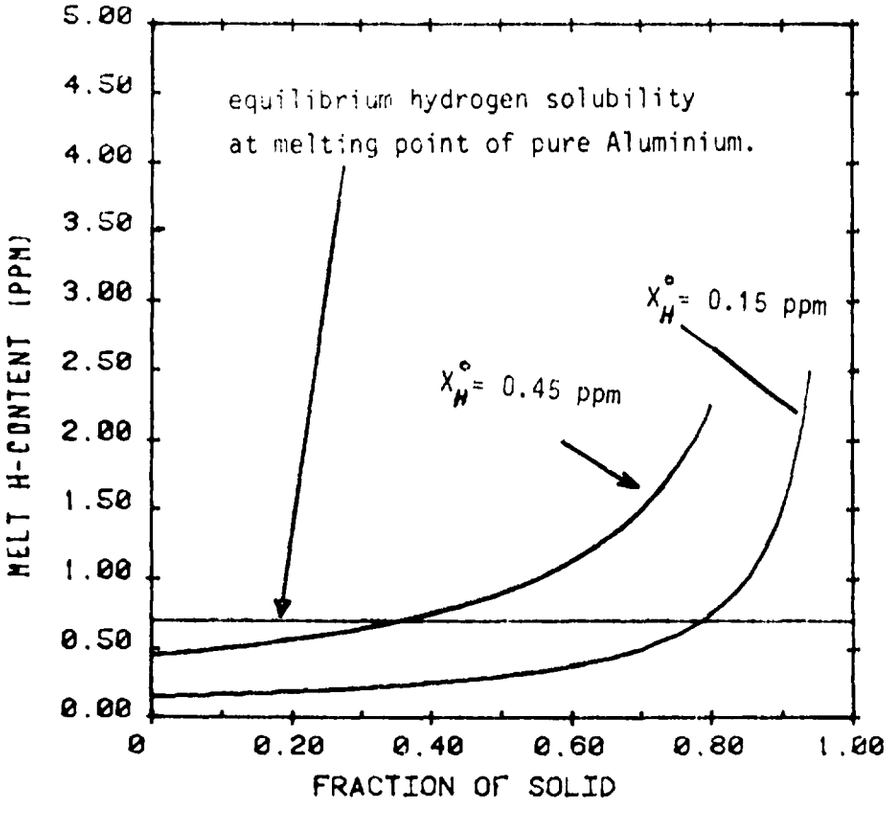

Figure 45. Enrichment of hydrogen in the melt during solidification.

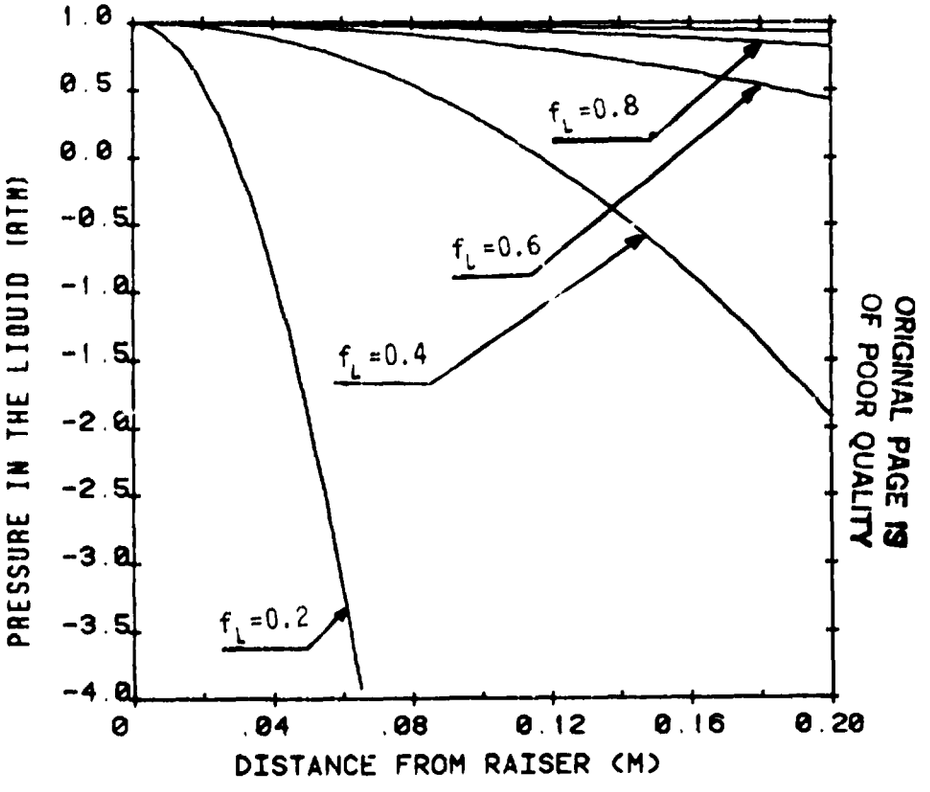

Figure 46. Pressure drop due to shrinkage.

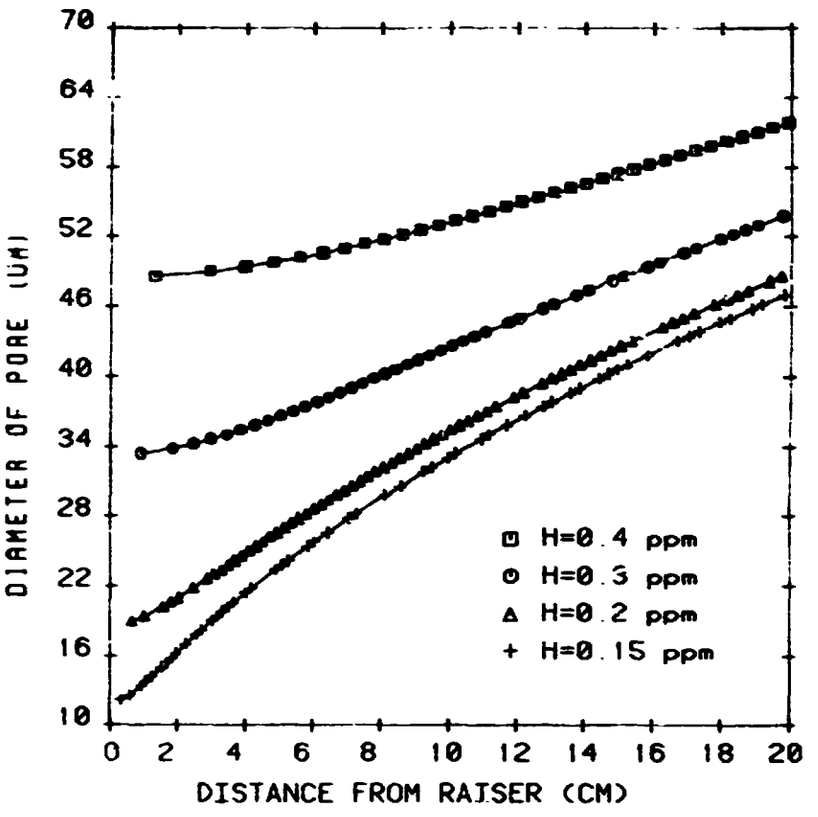

Figure 47. Calculated pore size (Eq. 19).

RAPIDLY SOLIDIFIED AMORPHOUS AND CRYSTALLINE ALLOYS
B.H. Kear, B.C. Giessen, and M. Cohen, editors

THE EFFECT OF HYDROGEN ON AN IRON BASED AMORPHOUS ALLOY

H. SHAHANI, H. SODERHJELM AND MATS NYGREN[X]
Department of Casting of Metals, The Royal Institute of Technology Stockholm, Sweden, [X]The Arrhenius Laboratory, Stockholm, Sweden

ABSTRACT

In this investigation we have systematically studied the brittleness and the atomic structure in an Fe(SiBC) alloy. Different amounts of hydrogen have been dissolved in the alloy. It has then been studied at different cooling rates.

Hydrogen gas of different partial pressures was dissolved into the melt. The alloy was then rapidly quenched by a chill block melt spinning method. The cooling rates were changed by changing the velocity on the chilling roll. The brittleness and the atomic structure were examined by bending tests and x-ray diffraction.

X-ray diffractions showed that the ribbons were amorphous when the cooling rate was sufficient. Amorphous ribbons without any hydrogen were ductile, crystalline ribbons of this alloy were brittle. The ribbons with dissolved hydrogen and amorphous structure were brittle even at small amounts of hydrogen. At the highest cooling rates the ribbons with low hydrogen content were ductile. There seems to be a connection between the hydrogen content and the amorphous ribbons ductility. The hydrogen content only has a slight influence to amorphous structure.

INTRODUCTION

Hydrogen easily dissolves in liquid metals. The solubility decreases rapidly when the metal solidifies and with decreasing temperature. Many alloys become brittle even when a small amount of hydrogen is present. In this investigation we have dissolved different amounts of hydrogen in a Fe ($Si_5B_{11}C_4$) liquid alloy. Ribbons were then directly cast from the melt by a chill-block melt-spinning method. Both amorphous and crystalline atomic structures were obtained by changing the velocity of the chilling substrate. The hydrogen content, the brittleness and the atomic structure were then examined on the ribbons.

EXPERIMENTAL

The ribbons were made by a single roller melt spinning equipment. The diameter of the copper roll was 159 mm. Three grams of the Fe (SiBC) alloy was used for each experiment and it was melted by a high frequency induction furnace. The crucible was made of quartz; in the crucible bottom there was a hole with a diameter of 0.5 mm. A gas mixture was blown for 30 seconds through a lance onto the top of the liquid alloy (Fig. 1). The gas mixture was a mixture of hydrogen and argon. The different amounts of hydrogen gas which were used in these experiments were 0, 5, 10, 50 and 100 volume %. The amount of gas was 200 liters per hour. The driving ejection pressure was 100 kPa; argon gas was used (Fig. 2). The distance between the crucible and the copper role was 3 mm and the melt jet inclination was 90°. The substrate velocities were 4, 8, 13, 17, 21, 25, 29 and 33 m/s.

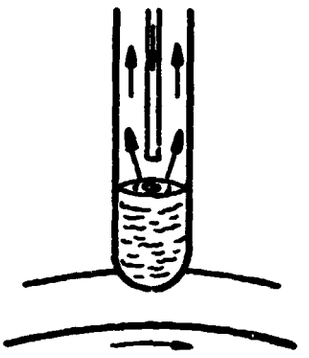

Fig. 1. Gas flow during the gas treatment.

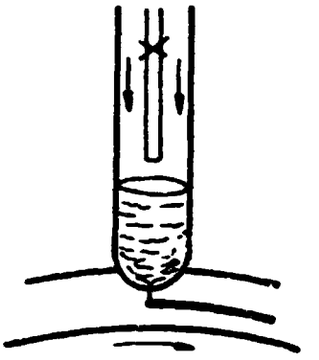

Fig. 2. Gas flow during casting

The atomic structure was determined by x-ray diffraction, using nickel filtered CuKα radiation. The amount of hydrogen in the specimens was measured by vacuum fusion with a Balzer analyzer EAH 220. Two grams of the sample were heated in graphite crucibles to 2000°C. This was done about one week after the ribbons were made.

Differential scanning calorimetry was carried out in a Mettler TA 2000 C. Samples of around 20 mg were heated in Pt cups with a rate of 5 K/min^{-1} from 460°C beyond the crystallization temperature in inert atmosphere. The temperature axis and the peak area were calibrated from melting endotherms of pure indium, aluminium and gold.

RESULTS

Several different examinations were made on the ribbons to determine the effect of hydrogen on the samples.

The hydrogen content was determined by vacuum fusion. The results are shown in Fig. 3 and Fig. 4.

In Fig. 3 it is shown how the hydrogen content in the ribbons varies with the amount of hydrogen gas in the gas mixture. The substrate velocity was 29 m/s. Fig. 4 shows how the hydrogen content in the ribbons varies with the substrate velocity. The amount of hydrogen gas in the gas mixture was 50%.

The thickness of the ribbons was measured with a micrometer. No noticeable difference could be seen on ribbons with or without hydrogen. The average thickness as a function of the substrate velocity is shown in Fig. 5.

The x-ray diffraction examination showed that the structure was crystalline when the thickness was over 50 μm. No noticeable difference could be seen on ribbons with or without hydrogen.

The brittleness of the ribbons was investigated in a rather simple way by a bending test. The ribbon was bent 180°; if it breaks it is brittle and if not, it is ductile. In Fig. 6 these results are shown. There is a definite difference in brittleness of ribbons with different amounts of hydrogen in the gas mixture. The ribbons which were treated with pure hydrogen showed brittle behaviour for all substrate velocities. Ribbons without any hydrogen become brittle at substrate velocities lower than 20 m/s. At velocities lower than 13 m/s, ribbons were crystalline.

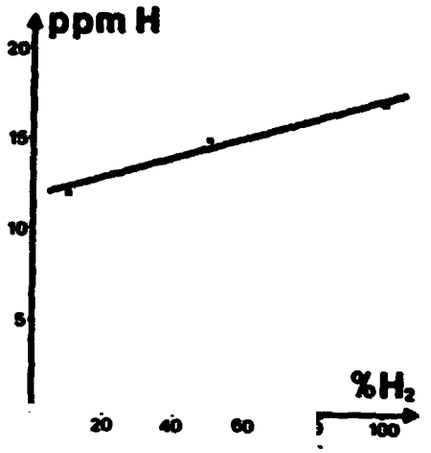

Fig. 3. The hydrogen content of the ribbons at different amounts of hydrogen gas in the gas mixture.

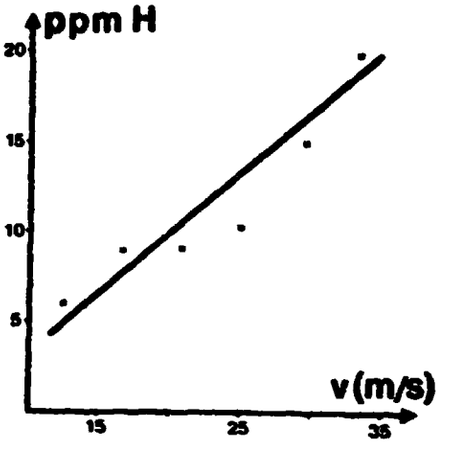

Fig. 4. The hydrogen content of the ribbons at different substrate velocities.

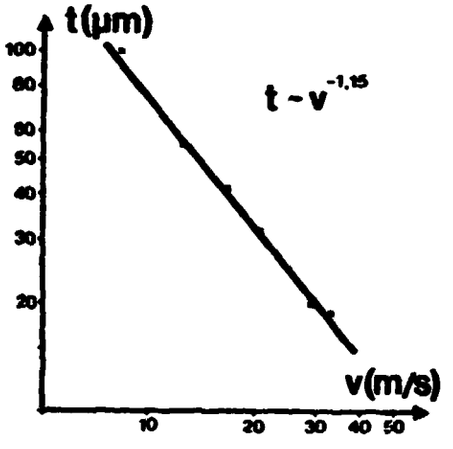

Fig. 5. The variation of thickness with substrate velocity.

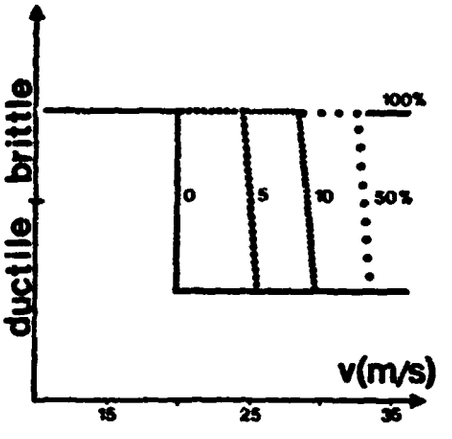

Fig. 6. Ductility of the ribbons at different substrate velocities and different amounts of hydrogen gas in the gas mixture.

Differenti l scanning calorimetry has been used to determine the crystallization temper re and heat of crystallization. Two series were determined, one in which the melt had been treated with 100 % H_2, and one in which 100 % Ar. Four representative DSC thermograms are shown in Fig. 7 and Fig. 8. All samples spun with between 33 and 13 m/s exhibit exothermic DSC peaks while no crystallization peaks could be observed for samples which were made at velocities lower than 13 m/s.

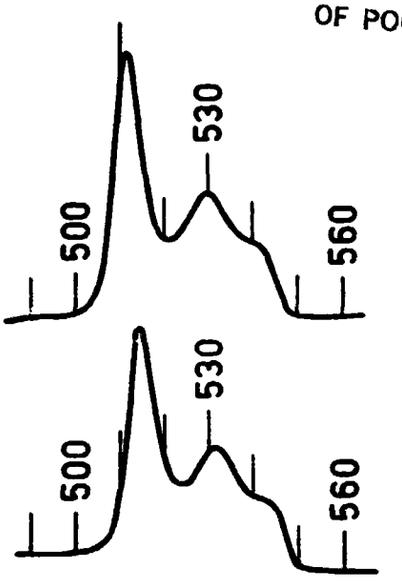

Fig. 7. DSC curves for the exothermal crystallization of amorphous ribbons: 100% Ar, 33 m/s (above); 100 % H_2, 33 m/s (below).

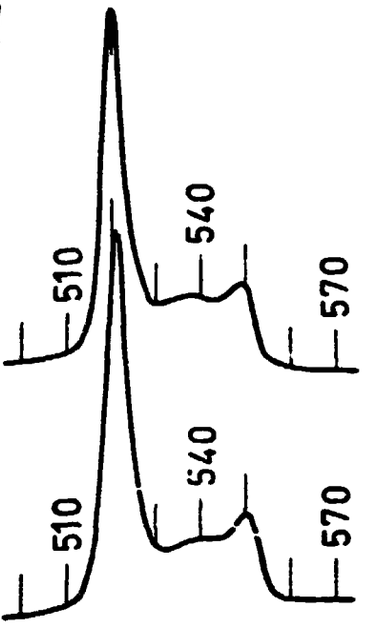

Fig. 8. DSC curves for the exothermal crystallization of amorphous ribbons: 100 % Ar, 13 m/s (above); 100% H_2, 13 m/s (below).

DISCUSSION

According to the x-ray diffraction evidence there was no noticeable difference in the atomic structure of the ribbons which were treated with or without hydrogen gas. It seems that hydrogen at these levels has no effect on the formation of the atomic structure for this alloy. This corresponds to the DSC thermograms. As can be seen in Figs. 7 and 8. the total crystallization peak seems to be composed of three overlapping peaks, indicating the kinetics of crystallization to consist of several processes. The total heat of crystallization has been found to be 1.34 kcal/mole, independent of the velocity and the hydrogen content. Our value is in good agreement with previous findings for Fe-P-C amorphous alloys (1). The shapes of the peaks of samples with the same velocity but different amounts of hydrogen were almost identical, but the shapes varied somewhat with the velocity as is to be seen in the figures.

It is known that amorphous alloys become brittle when certain amounts of hydrogen are present (2-6). The most common way of dissolving hydrogen used in these investigations was by cathodic polarization in an acid solution. The hydrogen content in the ribbons then becomes high and they cannot be bent 180° without breaking.

In this investigation the maximum content of dissolved hydrogen is limited by the solubility in the liquid phase which is about 25 ppm. At the highest cooling rates most of the hydrogen is left in the ribbons; thereafter the hydrogen content decreases with decreasing cooling rate. This can even be observed on ribbons made from melt treated with 100 % Ar. The amount of hydrogen is relatively high even though the melt has not been treated with hydrogen. This has also been reported by ref. (7).

Ribbons that are made at the highest substrate velocity, 33 m/s, become brittle when the hydrogen content is over about 20 ppm. The ribbons that are made at lower substrate velocity, 29 m/s, become brittle when the hydrogen content is over ca 15 ppm.

It seems that the cooling rate on amorphous alloys has an effect on the sensitivity to hydrogen embrittlement.

ACKNOWLEDGEMENT

Thanks are due to Professor Hasse Fredriksson for many stimulating discussions.

REFERENCES

1. M.G. Scott, P. Ramachandrarao, Mat. Sci. Eng., 29, (1977), p. 137.

2. R.K. Viswanadham, I.A.S. Green, W.G. Montague, Script. Metal., 10, (1976), p. 229.

3. N. Nagumo, T. Takahashi, Mat. Sci. Eng., 23, (1976), p. 257.

4. A. Kawashima, K. Hasimoto, T. Masumoto, Script. Metal., 14, (1980), p. 41.

5. A. Kawashima, K. Hasimoto, T. Masumoto, Corrosion, 36, (1980), p. 577.

6. S. Ashok, N.S. Stoloff, M. Glicksman, T. Slavin, Script. Metal., 15, (1981), p. 331.

7. A. Kawashima, K. Hasimoto, T. Masumoto, Corrosion Sci., 32, (1976), p. 935.